



RPSEA

Final Report

08123.02.Final

***Field Demonstration of Alkaline
Surfactant Polymer Floods in Mature
Oil Reservoirs, Brookshire Dome, Texas***

October 21, 2012

Chris Lewis
Layline Petroleum LLC

PI-Mukul M. Sharma
Bo Gao
The University of Texas at Austin
200 E. Dean Keeton St. Stop C0300
Austin, Texas 78712
(512) 471-3257
msharma@mail.utexas.edu

LEGAL NOTICE

This report was prepared by Layline Petroleum LLC as an account of work sponsored by the Research Partnership to Secure Energy for America, RPSEA. Neither RPSEA, members of RPSEA, the National Energy Technology Laboratory, the U.S. Department of Energy, nor any person acting on behalf of any of the entities:

- a. MAKES ANY WARRANTY OR REPRESENTATION, EXPRESS OR IMPLIED WITH RESPECT TO ACCURACY, COMPLETENESS, OR USEFULNESS OF THE INFORMATION CONTAINED IN THIS DOCUMENT, OR THAT THE USE OF ANY INFORMATION, APPARATUS, METHOD, OR PROCESS DISCLOSED IN THIS DOCUMENT MAY NOT INFRINGE PRIVATELY OWNED RIGHTS, OR
- b. ASSUMES ANY LIABILITY WITH RESPECT TO THE USE OF, OR FOR ANY AND ALL DAMAGES RESULTING FROM THE USE OF, ANY INFORMATION, APPARATUS, METHOD, OR PROCESS DISCLOSED IN THIS DOCUMENT.

THIS IS A FINAL REPORT. THE DATA, CALCULATIONS, INFORMATION, CONCLUSIONS, AND/OR RECOMMENDATIONS REPORTED HEREIN ARE THE PROPERTY OF THE U.S. DEPARTMENT OF ENERGY.


REFERENCE TO TRADE NAMES OR SPECIFIC COMMERCIAL PRODUCTS, COMMODITIES, OR SERVICES IN THIS REPORT DOES NOT REPRESENT OR CONSTITUTE AN ENDORSEMENT, RECOMMENDATION, OR FAVORING BY RPSEA OR ITS CONTRACTORS OF THE SPECIFIC COMMERCIAL PRODUCT, COMMODITY, OR SERVICE.

Abstract

A pilot alkaline/surfactant/polymer (ASP) flood has been conducted. A four-step design approach, composed of a) process and material selection; b) formulation optimization; c) core flood validation; 4) numerical simulation, was successfully conducted and this methodology could be applied to any other EOR project. The optimal chemical formulation recovered over 90% residual oil in a Berea core flood. The simulation model accurately history matches the core flood experiment and allowed us to scale from the lab scale to the pilot scale. Different operating strategies were simulated for the pilot. These cases allowed us to evaluate the sensitivities of project economics to various design parameters. A field execution plan was proposed based on the results of the simulation study.

Surface facilities for the pilot were built by Fabtech and the surfactant and polymer were provided by Stepan and TIORCO. Layline conducted a multi-well tracer test to ensure that the wells were communicating and that the active water drive would not skew the flood pattern. Out of pattern breakthrough of the tracer indicated that the injected fluids were going to be migrating outside the pattern. Production logging tools were run in the injection well to check on the vertical conformance. It was found that the upper layers were taking a disproportionate amount of water. A polymer pre-flush was implemented in the ASP to improve the vertical conformance.

The final design of the ASP was implemented over a period of 10 months. The results indicated oil breakthrough in many of the producers. However, the volumes of oil produced were not as large as predicted by the core floods and simulations. The key lessons learned throughout the project are summarized in this report and are invaluable for planning and designing future ASP pilot floods.


Chris Lewis
President, Layline Petroleum

1/15/13
Date

Table of Contents

Abstract.....	Error! Bookmark not defined.
Table of Contents.....	i
Executive Summary.....	1
A. Development of Surfactant Formulations for Field Pilot.....	4
A.1 Catahoula Sand Information.....	4
A.1.1 Geology and Petrophysics of Pilot Area.....	4
A.1.2 Crude Oil and Brine.....	5
A.1.3 Field Core Samples.....	7
A.2 Phase Behavior Measurements.....	8
A.2.1 Initial Screening and Oil Activity (B-1 to B-16).....	9
A.2.2 Alkyl Benzene Sulfonate (ABS) Trials (B-17 to B-26).....	15
A.2.3 Surfactant Mixture and New Molecules (B-27 to B-40).....	17
A.2.4 Formulation Optimization (B-41 to B-91).....	20
A.3 Coreflood Experiments.....	34
A.3.1 Experimental Equipment.....	34
A.3.2 Coreflood Description.....	35
Brine Flood.....	35
Oil Flood.....	35
Water Flood.....	35
Chemical Flood.....	36
A.3.3 Quality and Mobility Control for Polymer.....	36
A.3.4 Brookshire Coreflood GB-2.....	38
GB-2 Core Data.....	38
GB-2 Brine Flood.....	40
GB-2 Oil Flood.....	40
GB-2 Water Flood.....	41
GB-2 Chemical Flood Design.....	42

GB-2 Chemical Flood Recovery.....	45
A.4 Section Summary	47
B. Pilot-Scale ASP Flood Design	48
B.1 Coreflood History Matching.....	48
B.1.1 Phase Behavior: Experiments and Modeling.....	48
B.1.2 Polymer Rheology Modeling.....	51
B.1.3 Geochemical Input Data	53
B.1.4 Coreflood Simulation.....	54
B.2 Pilot Scale Simulation Study	59
B.2.1 Simulation Model Setup	59
Pattern Volume Calculation.....	60
Spinner Survey.....	61
Multi-well Tracer Test.....	64
B.2.2 Waterflood	67
B.2.3 General Operating Strategy Comparison (w/ 5-Layer Model) ...	70
Case 1: Base Case ASP Flood	72
Case 2: 2X ASP Injection	73
Case 3: ASP Bottom Injection.....	75
Case 4: Polymer Pre-Flush + ASP.....	77
Case 5: ASP with Doubled Production Rates.....	79
Summary	81
B.2.4 Sensitivity Simulations for ASP Flood (w/ 9-Layer Model)	83
Polymer Concentration Sensitivity	83
Total Chemical Mass Sensitivity	87
Alkali Consumption Sensitivity.....	91
B.3 Section Summary	95
C. Field Implementation and Performance Update.....	97
C.1 Field Implementation	97
C.1.1 Field Injection Plan.....	97
C.1.2 Project Timeline.....	98

C.2	Field Operation	100
C.2.1	Injection and Production Facilities	100
C.2.2	Field Laboratory Testing.....	101
C.3	Field Observations and Results.....	104
C.3.1	Injection Data.....	104
C.3.2	Residual Oil Mobilization.....	108
C.3.3	Chemical Detection.....	109
C.3.4	Production Response.....	110
C.4	Pilot Risks and Uncertainties	113
C.4.1	Higher Swept Pore Volume	113
C.4.2	Existence of Thief Zones / Unconstrained Fracture Growth	114
C.4.3	Higher Surfactant Retention	115
C.4.4	Viscous Microemulsion Formation.....	116
C.4.5	Low Initial Oil Saturation	119
C.5	Section Summary	119
	Conclusions.....	121
	Bibliography	125
	List of Tables	128
	List of Figures.....	130

Executive Summary

The largest onshore oil reserves in the US are the discovered mature oilfields that have been produced by primary and secondary recovery but still contain over 65% of the original oil in place. This represents 377 billion barrels of oil that is not recoverable by traditional methods. Recent oil prices are currently encouraging a tremendous growth in the study of chemical enhanced oil recovery. The vast amount of residual oil left behind after secondary recovery efforts are becoming increasingly appealing due to high demand and the price of oil. Chemical flooding has been studied for over half a century now. However, never have the conditions encouraging its growth been as good as right now. These conditions include new, improved technology and oil prices high enough to make implementation economical.

The primary objective of the project is to improve the oil recovery in a mature onshore oilfield, Brookshire Dome, using ASP (alkaline/surfactant/polymer) flooding. Extensive laboratory phase behavior and core flood studies, together with pilot flood implementation based on systematic planning and design, has directed the design of the ASP and the flood. The University of Texas at Austin conducted most of the laboratory studies necessary to design the appropriate ASP treatment. TIORCO aided in the supply chain steps needed to produce and supply the quantities of surfactant needed for the field study. Layline Petroleum provided the field area and oversaw the construction and implementation of the polymer flood. Primary tasks included field characterization, screening potential ASP candidates to select the best product for the project, and laboratory core floods and simulations to optimize the flood design. This was followed by a field tracer study and a final stage of field planning and flood design, then the actual field implementation of the flood.

Notable accomplishments include:

- Appropriate surfactants for the ASP flood were identified in the laboratory, based on phase behavior tests and core flood testing that showed excellent results.
- Computer simulations of ASP flooding in the Brookshire Dome were completed.
- Different scenarios with varying injection volumes of chemicals were investigated.
- Construction of facilities including an ASP system was completed and installed in the field.
- The ASP chemicals were injected into the pilot area over a seven month period and chemicals and oil recovery was monitored.

Based on the work completed thus far, the following significant conclusions have been arrived at:

- Injection of ASP chemicals was successfully achieved in the field. Polymer injectivities were much higher than anticipated based on simulations and polymer rheology.
- Inter-well tracer tests proved to be very useful in determining the fluid migration in the reservoir. The ASP responses were generally consistent with the results of the tracer tests.
- The phase behavior tests showed excellent oil solubilization, and the core flood tests showed more than 90% oil recovery.
- Oil cuts more than 10% were anticipated in the field pilot based on core floods and simulations. While an oil bank was observed in the field, oil cuts were much lower (in the range of 1-2%).

- The difference in the field performance compared to the lab tests may be due to two possible reasons: out of zone placement of the injected chemicals (due to faults or fractures), or insufficient chemical concentrations due to unexpectedly high adsorption of the chemicals on the reservoir rock.
- Oil production continues in the pilot wells and will continue to be monitored in the coming months.

This report is organized into three main sections. The purpose of **Section A** is to develop and test a surfactant formulation for the ASP field pilot. **Section B** discusses pilot execution plan and on-site pilot implementation. **Section C** is a summary of field operations and oil production results throughout the project. Finally the lessons learned from the pilot study are summarized in the **Conclusions** section.

A. Development of Surfactant Formulations for Field Pilot

A.1 CATAHOULA SAND INFORMATION

A.1.1 Geology and Petrophysics of Pilot Area

The target reservoir for field study is the Oligocene-aged Catahoula sandstone in the Brookshire Dome field in Texas. The field is about 35 miles to the west of Houston, off I-10. Discovered in 1996, the field is a piercement salt dome containing two main sands, the Catahoula and Plunk sands. Oil is found in the caprock above the salt dome (~3500ft). The Catahoula net sand ranges in thickness from 50 to 70ft thick within the pattern (Figure A.1). A spinner survey run on the injector (Martin 24) suggests some degree of heterogeneity. An inverted five-spot pattern was chosen for the pilot (highlighted area in Figure A.2). It comprises four producers (Martin 34, 37, 10A and 12) and a central well (Martin 24) converted for chemical injection. These wells are also referred to in the map as Layline 37, 34, 10A, 12 and 24. The short producer-to injector distance enables early flood response and ensures completion of the field trial within a relatively short period of time.

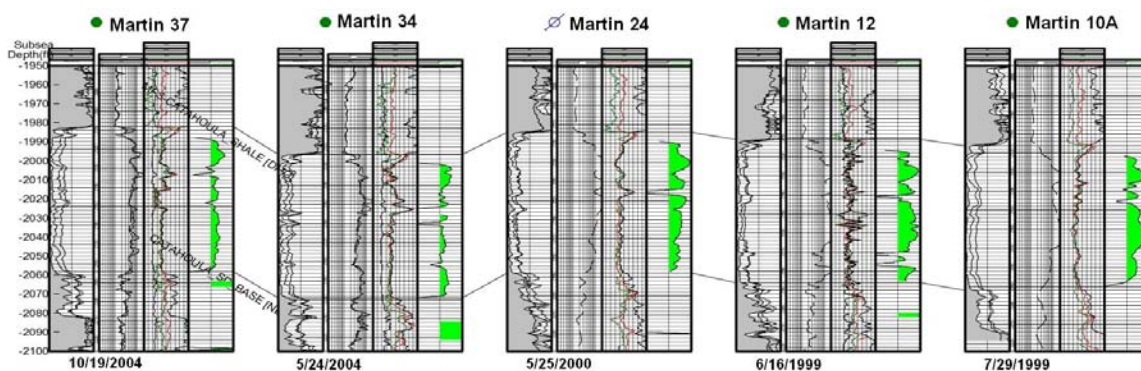


Figure A.1: Lateral Continuity of the Catahoula Sand within the Pattern (Injector: Martin 24; Producers: Martin 37, 34, 12 and 10A).

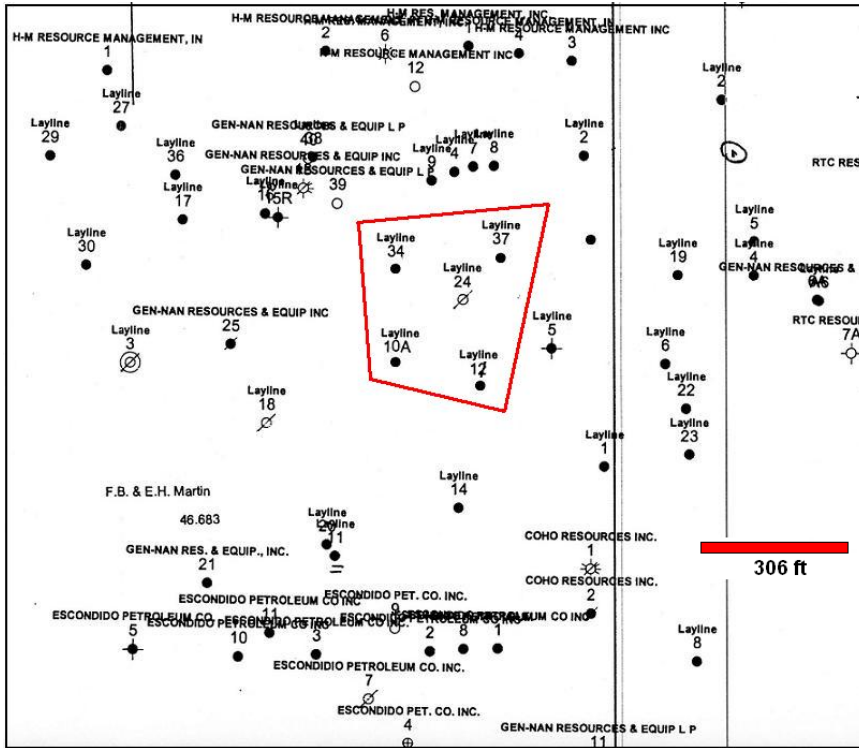


Figure A.2: Well Locations in Brookshire Dome Field (pilot pattern in red box).

A.1.2 Crude Oil and Brine

The crude oil is light to medium, $\sim 30^\circ$ API (lab measured density of 0.8762 g/cc @ 20°C), acidic and reactive. The viscosity was measured to be around 28cP at the reservoir temperature of 130°F (55°C). Because the Catahoula sand is a fairly shallow formation, the temperature is moderate, 130°F (55°C), thus sulfate surfactants can be used for the ASP formulation. The formation brine has a low salinity (~ 7000 to 8000ppm) and is fairly fresh. This poses a challenge for the surfactant selection process since most commercial surfactant systems have optimum salinities in the 20,000 to 35,000ppm range. Table A.1 shows the composition of a typical field water sample.

For lab testing purposes, the sulfate ions were removed to avoid precipitation issues at lab conditions. The synthetic version of this brine is referred to as Synthetic Brookshire Brine (SBB). SBB was prepared based on the composition of heater treater water, and by mixing appropriate amounts of CaCl₂, MgCl₂·6H₂O, NaHCO₃, and NaCl in DI water. Table A.2 below was used for preparing 1L SBB.

Table A.1: Composition of Field Water Samples (from Heater Treater).

Ion	Conc., mg/L	MW	Charge	Conc., meq/ml*
Ca ²⁺	88.80	40	2	0.00444
Mg ²⁺	8.40	24	2	0.00070
Na ⁺	2678.00	23	1	0.11643
Cl ⁻	3920.00	35.5	1	0.11042
SO ₄ ²⁻	10.60	96	2	0.00022
HCO ₃ ⁻	659.00	61	1	0.01080
Sr ²⁺	2.10	88	2	0.00005
Total	7366.90	---	---	0.24307

Table A.2: Mixing Sheet for Preparing 1L SBB (TDS = 7360.74 mg/L).

Compound	Mass (g/L)
CaCl ₂	0.246
MgCl ₂ ·6H ₂ O	0.070
NaHCO ₃	0.907
NaCl	6.174
DI	992.602

Table A.3: Composition of SBB (TDS = 7360.74 mg/L).

Ion	Conc., mg/L	MW	Charge	Conc., meq/ml
Ca ²⁺	88.80	40	2	0.00444
Mg ²⁺	8.40	24	2	0.00070
Na ⁺	2678.00	23	1	0.11643
Cl ⁻	3926.54	35.5	1	0.11061
SO ₄ ²⁻	0	96	2	0

HCO ₃ ⁻	659.00	61	1	0.01080
Sr ²⁺	0	88	2	0
Total	7360.74	---	---	0.24325

A.1.3 Field Core Samples

A good quality reservoir core is of key importance to the evaluation of candidate chemical formulations through coreflood experiments. Lack of reservoir core oftentimes poses challenges to laboratory evaluation of the ASP formulation. Unfortunately for this project, only poor quality sidewall cores were available. These core plugs were obtained from offset wells outside the pilot area. They were delivered either broken apart or severely contaminated by drilling mud (very muddy looking). Figure A.3 shows a picture of two plug samples.

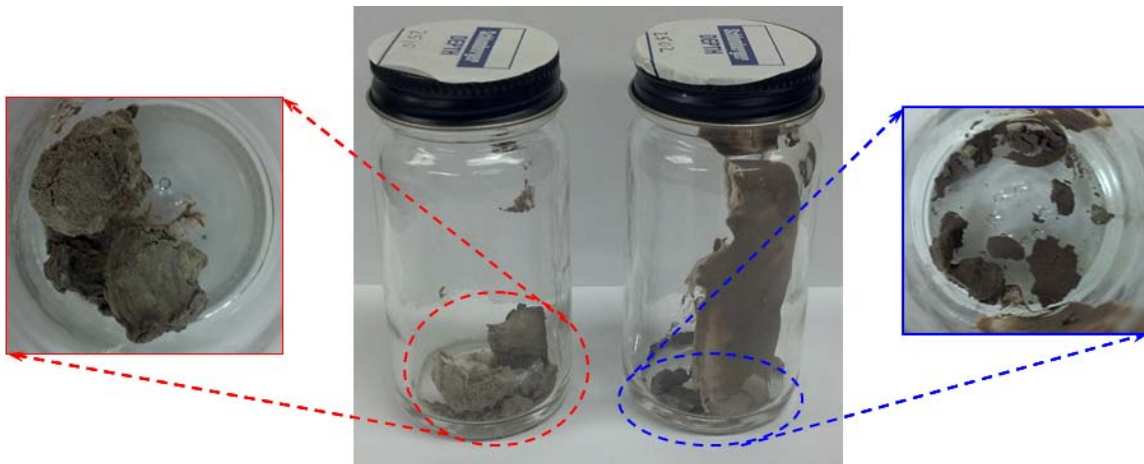


Figure A.3: Core Plugs from the Field (broken apart and muddy looking).

One relatively ‘cleaner’ sample was sent to Core Laboratories for mineralogy (XRD) analysis and the results are listed in Table A.4. About 15 grams of sample was sent out for the XRD work, and two independent runs were performed by Core Lab. The results are questionable from at least two aspects: 1) the inconsistency in quartz and clay

contents between the two runs; 2) the inconsistency between high content of smectite and the fact that the permeability is several hundred millidarcies with over 30% porosity. One possible explanation to these inconsistencies could be bentonite contamination which causes a high smectite (or bentonite) content. Due to the poor quality of these core plugs, coreflood experiments were only conducted with Berea sandstone cores, as will be discussed in later sections. It should be noted that the clay content in the field core sample is higher than in Berea.

Table A.4: X-Ray Diffraction Analysis of Core Sample at 2468' Depth (from CoreLab).

		Depth (ft)	
		2468'	2468' re-run
Bulk Mineralogy (%)	Quartz	81	91
	Plagioclase	4	3
	K-Feldspars	4	3
	Calcite	1	Trace
	Barite	1	Trace
	Pyrite	Trace (<0.5%)	Trace
	Total Clay	9	3
Clay Mineralogy (%)	Kaolinite	1	Trace
	Chlorite	Trace	Trace
	Illite	2	1
	MXL I/S*	6	2
	% Smectite in MXL I/S*	60-70	60-70

A.2 PHASE BEHAVIOR MEASUREMENTS

The methodology for using phase behavior and aqueous stability tests to find an optimum surfactant, co-solvent and alkali concentrations is described by many researchers (Levitt, 2006; Jackson, 2006; Flaaten, 2007; Sahni, 2009; Yang, 2010; Dean,

2011; Solairaj, 2011; Walker, 2011). This description explains how different formulations were evaluated, and how the best candidates were identified.

Formulations were given the name B-####, signifying Brookshire and the number of the experiment. Many different surfactants, co-surfactants, and co-solvents were used during the phase behavior evaluation phase. Propoxylate and ethoxylate are abbreviated PO and EO respectively. Internal olefin sulfonate is abbreviated IOS. Unless otherwise noted PO-sulfates and IOSs were Stepan branded surfactants.

Lot numbers of chemicals changed over time during these experiments. This led to certain phase behavior changes of formulations even though the same chemicals were used. For example, different TDA-9PO-SO₄ lots were delivered by Stepan and the phase behavior changed for various reasons including different tri-decyl alcohol feed stocks and different activities with varying amount of solvent in the delivered surfactant. This also happened many times with the C₁₅₋₁₈IOS manufactured by Stepan. It is, therefore, very important to keep track of different batches of chemicals used in every set of experiments.

After reviewing the background information on the reservoir and its fluid characteristics, the goal was to develop an inexpensive ASP formulation with suitable characteristics as discussed in detail below.

A.2.1 Initial Screening and Oil Activity (B-1 to B-16)

Because Brookshire reservoir is a light (to medium) oil reservoir, for the initial screening, Petrostep S1 (Neodol[®]C₁₆₋₁₇-7PO-SO₄) and similar molecules, e.g. Alfoterra L167-7S (C₁₆₋₁₇-7PO-SO₄) and Alfoterra L145-8S (C₁₄₋₁₅-8PO-SO₄) (Alfoterra surfactants from Sasol) were tried out as main surfactants with Petrostep S2 (C₁₅₋₁₈IOS) as the co-surfactant and IBA as the co-solvent. These surfactants have been shown in the

past to work with many light oil reservoirs. Both salinity and sodium carbonate (Na_2CO_3) scans were done on the above samples. However, the formulation with Alfoterra L167-7S formed high viscosity microemulsions. Also, some formulations had an aqueous stability limit lower than the optimum salinity. For most formulations, the optimum salinity (around 30,000 to 50,000ppm) was found to be much higher than that of SBB (7360ppm). The solubilization curves for one formulation with Alfoterra L167-7S are shown in Figure A.4.

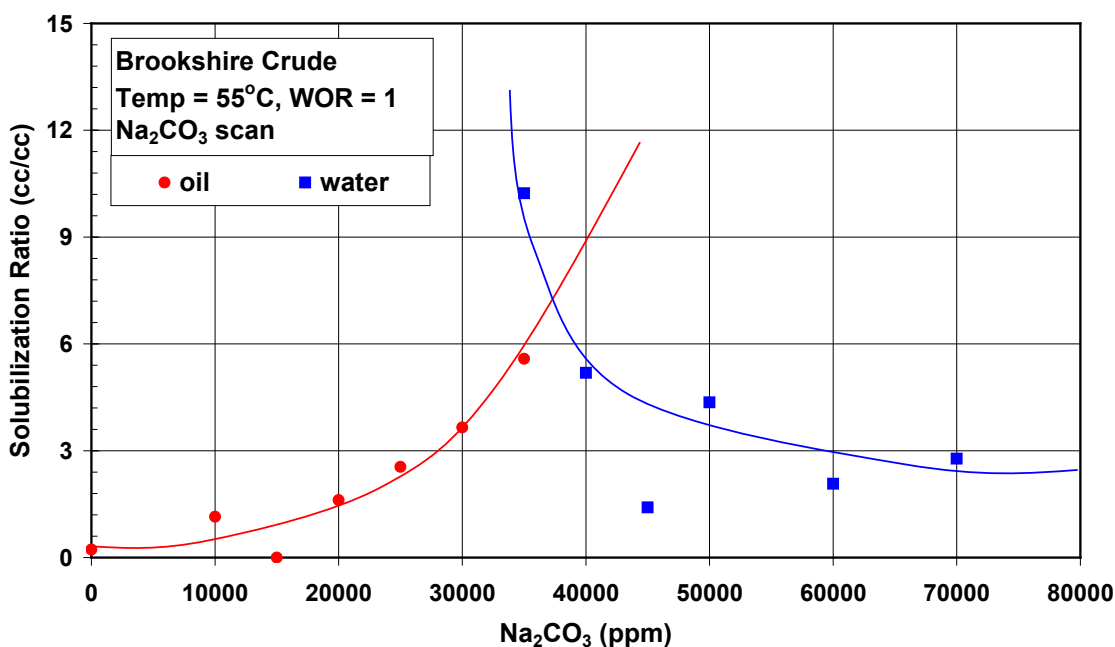


Figure A.4: B-3 Solubilization Plot after One Month Settling at WOR=1 (1.5wt% Alfoterra L167-7S + 0.5wt% Petrostep S-2 + 2wt% IBA).

It should be noted that phase behavior plots do not exist for many experiments due to an inability to read interfaces often attributed to undesirable long equilibration times. Sometimes, the chemical formulation was not a good fit for this oil and there was no solubilization, just a transition from Type I to Type II. Type I microemulsions are

formed when the surfactant is too hydrophilic whereas Type II microemulsions are formed when the a good bit of the oil is solubilized by the surfactant into a middle phase. When optimum salinities are mentioned without a phase behavior plot, the value came from qualitative observations of lowest interfacial tension when the fluids are mixed to form an emulsion in a pipette.

To check whether the oil was reactive or not, the above experiment using Alfoterra L167-7S and Petrostep S2 with 2% IBA as the co-solvent was repeated at a water oil ratio (WOR) of 4. The solubilization plot at this water oil ratio is shown in Figure A.5. It can be seen that the optimum salinity shifted lightly from 3.7wt% Na₂CO₃ to 4.2% Na₂CO₃ showing that the oil was reactive. Therefore, the addition of Na₂CO₃ should help promote soap generation and prevent surfactant adsorption.

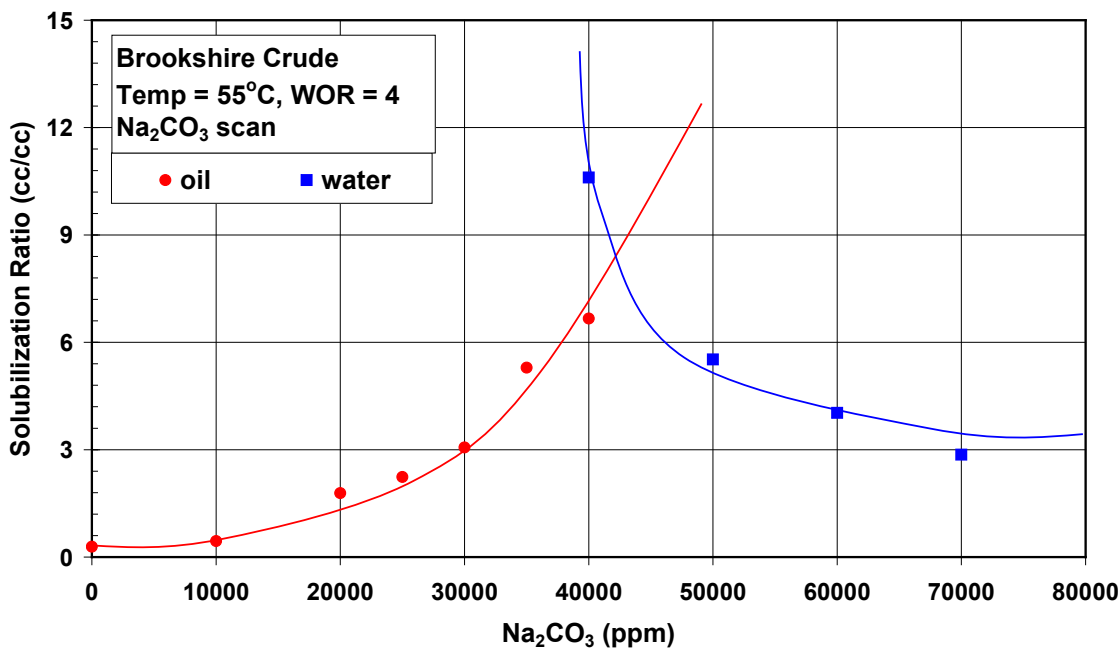


Figure A.5: B-4 Solubilization Plot after 20 Days Settling at WOR = 4(1.5 wt%Alfoterra L167-7S + 0.5 wt%Petrostep S-2 + 2wt% IBA).

A visual comparison of the phase behavior pipettes of a salinity (SBB) scan with those of a sodium carbonate (Na_2CO_3) scan illustrates the change in oil activity. Figure A.6 and Figure A.7 show such a comparison. The salinity scan in Figure A.6 shows only Type I microemulsion with a clear aqueous phase at the bottom. However, if Na_2CO_3 is used in the scan, the aqueous phase in all pipettes becomes the brownish messy-looking phase shown in Figure A.7. This appearance seems to be a direct result of soap generation and solubilization promoted by the alkali addition.

0.5% Petrostep S-1 + x% SBB (100% SBB = 7360 ppm)
@ WOR=1 and 1 week setting in oven at 55°C
x = 20 40 60 80 100 120 140 160 180 200



Figure A.6: B-11 Phase Behavior Pipettes after 1 Week Settling.

0.5% Petrostep S-1 + x wt% Na_2CO_3 (stable up to 1.6wt%)
@ WOR=1 and 1 week setting in oven at 55°C
x = 0.2 0.4 0.6 0.8 1.0 1.2 1.4 1.6 1.8 2.0



Figure A.7: B-12 Phase Behavior Pipettes after 1 Week Settling

Table A.5: Summary of Group 1 (Alcohol Ether Sulfates) Surfactant Screening.

Exp. No.	Surfactant		Co-surfactant		Co-solvent		Scan	WOR	Aqueous Limit	Optimum Salinity	Comment
	Name (Structure)	wt%	Name (Structure)	wt%	Name	wt%					
B-1	Petrostep S-1 (C16-17 7PO SO4)	1.50	Petrostep S-2 (C15-18 IOS)	0.50	IBA	2.0	SBB	1	all clear	4%	Type I→III→II
B-2	Alfoterra L67-7S (C16-17 7PO SO4)	1.50	Petrostep S-2 (C15-18 IOS)	0.50	IBA	2.0	SBB	1	all clear	3.85%	Type I→III→II
B-3							Na ₂ CO ₃	1	all clear	3.7%	Type I→III→II
B-4							Na ₂ CO ₃	4	all clear	4.2%	Type I→III→II
B-5	Petrostep S-1 (C16-17 7PO SO4)	0.50	---		IBA	0.0	SBB	1	all clear	---	Type I
B-6							Na ₂ CO ₃		all clear	---	Aqueous phase: messy & opaque; Oil phase: different from original
B-7	Petrostep S-1 (C16-17 7PO SO4)	0.50	---		IBA	1.0	SBB	1	all clear	---	Type I
B-8							Na ₂ CO ₃		all clear	---	Aqueous phase: messy & opaque; Oil phase: different from original
B-9	Petrostep S-1 (C16-17 7PO SO4)	0.50	---		IBA	2.0	SBB	1	all clear	---	Type I
B-10							Na ₂ CO ₃		all clear	---	Aqueous phase: messy & opaque; Oil phase: different from original
B-11	Alfoterra 145-8S (C14-15 8PO SO4)	0.50	---		IBA	0.0	SBB	1	all clear	---	Type I
B-12							Na ₂ CO ₃		1.6%	---	Aqueous phase: messy & opaque; Oil phase: different from original
B-13	Alfoterra 145-8S (C14-15 8PO SO4)	0.50	---		IBA	1.0	SBB	1	all clear	---	Type I
B-14							Na ₂ CO ₃		1.6%	---	Aqueous phase: messy & opaque; Oil phase: different from original
B-15	Alfoterra 145-8S (C14-15 8PO SO4)	0.50	---		IBA	2.0	SBB	1	all clear	---	Type I
B-16							Na ₂ CO ₃		1.6%	---	Aqueous phase: messy & opaque; Oil phase: different from original

A.2.2 Alkyl Benzene Sulfonate (ABS) Trials (B-17 to B-26)

The surfactant formulations tested above all rendered optimum salinities much higher than the formation brine and the solubilization ratios less than the target (at least 10). Therefore, in an effort to bring down the optimum salinity to within the range of the synthetic Brookshire brine (SBB), alkyl benzene/toluene sulfonates, which are known to give low optimal salinities, were tested. A series of experiments using different alkyl benzene/toluene sulfonates was conducted. Low concentrations of 0.2% surfactant were used and Neodol 25-12 (C₁₂₋₁₅-12EO) was used as the co-solvent (or non-ionic co-surfactant) in each case. The following surfactants were tried:

- ORS-41HF (Alkylaryl Sulfonate)
- Petrostep A-1 (C15-18 Branched Alkyl Benzene Sulfonate)
- Petrostep A-6 (C16-18 Branched Alkyl Xylene Sulfonate)
- Petrostep M-2 (C16-18 Branched Alkyl Benzene Sulfonate)
- ORS-47HF (C15.8 Alkyl Benzene Sulfonate)
- Shell C16 (C16 Xylene Sulfonate)

Some of these surfactants, are known for low aqueous solubilities. For instance, ORS-41HF (trade name ORS-## from Oil Chem Technology) was tested with 0.1, 0.2, 0.3 and 0.4wt% of Neodol 25-12 as the co-solvent and it was found to require at least 0.3wt% Neodol 25-12 for reasonable aqueous stability. All other surfactants were tried out with 0.2wt% co-solvent and were found to have reasonable aqueous stability limits as shown in Table A.6. However, the phase behavior experiments on the above formulations resulted in optimum salinities far below the TDS of SBB. In fact, all samples in the salinity range from 1300ppm TDS to 7360ppm TDS formed Type II systems.

Table A.6: Summary of Group 2 (ABS) Surfactant Screening.

Exp. No.	Surfactant		Co-solvent		Scan	WOR	Aqueous Limit	Optimum Salinity	Comment
	Name (Structure)	wt%	Name (Structure)	wt%					
B-17	Petrostep S-1 (C16-17 7PO SO4)	0.20	Neodol 25-12 (C12-15 12EO)	0.10	SBB	1	2680 ppm	---	Extremely low optimum salinity, all Type II
B-18	ORS-41HF (Alkylaryl Sulfonate)	0.20	Neodol 25-12 (C12-15 12EO)	0.10	SBB	1	<1340 ppm	---	
B-19	ORS-41HF (Alkylaryl Sulfonate)	0.20	Neodol 25-12 (C12-15 12EO)	0.20	SBB	1	1340 ppm	---	
B-20	ORS-41HF (Alkylaryl Sulfonate)	0.20	Neodol 25-12 (C12-15 12EO)	0.30	SBB	1	7360 ppm	---	
B-21	ORS-41HF (Alkylaryl Sulfonate)	0.20	Neodol 25-12 (C12-15 12EO)	0.40	SBB	1	7360 ppm	---	
B-22	ORS-41HF (Alkylaryl Sulfonate)	0.20	Neodol 25-12 (C12-15 12EO)	0.20	SBB	1	3680 ppm	---	
B-23	Petrostep A-6 (C16-18 BAXS)	0.20	Neodol 25-12 (C12-15 12EO)	0.20	SBB	1	3680 ppm	---	
B-24	Petrostep M-2 (C16-18 BABS)	0.20	Neodol 25-12 (C12-15 12EO)	0.20	SBB	1	5350 ppm	---	
B-25	ORS-47HF (C15.8 ABS)	0.20	Neodol 25-12 (C12-15 12EO)	0.20	SBB	1	7360 ppm	---	
B-26	Shell C16 (C16 AXS)	0.20	Neodol 25-12 (C12-15 12EO)	0.20	SBB	1	3345 ppm	---	

A.2.3 Surfactant Mixture and New Molecules (B-27 to B-40)

Two different approaches were then employed in order to obtain an intermediate to low optimum salinity: a) mixing Group 1 (alcohol ether sulfates) and Group 2 (ABS) surfactants to adjust the optimum condition; b) looking into other molecules that have easily tailored structures (by manipulating PON or alkyl chain length). Table A.7 summarizes these efforts.

Experiments B-27 to B-32 were trials using surfactant mixtures. Unfortunately, many of the test tubes did not even show any volume of middle phase so it was difficult to identify optimum salinities and quantify solubilization ratios. A C_{13} -13PO-SO₄ molecule was then tested for both SBB and Na₂CO₃ scans. With this surfactant, a large volume of middle phase microemulsion was observed within a short period of time and was fairly stable over time. The optimum salinity was relatively low compared to other systems tested before. The aqueous stability was marginally acceptable but could be further improved. Therefore, it was determined that Petrostep S8-D (and other structurally similar molecules) would be used as the primary surfactant and detailed formulation optimization should be planned and conducted accordingly. Figure A.8 and Figure A.9 below show the phase behavior pipettes of B-33 and B-34 after 3 weeks' settling in the oven. Notice in Figure A.9 (Na₂CO₃ scan) at 1.4wt%, almost all the original oil and water phases were solubilized into the huge middle phase, indicating an extremely high solubilization ratio and ultralow interfacial tension.

Table A.7: Summary of Group 3 (Surfactant Mixtures or New Molecules) Surfactant Screening.

Exp. No.	Surfactant		Co-surfactant		Co-solvent		Scan	WOR	Aqueous Limit	Optimum Salinity	Comment
	Name (Structure)	wt%	Name (Structure)	wt%	Name (Structure)	wt%					
B-27	Petrostep S-1 (C16-17 7PO SO4)	0.20	ORS-41HF (Alkylaryl Sulfonate)	0.20	Neodol 25-12 (C12-15 12EO)	0.20	SBB	1	all clear	---	Type I→II, very little middle phase
B-28	Alfoterra L67-7S (C16-17 7PO SO4)	0.20	ORS-41HF (Alkylaryl Sulfonate)	0.20	Neodol 25-12 (C12-15 12EO)	0.20	SBB	1	all clear	---	Type I→II, very little middle phase
B-29	Petrostep S-2 (C15-18 IOS)	0.20	ORS-41HF (Alkylaryl Sulfonate)	0.20	Neodol 25-12 (C12-15 12EO)	0.20	SBB	1	all clear	---	Type I→III→II
B-30	Petrostep S-1 (C16-17 7PO SO4)	0.30	Petrostep A-1 (C15-18 BABS)	0.10	IBA	0.00	SBB	1	1.84%	---	Type I→II, very little middle phase
B-31					IBA	1.00			2.21%	2.58%	Type I→III→II
B-32					IBA	2.00			---	2.58%	Type I→III→II
B-33	Petrostep S8-D (Sasol TDA 13PO SO4)	0.50	---		IBA	0.0	SBB	1	all clear	---	All Type I
B-34							Na ₂ CO ₃		1.40%	1.4%	Type I→III→II, $\sigma^* \sim 150$
B-35	Petrostep S8-D (Sasol TDA 13PO SO4)	0.50	---		IBA	1.0	SBB	1	all clear	---	All Type I
B-36							Na ₂ CO ₃		1.40%	1.4%	Type I→III, $\sigma^* \sim 150$
B-37	Petrostep S8-D (Sasol TDA 13PO SO4)	0.50	---		IBA	2.0	SBB	1	all clear	---	All Type I
B-38							Na ₂ CO ₃		1.20%	1.4%	Type I→III, $\sigma^* \sim 150$
B-39	Petrostep S3-A (C20-24 IOS Shell feedstock)	0.50	---		IBA	0.0	SBB	1	<3680 ppm	---	Type I→II
B-40									IBA	1.0	3680 ppm

0.5% Petrostep S8-D + x% SBB (100% SBB = 7360 ppm)
 @ WOR=1 and 3 week setting in oven at 55°C
 x = 20 40 60 80 100 120 140 160 180 200



Figure A.8: B-33 Phase Behavior Pipettes after 3 Weeks' Settling.

0.5% Petrostep S8-D + x wt% Na_2CO_3
 @ WOR=1 and 3 week setting in oven at 55°C
 x = 0.2 0.4 0.6 0.8 1.0 1.2 1.4 1.6 1.8 2.0



Figure A.9: B-34 Phase Behavior Pipettes after 3 Weeks' Settling.

A.2.4 Formulation Optimization (B-41 to B-91)

After identifying TDA (C13) PO sulfate as the primary surfactant, more tests were performed to determine relevant formulation parameters, including TDA feedstock selection (Sasol vs. Exxal), optimal HLB of the molecule (PO number adjustment), effective (and economic) surfactant concentration, co-solvent type and concentration, as well as impact of WOR (activity map). Table A.8 is a complete summary of aqueous stability and phase behavior tests conducted for formulation optimization.

Several general observations can be made from these fifty sets of experiments:

- Formulations with Petrostep S8-D as the primary surfactant take more time to reach equilibrium and often give rise to gel or macroemulsion formation;
- The Petrostep S13 surfactant series generally performs better than the Petrostep S8 series, in terms of faster equilibration and a more fluid interface. This is possibly due to different tridecyl alcohol feed stocks used to make the surfactants (Sasol vs. Exxal TDA);
- Within the aqueous stability limit, adding polymer into the aqueous phase does not change the phase behavior (optimum salinity and solubilization ratio);
- Phase behavior does not change much with surfactant concentration reduced to 0.2wt%, which is very beneficial in terms of project economics;
- At least 0.1wt% of Neodol 25-12 is needed in the formulation to achieve desirable aqueous stability; too much Neodol, on the other hand, causes optimum salinity to increase drastically. Co-solvent concentration should, therefore, be carefully controlled;
- Coexistence of divalent ions (Ca^{2+} , Mg^{2+}) with carbonate ions does not severely affect aqueous stability because of their low concentrations; the

stability is further secured when sufficient co-solvent is added; EDTA could be added to ensure a clear surfactant slug injection in the field;

- Oil concentration scans show that as WOR goes up, the optimum salinity increases and solubilization ratio in general decreases. The activity map (Figure A.20 and Figure A.21) shows a negative slope;
- Petrostep S13-B and S13-C perform comparably well at low concentration, with S13-C offering a lower optimum salinity and slightly higher solubilization ratio.

Based on the information collected, the proposed formulation for the coreflood experiment contains 0.3wt% Petrostep S13-C, 0.1wt% Neodol 25-12, and 1wt% Na_2CO_3 . Phase behavior pipettes and solubilization plots of several formulations tested in this section are shown in Figure A.10 to Figure A.19. A large volume of middle-phase microemulsion indicates good solubilization of oil and is an indication that the surfactant has the right degree of hydrophobicity.

Table A.8: Summary of Screening Experiments for Formulation Optimization.

Exp. No.	Surfactant		Co-solvent		Scan	WOR	Aqueous Limit	Optimum Salinity	Comment
	Name (Structure)	wt%	Name (Structure)	wt%					
B-41	Petrostep S8-D (Sasol TDA 13PO SO4)	0.50	Neodol 25-12 (C12-15 12EO)	1.0	SBB	1	all clear	---	All Type I
B-42					Na ₂ CO ₃	1	all clear	---	Na ₂ CO ₃ up to 2wt% Aqueous phase looks messy
B-43					Na ₂ CO ₃	1	all clear	3.6%	Na ₂ CO ₃ up to 4wt%; at 3.6% Type III observed; aqueous phase looks messy; $\sigma^* \sim 80$
B-44	Petrostep S8-B (Sasol TDA 7PO SO4)	0.5	Neodol 25-12 (C12-15 12EO)	1.0	SBB	1	all clear	---	All Type I
B-45					Na ₂ CO ₃	1	all clear	> 4.0%	Na ₂ CO ₃ up to 4wt%; at 4.0% Type III observed; aqueous phase looks messy; $\sigma^* \sim 80$
B-46	Petrostep S8-D (Sasol TDA 13PO SO4)	0.50	---		Na ₂ CO ₃	4	all clear	1.1%	Na ₂ CO ₃ up to 4wt% in 100% SBB; at 0.8% Type III observed; $\sigma^* \sim 80$
B-47						1	all clear	0.9%	Na ₂ CO ₃ up to 4wt% in 100% SBB; at 0.8% Type III observed; $\sigma^* \sim 30$
B-48	Petrostep S8-D (Sasol TDA 13PO SO4)	1.00	Neodol 25-12 (C12-15 12EO)	1.0	Na ₂ CO ₃	4	all clear	3.8%	Na ₂ CO ₃ up to 4wt% in 100% SBB; at 3.6% Type III observed; $\sigma^* \sim 30$
B-49						1	all clear	3.6%	Na ₂ CO ₃ up to 4wt% in 100% SBB; at 2.8% Type III observed; $\sigma^* \sim 110$
B-50	Petrostep S8-D (Sasol TDA 13PO SO4)	0.50	IBA	1.0	Na ₂ CO ₃	4	all clear	0.8%	Na ₂ CO ₃ up to 4wt% in 100% SBB; at 0.8% Type III observed; $\sigma^* \sim 40$
B-51						1	all clear	---	Na ₂ CO ₃ up to 4wt% in 100% SBB; at 1.2% Type III observed

Table A.8: Summary of Screening Experiments for Formulation Optimization (Cont.).

Exp. No.	Surfactant		Co-solvent		Scan	WOR	Aqueous Limit	Optimum Salinity	Comment	
	Name (Structure)	wt%	Name (Structure)	wt%						
B-52	Petrostep S8-D (Sasol TDA 13PO SO4)	0.50	Neodol 25-12 (C12-15 12EO)	1.0	Na ₂ CO ₃	4	all clear	---	Na ₂ CO ₃ up to 4wt% in 100% SBB; aqueous phase looks messy	
B-53						1		3.0%	Na ₂ CO ₃ up to 4wt% in 100% SBB; at 2.8% Type III observed; $\sigma^* \sim 70$	
B-54	Petrostep S8-D (Sasol TDA 13PO SO4)	0.50	---	---	SBB	4	---	---	Up to 500% SBB in 1% Na ₂ CO ₃ ; at 100% SBB Type III observed	
B-55						1		---	Up to 500% SBB in 1% Na ₂ CO ₃ ; at 100% SBB Type III observed	
B-56	Petrostep S8-D (Sasol TDA 13PO SO4)	1.00	---	---	SBB	4	---	---	Up to 500% SBB in 1.4% Na ₂ CO ₃ ; at 50% SBB Type III observed	
B-57						1		---	Up to 500% SBB in 1.4% Na ₂ CO ₃	
B-58	Petrostep S8-D (Sasol TDA 13PO SO4)	0.50	IBA	1.0	SBB	4	all clear	---	Up to 500% SBB in 1% Na ₂ CO ₃ ; at 100% SBB Type III observed	
B-59						1		---	Up to 500% SBB in 1% Na ₂ CO ₃ at 50% SBB Type III observed	
B-60	Petrostep S8-D (Sasol TDA 13PO SO4)	0.50	Neodol 25-12 (C12-15 12EO)	1.0	SBB	4	all clear	---	Up to 500% SBB in 1% Na ₂ CO ₃ ; aqueous phase looks messy	
B-61						1		3.18%	Up to 500% SBB in 1% Na ₂ CO ₃ ; at 400% SBB Type III observed; $\sigma^* \sim 90$	
B-62	Petrostep S8-D (Sasol TDA 13PO SO4)	0.50	Neodol 25-12 (C12-15 12EO)	0.20	Na ₂ CO ₃	1	1.5%	---	Na ₂ CO ₃ up to 5wt%	
B-63		0.30								2.0%
B-64		0.20								2.5%

Table A.8: Summary of Screening Experiments for Formulation Optimization (Cont.).

Exp. No.	Surfactant		Co-solvent		Scan	WOR	Aqueous Limit	Optimum Salinity	Comment
	Name (Structure)	wt%	Name (Structure)	wt%					
B-65	Petrostep S13-B (Exxal TDA 7PO SO4)	0.50	Neodol 25-12 (C12-15 12EO)	0.20	Na ₂ CO ₃	1	2.5%	2.5%	Na ₂ CO ₃ up to 5wt%; $\sigma^* \sim 70$
B-66						1.5	3.0%	2.65	Na ₂ CO ₃ up to 5wt%; $\sigma^* \sim 105$
B-67						2.33	3.0%	3.5%	Na ₂ CO ₃ up to 5wt%; $\sigma^* \sim 47$
B-68						4	3.5%	4.45%	Na ₂ CO ₃ up to 5wt%; $\sigma^* \sim 28$
B-69						9	4.0%	> 5%	Na ₂ CO ₃ up to 5wt%
B-70	Petrostep S13-B (Exxal TDA 7PO SO4)	0.50	Neodol 25-12 (C12-15 12EO)	0.20	Na ₂ CO ₃	4	3.0%	4.45%	With polymer added; up to 5% Na ₂ CO ₃ ; $\sigma^* \sim 28$
B-71						1		2.1%	With polymer added; up to 5% Na ₂ CO ₃ ; $\sigma^* \sim 66$
B-72	Petrostep S13-B (Exxal TDA 7PO SO4)	0.30	Neodol 25-12 (C12-15 12EO)	0.20	Na ₂ CO ₃	1	---	---	Na ₂ CO ₃ up to 5wt%; gel formation
B-73		0.20						1.85%	Na ₂ CO ₃ up to 5wt%; $\sigma^* \sim 85$
B-74	Petrostep S13-C (Exxal TDA 9PO SO4)	0.50	Neodol 25-12 (C12-15 12EO)	0.20	Na ₂ CO ₃	1	3.0%	2.0%	Na ₂ CO ₃ up to 5wt%; $\sigma^* \sim 135$
B-75		0.30					3.5%	1.95%	Na ₂ CO ₃ up to 5wt%; $\sigma^* \sim 92$
B-76		0.20					3.5%	---	Na ₂ CO ₃ up to 5wt%

Table A.8: Summary of Screening Experiments for Formulation Optimization (Cont.).

Exp. No.	Surfactant		Co-solvent		Scan	WOR	Aqueous Limit	Optimum Salinity	Comment
	Name (Structure)	wt%	Name (Structure)	wt%					
B-77	Petrostep S13-C (Exxal TDA 9PO SO4)	0.50	Neodol 25-12 (C12-15 12EO)	0.20	Na ₂ CO ₃	1.5	2.5%	2.3%	Na ₂ CO ₃ up to 5wt%; $\sigma^* \sim 125$
B-78						2.33	2.8%	2.6%	Na ₂ CO ₃ up to 5wt%; $\sigma^* \sim 85$
B-79						4	3.0%	3.5%	Na ₂ CO ₃ up to 5wt%; $\sigma^* \sim 180$
B-80						9	3.0%	4.6%	Na ₂ CO ₃ up to 5wt%; $\sigma^* \sim 70$
B-81	Petrostep S13-B (Exxal TDA 7PO SO4)	0.30	Neodol 25-12 (C12-15 12EO)	0.10	Na ₂ CO ₃	1	3.0%	2%	Na ₂ CO ₃ up to 5wt%; $\sigma^* \sim 145$
B-82	Petrostep S13-C (Exxal TDA 9PO SO4)	0.30	Neodol 25-12 (C12-15 12EO)	0.10	Na ₂ CO ₃	1	3.0%	2%	Na ₂ CO ₃ up to 5wt%; $\sigma^* \sim 150$
B-83	Petrostep S13-B (Exxal TDA 7PO SO4)	0.25	Neodol 25-12 (C12-15 12EO)	0.20	Na ₂ CO ₃	1	2.8%	2.7%	Na ₂ CO ₃ up to 5wt%; $\sigma^* \sim 75$
	Petrostep S13-C (Exxal TDA 9PO SO4)	0.25							
B-84	Petrostep S13-B (Exxal TDA 7PO SO4)	0.10	Neodol 25-12 (C12-15 12EO)	0.10	Na ₂ CO ₃	1	3.0%	1.38%	Na ₂ CO ₃ up to 5wt%; $\sigma^* \sim 380$
	Petrostep S13-C (Exxal TDA 9PO SO4)	0.10							

Table A.8: Summary of Screening Experiments for Formulation Optimization (Cont.).

Exp. No.	Surfactant		Co-solvent		Scan	WOR	Aqueous Limit	Optimum Salinity	Comment
	Name (Structure)	wt%	Name (Structure)	wt%					
B-85	Petrostep S13-B (Exxal TDA 7PO SO4)	0.15	Neodol 25-12 (C12-15 12EO)	0.10	Na ₂ CO ₃	1	3.0%	1.9%	Na ₂ CO ₃ up to 5wt%; $\sigma^* \sim 100$
	Petrostep S13-C (Exxal TDA 9PO SO4)	0.15							
B-86	Petrostep S13-B (Exxal TDA 7PO SO4)	0.15	Neodol 25-12 (C12-15 12EO)	0.20	Na ₂ CO ₃	1	3.5%	2.0%	Na ₂ CO ₃ up to 5wt%; $\sigma^* \sim 230$
	Petrostep S13-C (Exxal TDA 9PO SO4)	0.15							
B-87	Petrostep S13-B (Exxal TDA 7PO SO4)	0.10	Neodol 25-12 (C12-15 12EO)	0.10	Na ₂ CO ₃	1	3.5%	0.9%	Na ₂ CO ₃ up to 4wt% in 100% SBB; $\sigma^* \sim 380$
	Petrostep S13-C (Exxal TDA 9PO SO4)	0.10							
B-88	Petrostep S13-B (Exxal TDA 7PO SO4)	0.15	Neodol 25-12 (C12-15 12EO)	0.10	Na ₂ CO ₃	1	3.5%	0.75%	Na ₂ CO ₃ up to 4wt% in 100% SBB; $\sigma^* \sim 210$
	Petrostep S13-C (Exxal TDA 9PO SO4)	0.15							
B-89	Petrostep S13-B (Exxal TDA 7PO SO4)	0.15	Neodol 25-12 (C12-15 12EO)	0.20	Na ₂ CO ₃	1	3.0%	1.2%	Na ₂ CO ₃ up to 4wt% in 100% SBB; $\sigma^* \sim 210$
	Petrostep S13-C (Exxal TDA 9PO SO4)	0.15							

Table A.8: Summary of Screening Experiments for Formulation Optimization (Cont.).

Exp. No.	Surfactant		Co-solvent		Scan	WOR	Aqueous Limit	Optimum Salinity	Comment
	Name (Structure)	wt%	Name (Structure)	wt%					
B-90	Petrostep S13-B (Exxal TDA 7PO SO4)	0.30	Neodol 25-12 (C12-15 12EO)	0.10	Na ₂ CO ₃	1	3.0%	1.3%	Na ₂ CO ₃ up to 4wt% in 100% SBB; σ*~95
B-91	Petrostep S13-C (Exxal TDA 9PO SO4)	0.30	Neodol 25-12 (C12-15 12EO)	0.10	Na ₂ CO ₃	1	3.0%	1.0%	Na ₂ CO ₃ up to 4wt% in 100% SBB; σ*~220

0.5% Petrostep S13-B + 0.2% Neodol 25-12 + x wt% Na₂CO₃
 @ WOR=1 and 2 week setting in oven at 55°C
 x = 0.5 1.0 1.5 2.0 2.5 3.0 3.5 4.0 4.5 5.0

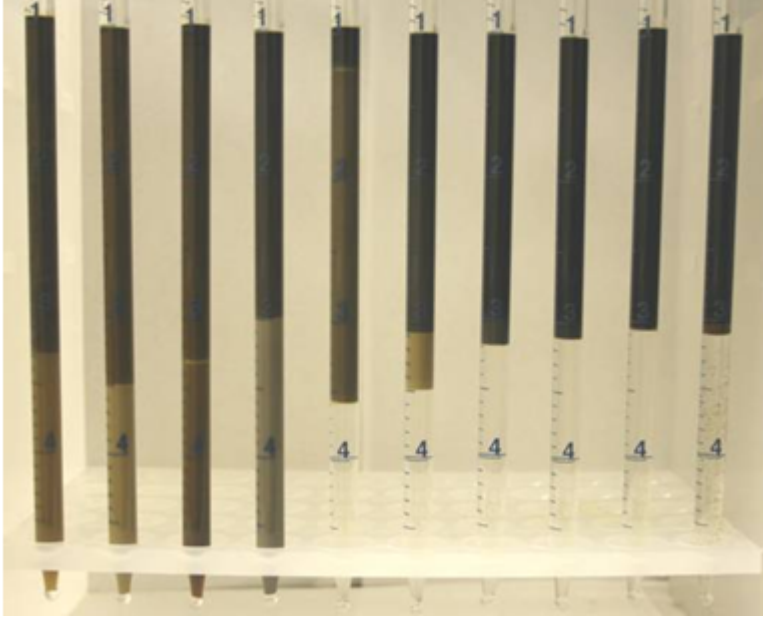


Figure A.10: B-65 Phase Behavior Pipettes after 2 Weeks' Settling.

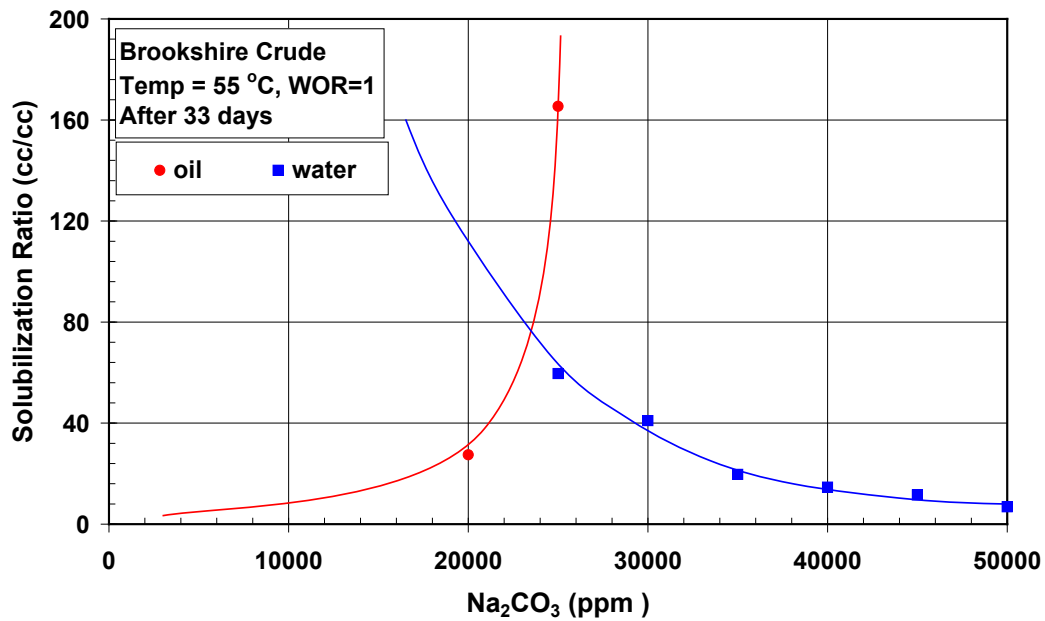


Figure A.11: B-65 Solubilization Plot after 33 Days Settling at WOR = 1 (0.5 wt% Petrostep S13-B + 0.2 wt% Neodol 25-12).

0.5% Petrostep S13-B + 0.2% Neodol 25-12 + x wt% Na₂CO₃
 @ WOR=2.33 and 2 week setting in oven at 55°C

x = 0.5 1.0 1.5 2.0 2.5 3.0 3.5 4.0 4.5 5.0

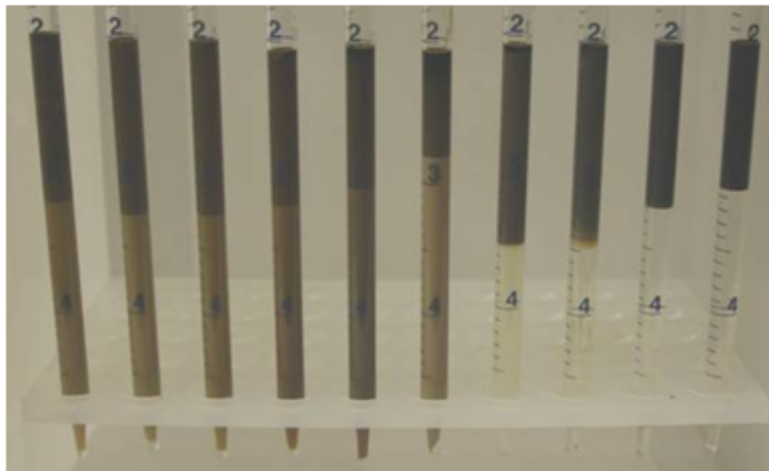


Figure A.12: B-67 Phase Behavior Pipettes after 2 Weeks' Settling.

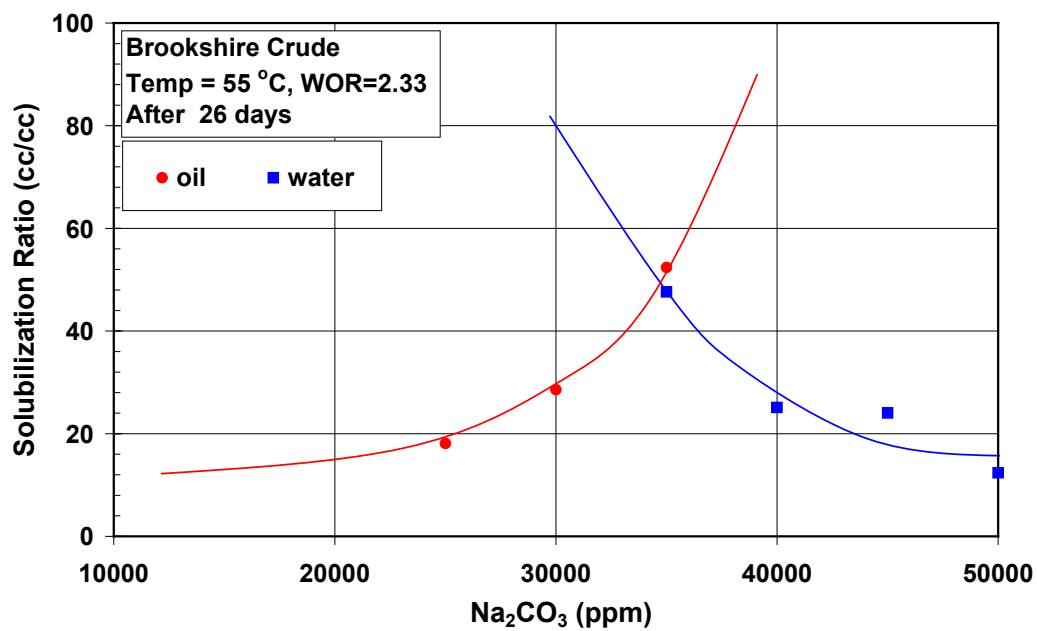


Figure A.13: B-67 Solubilization Plot after 26 Days Settling at WOR = 2.33 (0.5 wt% Petrostep S13-B + 0.2 wt% Neodol 25-12).

0.2% Petrostep S13-B + 0.2% Neodol 25-12 + x wt% Na₂CO₃
 @ WOR=1 and 2 week setting in oven at 55°C

x = 0.5 1.0 1.5 2.0 2.5 3.0 3.5 4.0 4.5 5.0

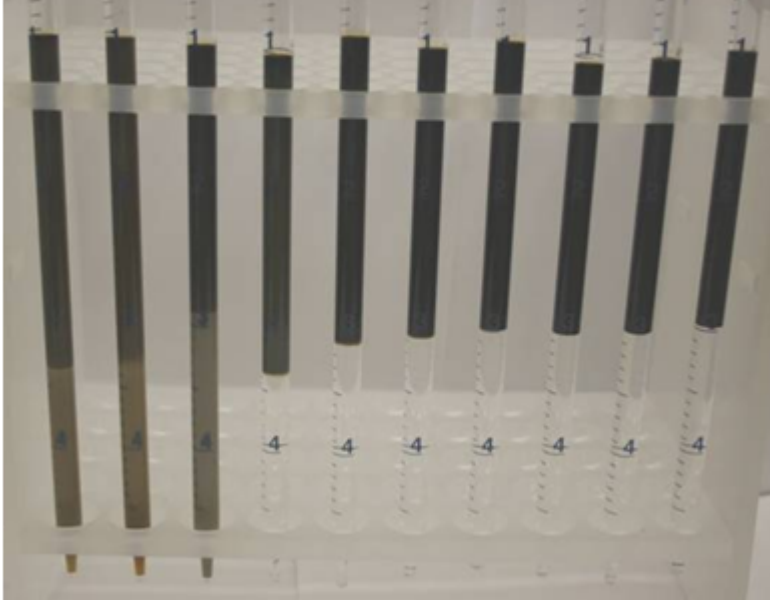


Figure A.14: B-73 Phase Behavior Pipettes after 2 Weeks' Settling.

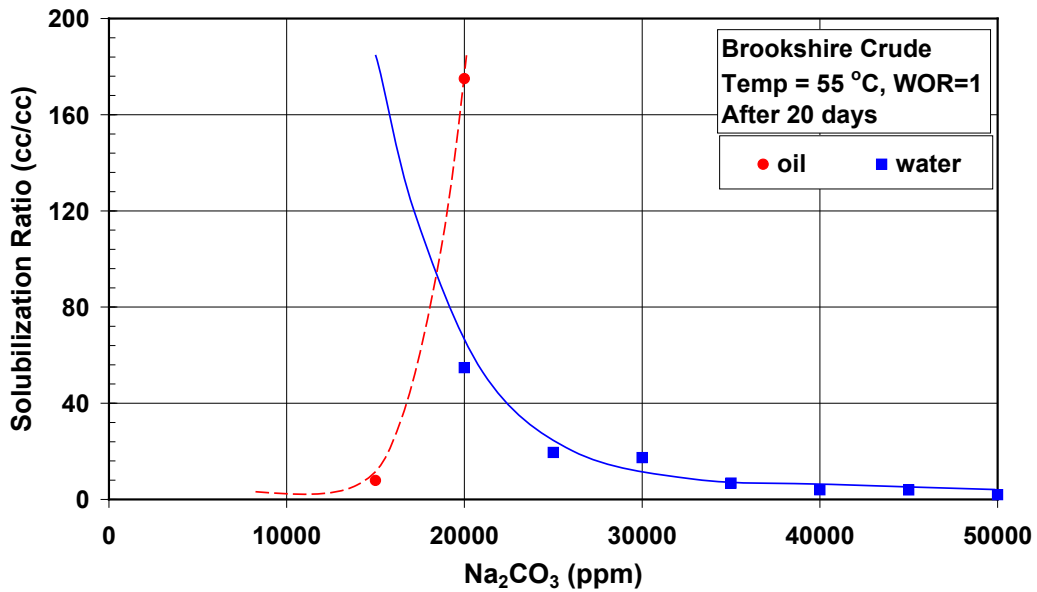


Figure A.15: B-73 Solubilization Plot after 20 Days Settling at WOR = 1 (0.2 wt% Petrostep S13-B + 0.2 wt% Neodol 25-12).

0.5% Petrostep S13-C + 0.2% Neodol 25-12 + x wt% Na_2CO_3
 @ WOR=1 and 3 week setting in oven at 55°C

x = 0.5 1.0 1.5 2.0 2.5 3.0 3.5 4.0 4.5 5.0

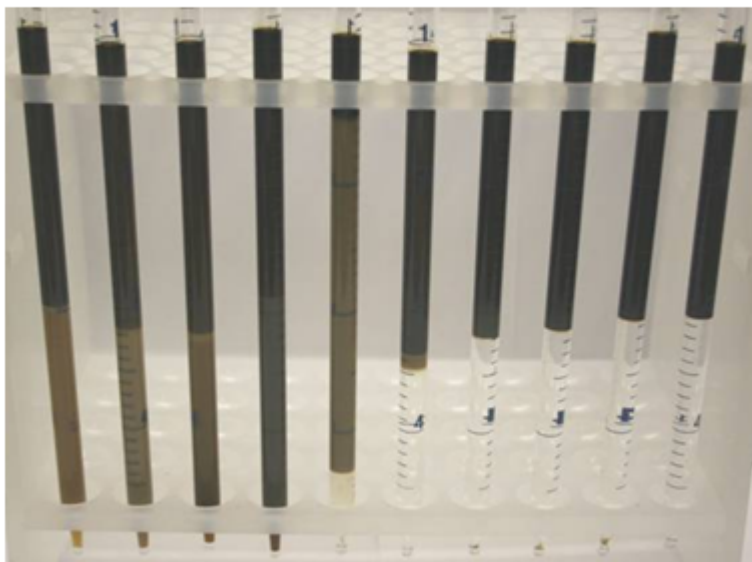


Figure A.16: B-74 Phase Behavior Pipettes after 3 Weeks' Settling.

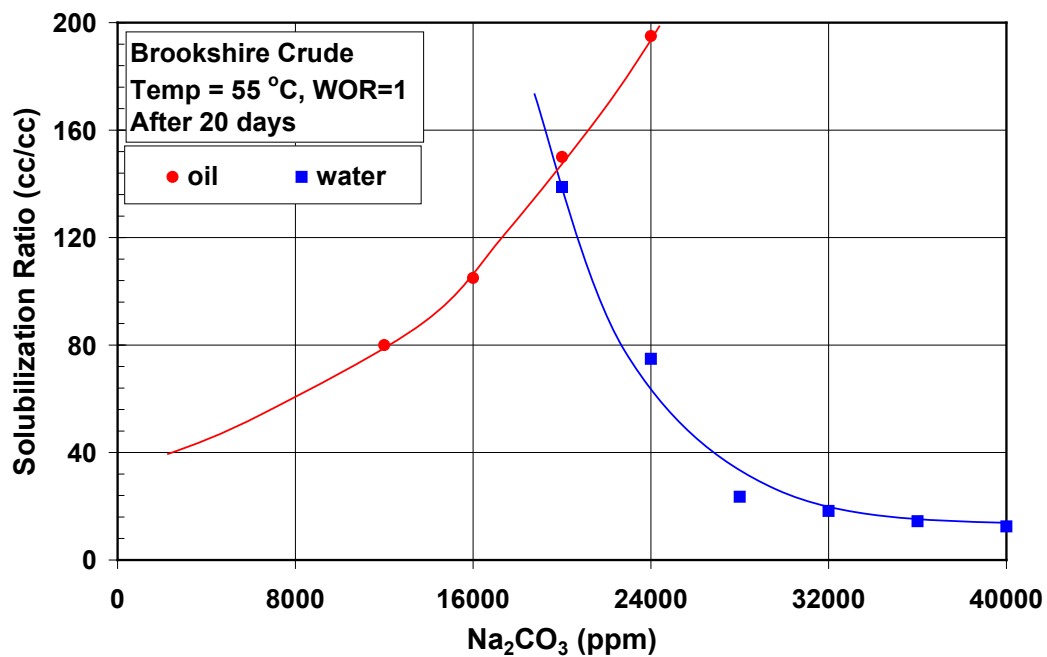


Figure A.17: B-74 Solubilization Plot after 20 Days Settling at WOR = 1 (0.5 wt% Petrostep S13-C + 0.2 wt% Neodol 25-12).

0.3% Petrostep S13-C + 0.1% Neodol 25-12
 in 100% SBB + x wt% Na₂CO₃
 @ WOR=1 and 3 week setting in oven at 55°C
 x = 0.4 0.8 1.2 1.6 2.0 2.4 2.8 3.2 3.6 4.0

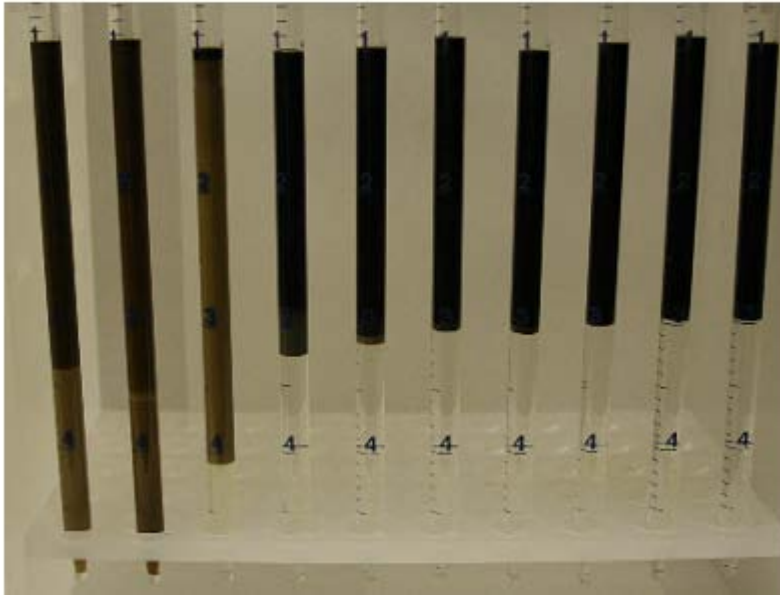


Figure A.18: B-91 Phase Behavior Pipettes after 3 Weeks' Settling.

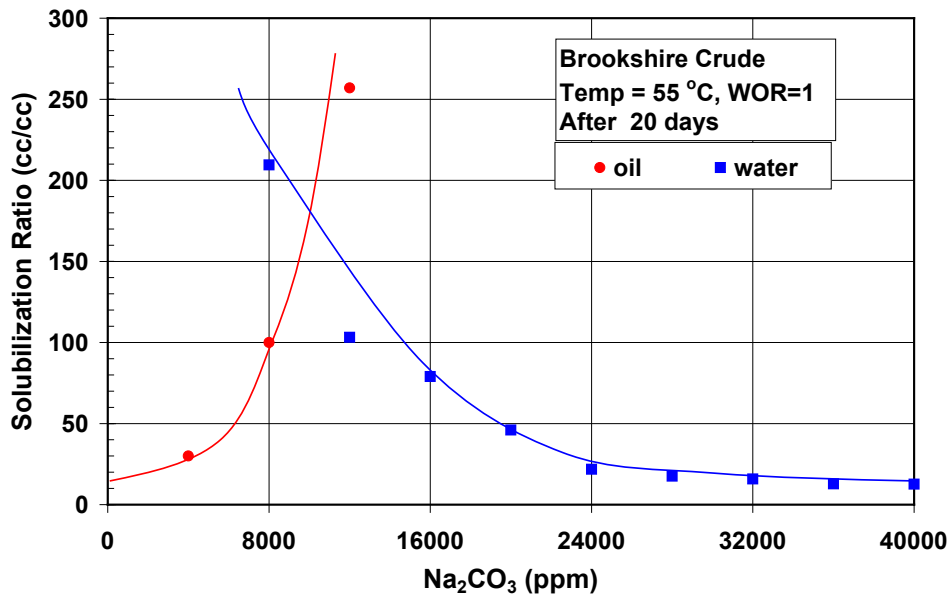


Figure A.19: B-91 Solubilization Plot after 20 Days Settling at WOR = 1 (0.3wt% Petrostep S13-C + 0.1 wt% Neodol 25-12).

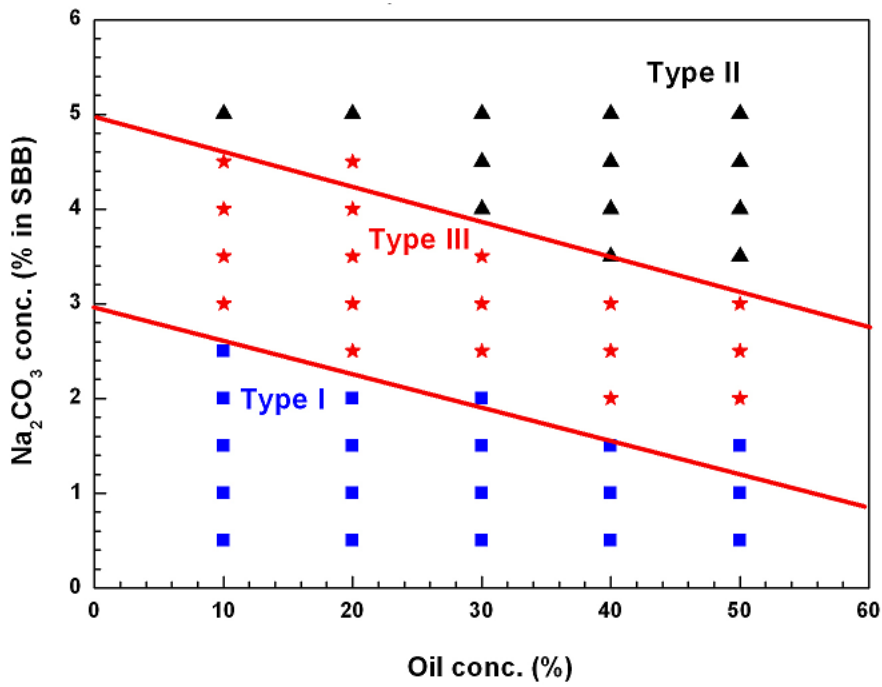


Figure A.20: Activity Map for 0.3wt% Petrostep S13-B + 0.1 wt% Neodol 25-12.

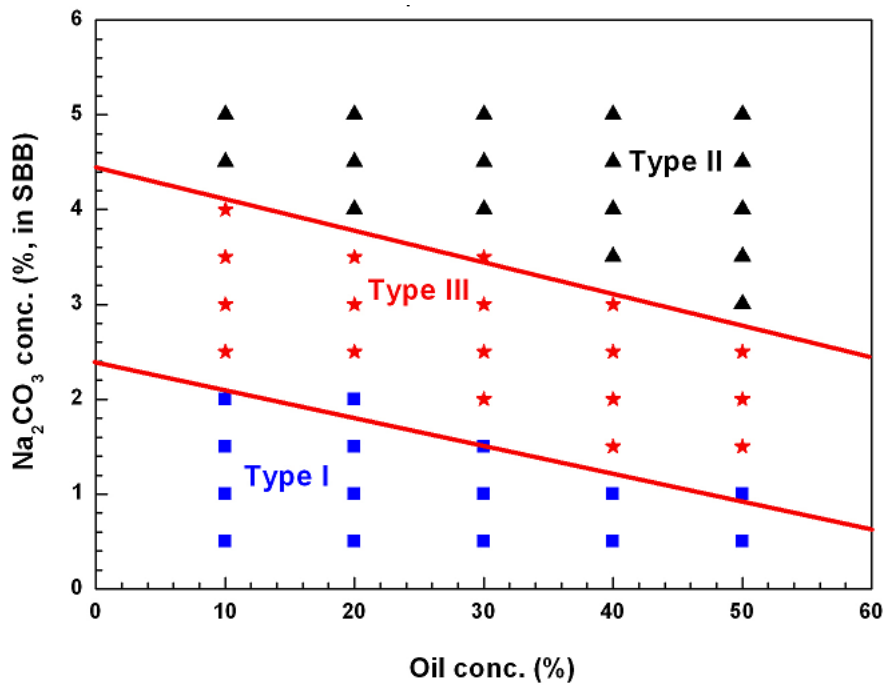


Figure A.21: Activity Map for 0.3wt% Petrostep S13-C + 0.1 wt% Neodol 25-12.

A.3 COREFLOOD EXPERIMENTS

Coreflood experiments are conducted to test the performance of the optimal formulation in an idealized laboratory setting. Coreflooding procedures are well documented in many theses and papers published earlier (Levitt *et al.*, 2006 & 2009; Jackson *et al.*, 2006; Flaaten *et al.*, 2007 & 2008; Zhao *et al.*, 2008; Yang *et al.*, 2010; Dean, 2011; Solairaj, 2011; Walker, 2011).

A.3.1 Experimental Equipment

The experimental setup was built upon an existing system designed by Dr. Choi in his study of polymer transport properties (Choi, 2008). A LC-5000 syringe pump (ISCO Inc.) was used to inject the fluids at a constant rate. The pump was filled with mineral oil to displace the fluid in the columns into core. It can pump in the range between 0 to 400ml/hr, with maximum 500ml storage capacity. A Hassler-type steel core holder was chosen to safely operate at high pressure. A glass column was used for aqueous fluid (brine, surfactant slug or polymer drive) injection under lower pressure. A high pressure steel column was used for the oil flood experiment. The pressure drops for different sections across the core are measured by pressure transducers (Model DP15-30, Validyne Engineering Corp.) In order to confirm the proper operation of pressure transducers, the pressure drop across the entire core was also measured and compared with the sum of three pressure drops. The effluents from the core were collected at regular intervals with a fraction collector (Retriever II, ISCO Inc.). The signals from the pressure transducers were collected and transformed by a data collector (Model MCI-20, Validyne Engineering Corp.) and the data were displayed in real time using LabVIEW 8.0 (National Instruments). Heating tape with a temperature controller (Thermo Scientific) was used together with fiberglass cloth insulation to provide the desired experimental core flood temperature.

A.3.2 Coreflood Description

The coreflood procedure includes a method of core preparation and assembly, brine flooding, oil flooding, water flooding and chemical flooding, collecting and analyzing the effluent samples. This section describes the flooding procedure.

Brine Flood

After finishing core preparation and assembly, the core was vacuum saturated and flushed with synthetic formation brine. The objective of this brine flooding was to determine the absolute brine permeability. Several pore volumes of formation brine were injected at a flow rate 2-4ml/min into the core until pressure stabilized. The pressure drop was recorded to determine the average absolute brine permeability of the core.

Oil Flood

After brine flooding, oil flooding was conducted at high injection pressure and at reservoir temperature. The main purpose of the oil flooding was to determine initial oil saturation, residual water saturation, effective oil permeability, and the relative oil permeability. Prior to oil flooding, the crude was filtered by a 0.45 μ m filter paper at reservoir temperature. Oil flooding was conducted under a constant pressure to saturate the pore volume with oil and obtain accurate residual water saturation. Approximately, 1.5PV of oil was injected. The effluent fluids were collected in 100ml burettes and the volume of displaced water was the volume of saturated oil inside the core. Oil flooding was continued until the water cut was less than 1% and pressure stabilized.

Water Flood

Oil flooding was followed by water flooding with filtered synthetic injection brine. Water flooding was conducted in order to determine the residual oil saturation, effective water permeability, and relative water permeability. Approximately 1.5PV of

synthetic brine was injected into the core at low constant flow rate (0.4-0.5 ml/min) to achieve residual oil saturation after water flooding. The effluent fluids were collected in a burette and water flooding was stopped when the oil cut was less than 1% and pressure stabilized.

Chemical Flood

A chemical (ASP) slug was injected after water flooding in order to check the performance of the formulation by measuring the incremental recovery of residual oil in the core (tertiary recovery). Typically, 0.3-0.5PV of ASP slug was injected into the core at reservoir temperature and followed by approximately 1.5-2.0PV polymer drive. Chemical flooding was performed at a constant flow rate of about 1-2ft/day and the flooding was performed until no more emulsion was produced. The effluent fluids were collected by a fraction collector for estimating the oil-water ratio and for further analyses. Oil recovery and residual oil saturation were determined after chemical flooding by material balance and measuring volumes of oil produced.

A.3.3 Quality and Mobility Control for Polymer

For a study of this type, steps should be taken to ensure that no problems arise because of polymer use. High quality, properly hydrated polymer must be used. All polymer solutions should have their filtration ratio measured. For this experiment, the filtration ratio was measured at 15psi using a 1.2 μ m filter paper. The filtration ratio checks to ensure that the last volumes of polymer flow out at the same rate as the volumes of polymer near the beginning of the test. It is therefore a measure of the plugging occurring during polymer flow. The filtration ratio is expressed as,

$$F.R. = \frac{t_{200ml} - t_{180ml}}{t_{80ml} - t_{60ml}} \quad (A.1)$$

This check ensures that no large, contaminated, or improperly mixed polymer is filtering out causing the polymer flow rate to decrease with time as a polymer filter cake builds up on the filter paper. The quality control cut-off is a filtration ratio of 1.2. Any polymer sample with a filtration ratio above 1.2 is not used for coreflooding.

Proper mobility control must be achieved with the correct concentration of polymer. This is done following these steps:

- 1). In order to select the correct concentration, the inverse of the estimated maximum oil bank mobility (i.e. necessary slug viscosity) is calculated using Corey exponents of 2, water and oil viscosities, and water and oil endpoint relative permeabilities. Notice that this estimation is on the more conservative side. A more aggressive approach is to use an estimated oil bank saturation to evaluate the required apparent slug viscosity. Polymer drive viscosity should be higher or equal to surfactant slug viscosity to prevent viscous fingering.

$$\mu_{app} = \frac{1}{\lambda_t} = \frac{1}{\left(\frac{k_w}{\mu_w} + \frac{k_o}{\mu_o} \right)} \quad (\text{A.2})$$

- 2). An existing polymer database can be used to give a close estimation of the range of polymer concentration necessary with a given salinity and hardness at a given temperature. The desired viscosity is achieved typically at a target shear rate of 10s^{-1} , due to flooding rates and common ranges of permeabilities.
- 3). Several samples are made over a range of polymer concentration close to the estimated value. The samples must have the correct salinity hardness, and they should also contain all chemicals when designing the slug. Viscosities (from a rheometer) at 10s^{-1} can be plotted as a function of polymer concentration. The

polymer concentration can then be selected from a fitted curve and used when mixing the slug.

A.3.4 Brookshire Coreflood GB-2

The surfactant formulation (0.3wt% Petrostep S13-C, 0.1wt% Neodol 25-12, and 1wt% Na₂CO₃ in 100% SBB) was tested in a sandstone coreflood experiment at reservoir temperature to verify that it is effective at recovering residual oil. The standard laboratory protocol is to test a new chemical formulation in an outcrop rock such as Berea sandstone before testing it in the reservoir rock. Berea sandstone cores are often employed in experiments because of their consistent properties, and also because of the fact that many surfactant floods have been done using Berea that serve as a useful benchmark.

GB-2 Core Data

A Berea sandstone core was weighed and its dimensions (length and diameter) were measured. The closed system for the core holder was prepared by shutting off the valves and pulling a vacuum overnight. The core was then saturated with pure CO₂ gas, twice at 30 minute intervals, at the beginning of vacuum evacuation to effectively eliminate any air trapped in the pores of the core. The core was then saturated by imbibing 0.45µm filtered SBB. The pore volume was calculated by subtracting the dead volume of the closed system (the amount of brine saturated in unnecessary parts, such as valves or lines) from the total amount of imbibed brine. The porosity is given by,

$$\phi = \frac{V_p}{V_b} = \frac{\Delta V - V_{dead}}{\pi d^2 L / 4} \quad (\text{A.3})$$

The core properties of the GB-2 coreflood experiment are shown below in Table A.9. The permeability values are listed in Table A.10. These values are calculated from

pressure data and flow rates after flooding experiments. The flooding experiments consisted of brine flooding, oil flooding, water flooding, chemical flooding, and finally followed by polymer flooding. Then the oil permeability and relative oil permeability, 437md and 0.89 respectively, are acquired after the oil flood at the residual water saturation. Initial oil saturation of 0.64 is calculated using the volume of oil from the core. After water flooding with synthetic brine, a water permeability of 58.4md and a relative water permeability of 0.119 and residual oil saturation of 0.314 were measured. Oil saturation data for the GB-2 core are shown in Table A.11.

Table A.9: Berea Core Properties for Coreflood GB-2.

Core	GB-2
Source	Berea Sandstone
Mass (g)	310.6
Porosity	0.2014
Length (cm)	29.067
Diameter (cm)	2.54
Area (cm ²)	5.067
Temperature (°C)	55
Pore Volume (ml)	29.66

Table A.10: Permeability and Relative Permeability Values of Berea Core GB-2.

Absolute Brine Permeability, k_{brine} (md)	491
Oil Permeability, k_{oil} (md)	437
Water Permeability, k_{water} (md)	58.4
Relative Oil Permeability, k_{ro}° (end point)	0.89
Relative Water Permeability, k_{rw}° (end point)	0.119

Table A.11: Saturation Data for Berea Core GB-2.

Initial Oil Saturation, S_{oi}	0.64
Residual Water Saturation, S_{wr}	0.36

GB-2 Brine Flood

Initially GB-2 core was saturated with SBB and then flooded with SBB to measure the brine permeability. The composition of SBB was described in previous sections. The brine flood was done at a rate of 2.64ml/min and the pressure data measured is shown in Figure A.22. The measured absolute permeability is again 491md.

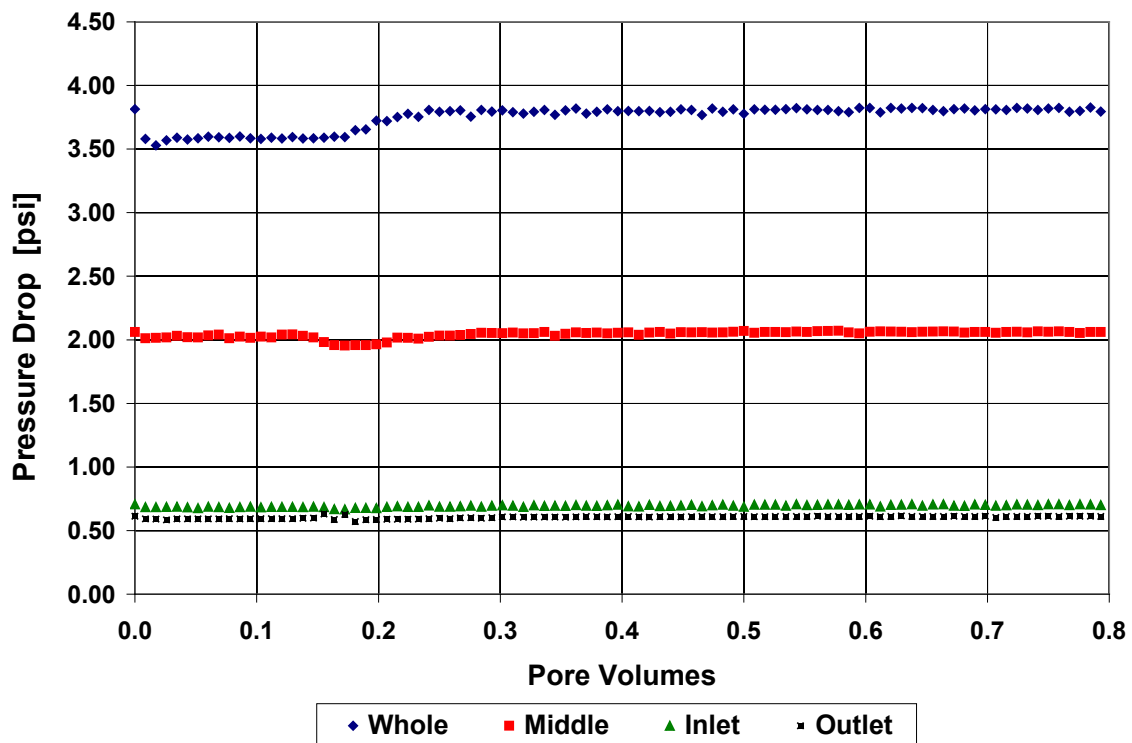


Figure A.22: GB-2 Brine Flood Pressure ($q = 2.64\text{ml/min}$, $\mu_w = 0.54\text{cP}$).

GB-2 Oil Flood

The crude was filtered through a $0.45\mu\text{m}$ filter paper under a pressure of 50psi at reservoir temperature. Prior to the oil flood, filtered oil viscosity was measured by a rheometer at the reservoir temperature (28cP at 10s^{-1}). Then, the oil flood experiment was

conducted with 1.5-2 pore volumes of filtered oil. The flood was continued until the water cut was less than 1%. The oil permeability to residual water was calculated to be 437md and the relative endpoint permeability of oil was 0.89. The initial oil saturation after oil flood was 0.64, for a residual water saturation of 0.36. The pressure data is shown for the GB-2 oil flood in Figure A.23.

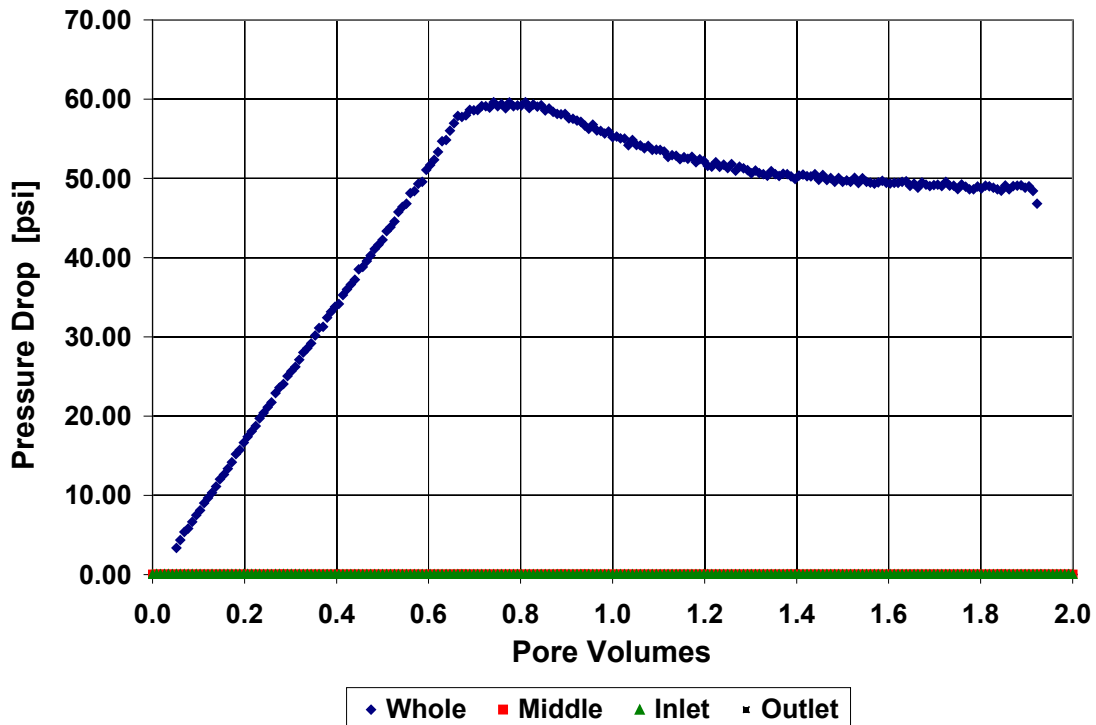


Figure A.23: GB-2 Oil Flood Pressure ($q = 0.54\text{ml/min}$, $\mu_o = 28\text{cP}$).

GB-2 Water Flood

The core was water flooded with SBB at a flow rate of 0.054ml/min until the produced oil cut was less than 1%. The pressure data for GB-2 water flood is illustrated in Figure A.24. After 1.4 PV of water flood, residual oil saturation was obtained to be

0.314. The permeability of water was evaluated to be 58.4md, corresponding to endpoint relative permeability of 0.119.

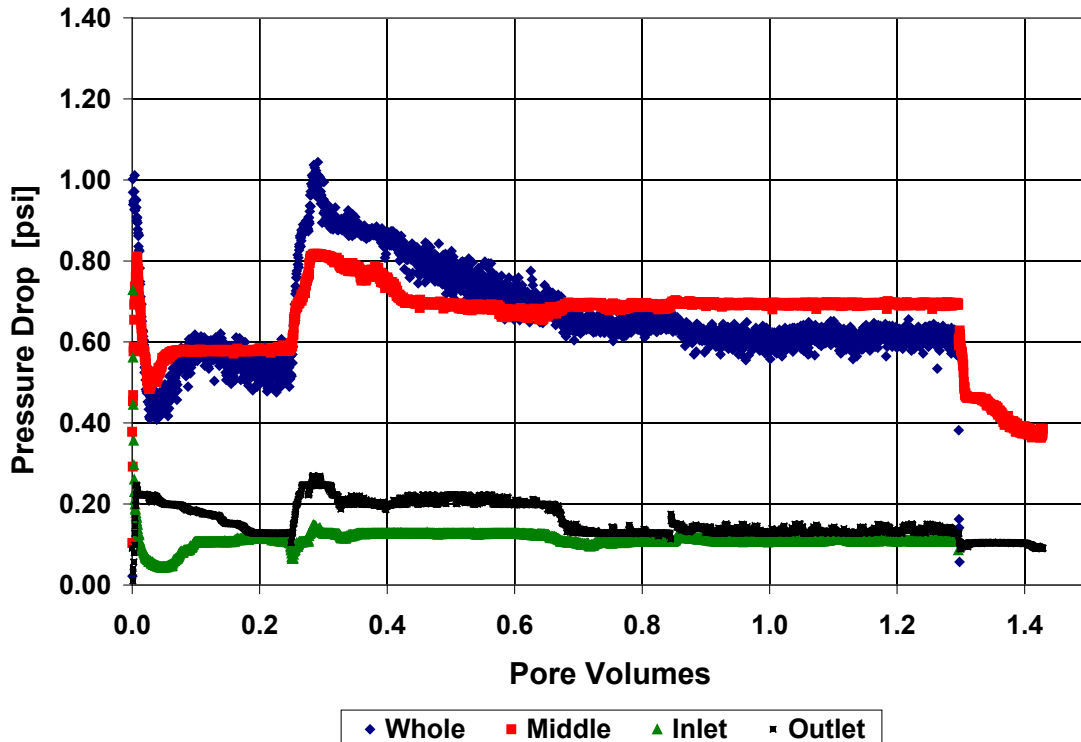


Figure A.24: GB-2 Water Flood Pressure ($q = 0.054\text{ml/min}$, $\mu_w = 0.54\text{cP}$).

GB-2 Chemical Flood Design

The chemical flood is designed using data from the phase behavior, aqueous stability, activity diagram, and polymer viscosity experiments. The phase behavior and solubilization plot for the optimal formulation (0.3wt% Petrostep S13-C, 0.1wt% Neodol 25-12, and 1wt% Na_2CO_3 in 100% SBB) are illustrated from Figure A.18 and Figure A.19. The aqueous stability test was conducted with FloppamTM 3330S polymer (SNF Floerger). The designed viscosity was estimated from the inverse of the minimum total mobility as described in eq. (A.2). Figure A.25 below illustrates relative permeability

curves calculated using the Corey model and values from Table A.10 and Table A.11. An oil bank saturation of 0.5 requires the apparent viscosity for the slug to be at least 18cP (based on eq. (A.2) and Corey Model). The polymer drive should have a viscosity greater than the slug viscosity.

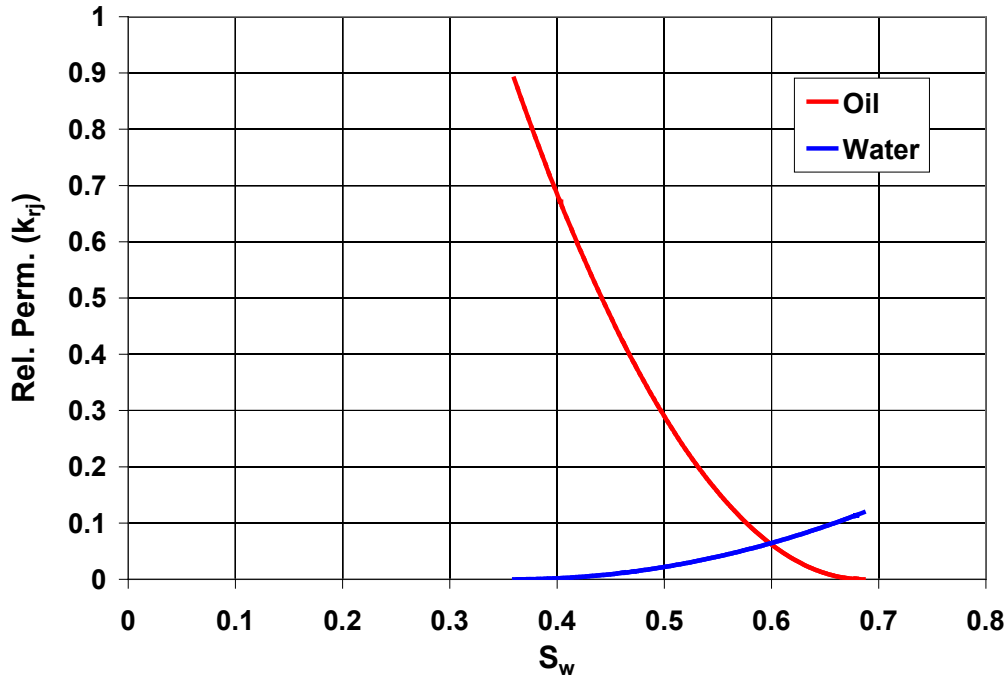


Figure A.25: Corey Model Estimation of Relative Permeability ($n = 2$).

The concentrations of polymer for the ASP slug and polymer drive were determined based on the polymer viscosity experiments at reservoir temperature show in Figure A.26. As can be seen in the figure, at 0.2wt% (2000ppm) polymer concentration, the ASP slug will have a viscosity of 23cP, which is greater than oil bank apparent viscosity (18cP), and the polymer drive will have a more than sufficient value of 32cP. All the measured fluid viscosities at reservoir temperature are listed in Table A.12.

Characteristics and chemical composition for the ASP slug and polymer drive for coreflood experiment GB-2 are tabulated in Table A.13 and Table A.14 respectively.

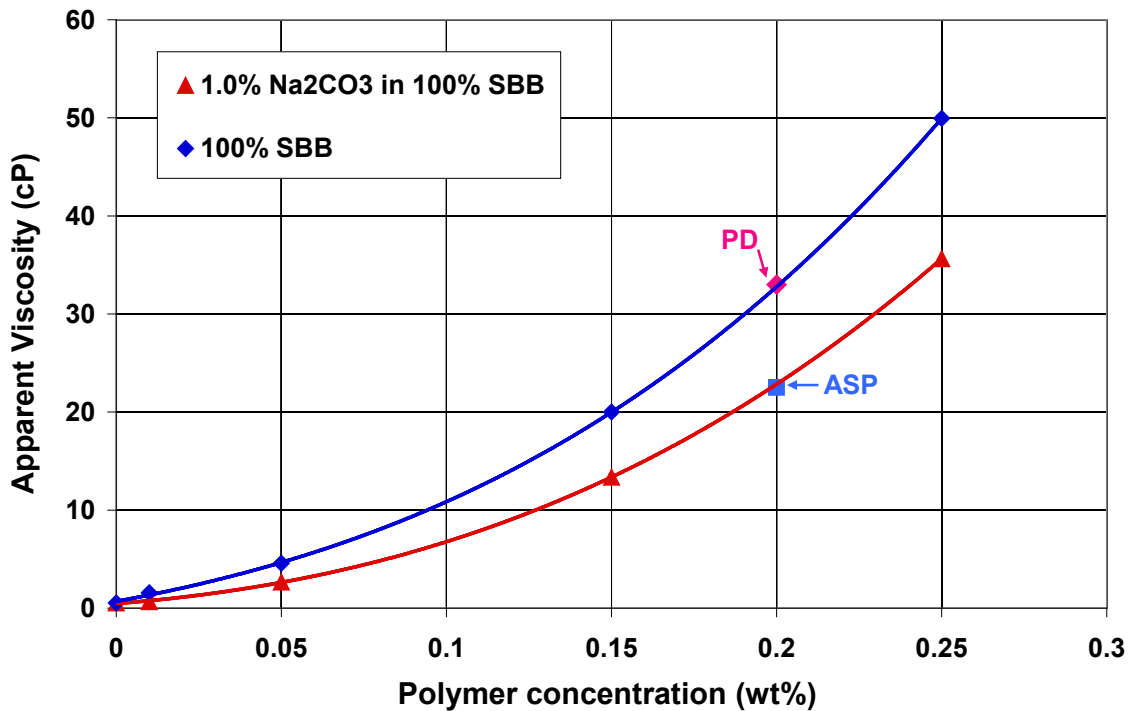


Figure A.26: Polymer Viscosities for GB-2 at 55°C and 10s⁻¹.

Table A.12: Fluid Viscosities Measured at 55°C and 10s⁻¹.

Brine Viscosity (cP)	0.54
Crude Oil Viscosity (cP)	28
ASP Slug Viscosity (cP)	23
Polymer Drive Viscosity (cP)	32

Table A.13: Alkali Surfactant Polymer Slug Data for GB-2 Coreflood.

Pore Volume Injected (PV)	0.3
Petrostep S-13C (C ₁₃ -9PO-SO ₄)	0.3%
Neodol 25-12 (C ₁₂₋₁₅ -12EO)	0.1%
Sodium Carbonate (ppm)	10000

TDS (ppm)	17360
Floppam 3330S (ppm)	2000
Front Velocity (ft/day)	2
Slug Viscosity (cP)	23

Table A.14: Polymer Drive Data for GB-2 Coreflood.

Polymer Drive Injected (PV)	2
TDS (ppm)	7360
Floppam 3330S	2000
Front Velocity (ft/day)	2
Drive Viscosity (cP)	32

GB-2 Chemical Flood Recovery

A 0.3PV ASP slug with 2000ppm Floppam 3330S polymer concentration (23cP) was injected at 2 ft/day followed by a polymer drive with 2000ppm 3330S (32cP) at the same rate. Figure A.27 below shows the pressure data for the chemical flood process.

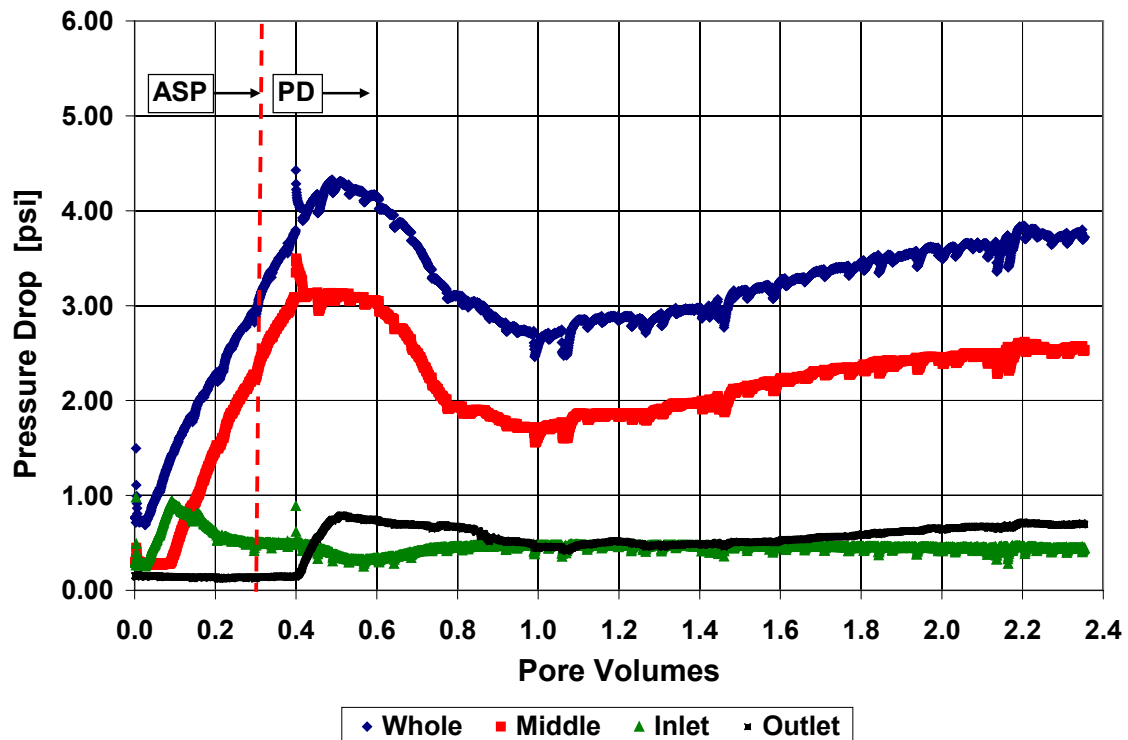


Figure A.27: GB-2 ASP Pressure ($q = 0.04\text{ml/min}$).

The oil breakthrough occurred at 0.3PV and the emulsion breakthrough occurred at 0.88PV. The total oil recovery was calculated to be 92% of residual oil. A high oil cut (around 50%) was observed and most of the free oil was recovered before emulsion breakthrough. The residual oil saturation after the chemical flood was 2.5%.

Figure A.28 shows the oil recovery data for the GB-2 coreflood. Effluent pH was measured periodically using a pH meter. Figure A.29 shows the effluent pH and emulsion cut history during the chemical flood. It seems that alkali and surfactant (contained in the emulsion phase) were able to travel together and thus provide optimum conditions inside the core, which obviously resulted in high oil recovery. Since the coreflood was not performed on a reservoir core, the surfactant retention was not measured in this experiment. Based on the high oil recovery and highly reactive crude oil, it was believed that the retention level would be quite low (Solairaj *et al.*, 2012).

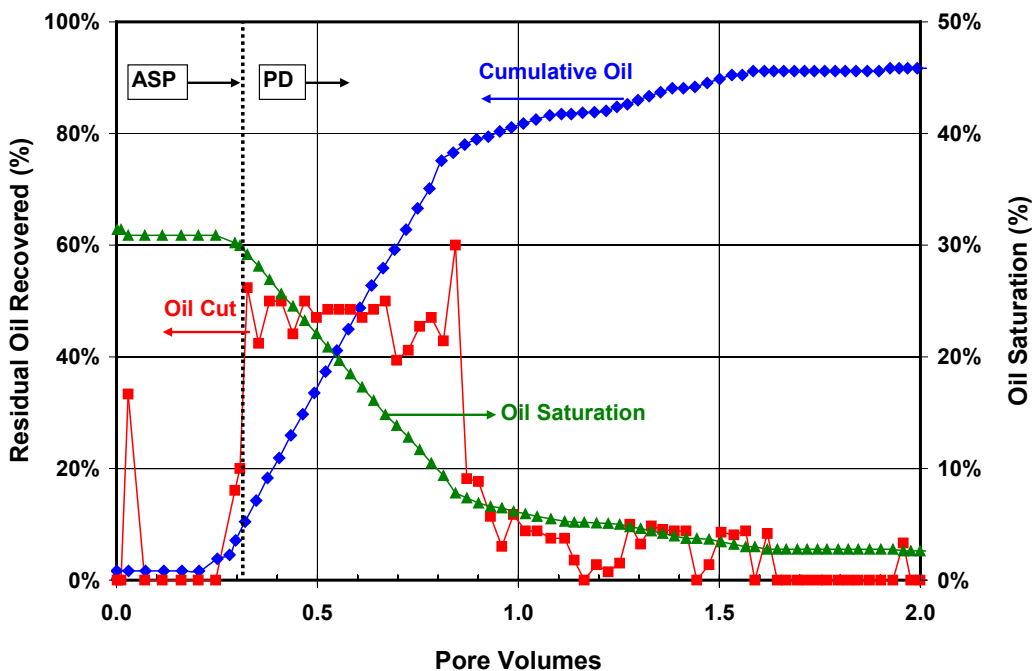


Figure A.28: GB-2 Oil Recovery.

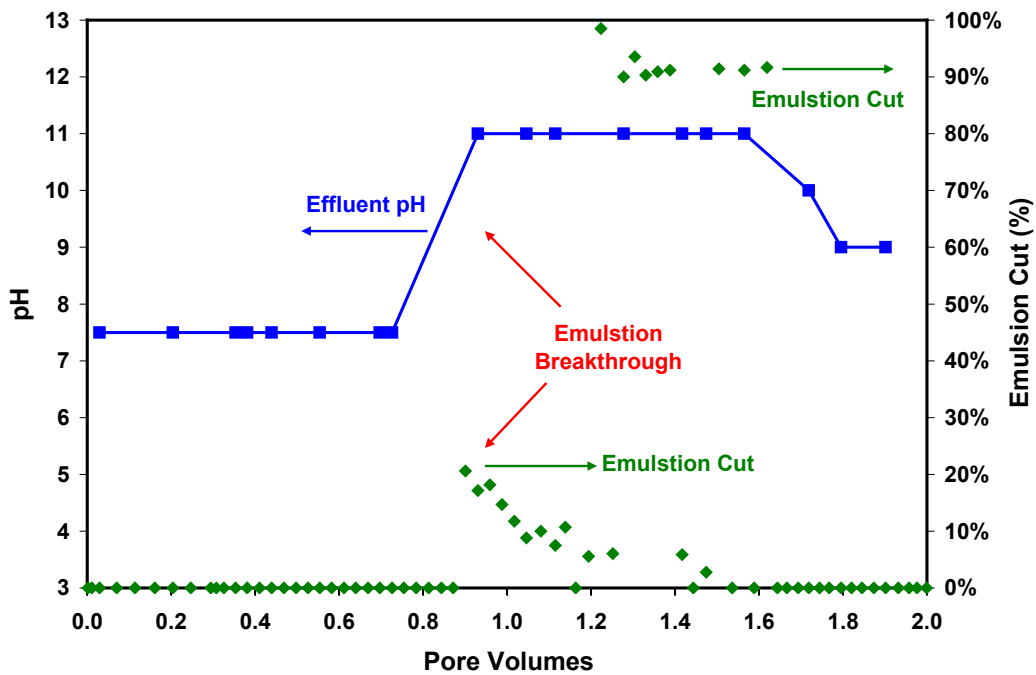


Figure A.29: GB-2 Effluent pH and Emulsion Cut.

A.4 SECTION SUMMARY

A systematic laboratory design study was carried out to identify, test, and verify the optimum chemical formulation for the Brookshire Dome ASP flood pilot project. The optimum ASP formulation (0.3wt% Petrostep S13-C, 0.1wt% Neodol 25-12, and 1wt% Na_2CO_3 in 100% SBB, with 2000 ppm 3330S) successfully recovered over 90% waterflood residual oil in a Berea sandstone coreflood. The poor quality of core plugs from the field prevented us from conducting coreflood experiments using reservoir core, which leaves some uncertainties in the design process.

B. Pilot-Scale ASP Flood Design

This section presents modeling and simulation of a pilot scale ASP flood. The primary goal of the simulation was to optimize the field scale performance by simulating and comparing various injection and operating strategies.

The University of Texas Chemical Compositional Simulator, UTCHEM (Delshad *et al.*, 1996; UTCHEM, 2000) is used for modeling the ASP process. The simulator is a 3D multi-component chemical flooding simulator. Various physical and chemical phenomena modeled include microemulsion phase behavior and interfacial tension models, compositional phase viscosity models, phase trapping models, three-phase relative permeability models that depend on trapping number, chemical adsorption models, and polymer rheology models. It is worth stressing from the onset that setting up a UTCHEM ASP simulation is quite an involved process. Invaluable inputs from Mr. Faiz Veedu, Mr. Abhinav Sharma and Dr. Delshad at UT Austin are greatly appreciated.

B.1 COREFLOOD HISTORY MATCHING

B.1.1 Phase Behavior: Experiments and Modeling

Before the pilot simulations were started, phase behavior and laboratory coreflood data were used to estimate as many simulation parameters as possible. Phase behavior experiments identify surfactants with acceptably high oil solubilization, rapid coalescence time, and minimal tendency to form liquid crystals, gels, or macroemulsions. Solubilization ratio diagrams are routinely used to represent the phase behavior. They provide an understanding of the sensitivity of the surfactant solution behavior to additional electrolytes. They also provide information on the electrolyte concentrations at which a transition from Type I to Type III to Type II is observed. The salinity at which

the transition occurs from Type I to Type III is called lower critical salinity (CSEL) and the salinity at which transition occurs from Type III to Type II is called upper critical salinity (CSEU). In addition, these diagrams provide information on the solubilization of the oil in the middle phase and the optimum salinity.

As discussed in the previous section, numerous surfactant / co-solvent / alkali / polymer combinations were tested to examine both the aqueous and microemulsion phase behavior using the field crude oil, and the best formulation was selected for testing in coreflood experiment. Alkali (Na_2CO_3) was added into synthetic Brookshire brine (SBB) to increase the pH and thereby reduce the surfactant adsorption. With the reactive Brookshire crude, one other primary use of alkali is to react with naphthenic acids in the crude oil to produce in-situ hydrophobic surfactant or soap. It also adds ionic strength along with SBB to bring the salinity up to optimum value. The surfactant formulation identified from laboratory design consists of 0.3wt% Petrostep S13-C (Exxal TDA-9PO-SO₄), 0.1wt% Neodol 25-12 (C₁₂₋₁₅-12EO).

Figure B.1 shows data for the phase behavior experiment done on the above surfactant system where the oil concentration is fixed at WOR=1 (50% oil and 50% water). The optimum salinity observed from the surfactant phase behavior was 1% Na_2CO_3 in SBB (0.310meq/ml salinity in total). One thing worth noting is the salinity calculation employed here. Both Na_2CO_3 and background brine salinity contribute to the total salinity, and thus they should both be considered in modeling phase behavior. The phase behavior is modeled in UTCHEM using Hand's rule of bimodal curve (UTCHEM, 2000). The equations derived from Hand's model for phase behavior calculations are solved using the height of bimodal curve as input parameters, which in UTCHEM are HBNC70, HBNC71 and HBNC72, representing the height of bimodal curve at zero, optimum and twice optimum salinity conditions. The values of these parameters are

obtained by matching the laboratory measured phase behavior data. This matching step is crucial to get the height of bimodal curve (HBNC) parameters and the salinity window (CSEL and CSEU) which are to be used for coreflood modeling and further to conduct pilot scale simulations. UTCHEM batch mode simulations were conducted by Mr. Faiz Veedu to predict the phase behavior of the current surfactant system. The curves in Figure B.1 are UTCHEM simulated results. Figure B.2 shows the phase behavior match at 30% oil concentration. Table B.1 lists the phase behavior parameters used to obtain these matches.

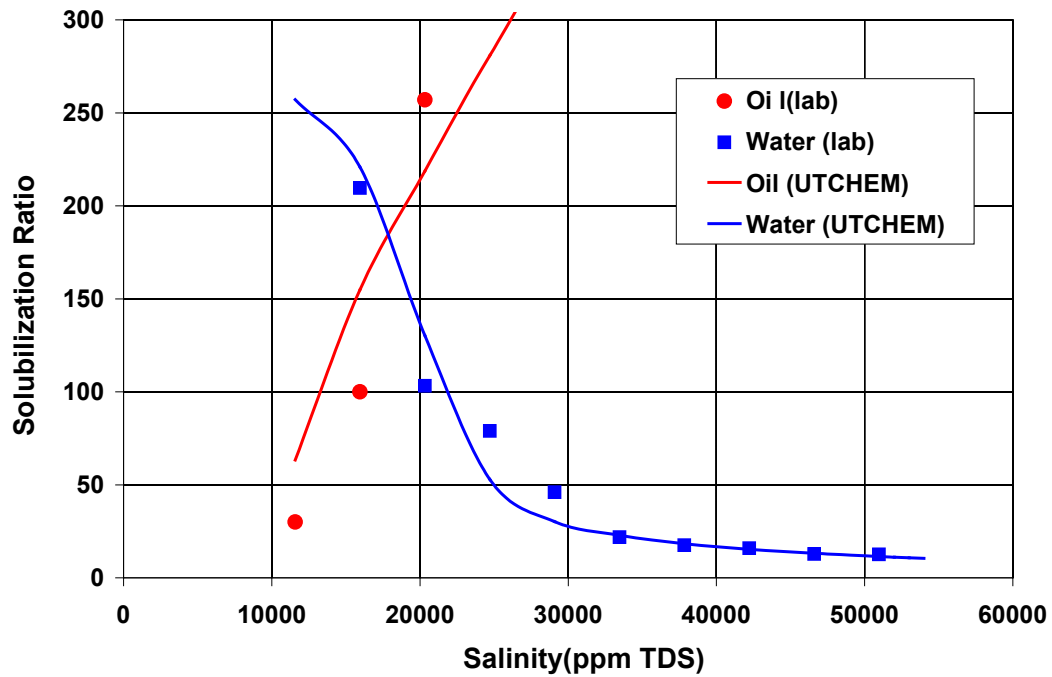


Figure B.1: Phase Behavior Match for 50% Oil Concentration.

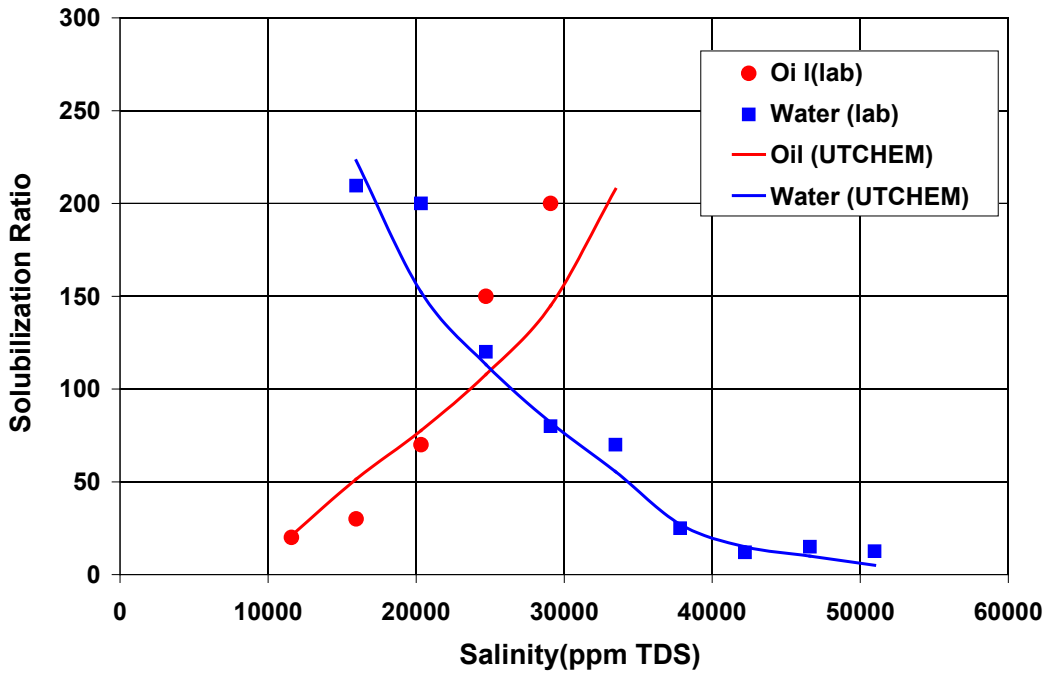


Figure B.2: Phase Behavior Match for 30% Oil Concentration.

Table B.1 Phase Behavior Parameters to Match the Experimental Data Shown in Figure B.1 and Figure B.2.

Height of Binodal Curve at Zero Salinity, HBNC70	0.007
Height of Binodal Curve at Optimum Salinity, HBNC71	0.002
Height of Binodal Curve at Twice Optimum Salinity, HBNC71	0.007

B.1.2 Polymer Rheology Modeling

The basic idea of adding polymer is to provide a viscosity of about 20cP in the surfactant slug (see Section A) and greater than 20cP in the polymer drive. To achieve this in the slug at 0.310meq/ml total salinity, 2000ppm Floppam 3330S was added. Moreover, for the polymer drive, 2000ppm 3330S was used to provide about 30cP viscosity at 0.243meq/ml. Figure B.3 through Figure B.5 present a comparison of polymer lab data along with the UTCHEM model under reservoir conditions at various concentrations, salinities and shear rates.

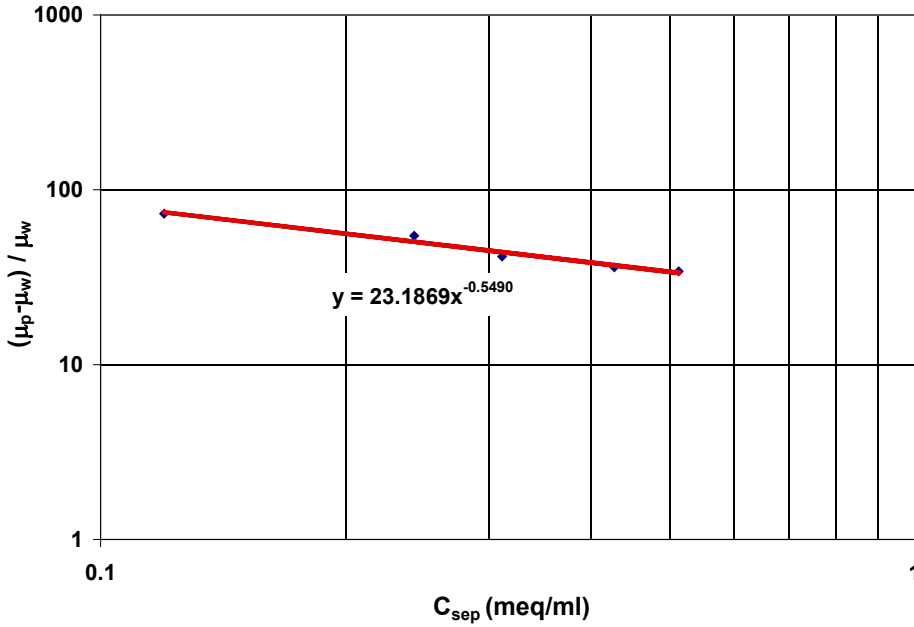


Figure B.3: UTCHEM Model Fit to Lab Data: Viscosity vs. Salinity (2000ppm Floppam 3330S at 55°C).

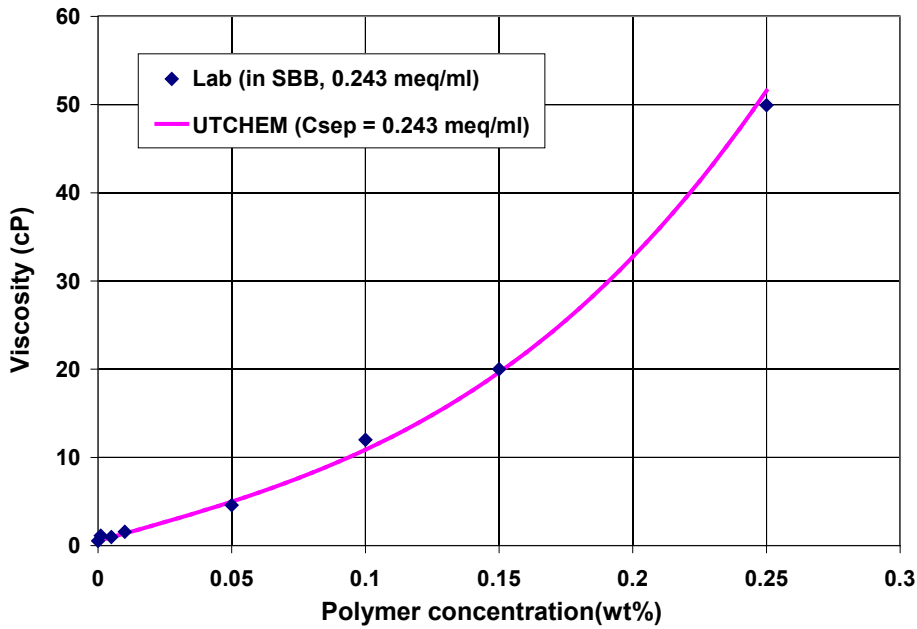


Figure B.4: UTCHEM Model Fit to Lab Data: Viscosity vs. Concentration (Floppam 3330S in SBB of 0.243meq/ml at 55°C).

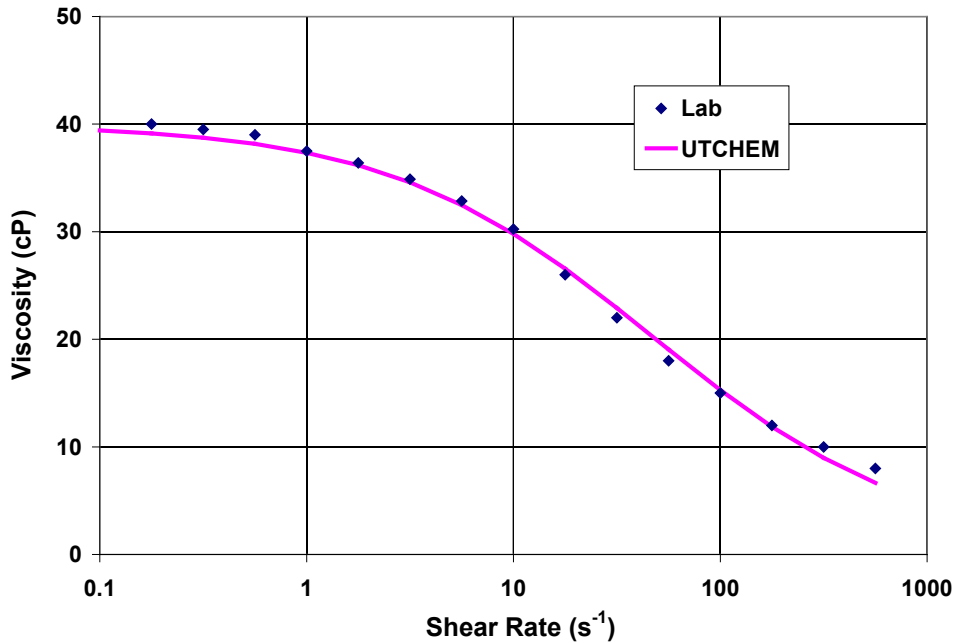


Figure B.5: UTCHEM Model Fit to Lab Data: Viscosity vs. Shear Rate (2000ppm Floppam 3330S in 100% SBB at 55°C).

B.1.3 Geochemical Input Data

The UTCHEM geochemistry model (Hourshad, 2008) is based on a local thermodynamic equilibrium assumption to compute the detailed composition of the reservoir rock and fluids in the presence of reactions among the injected species and reservoir rock and fluids. The reactions include aqueous electrolytes chemistry, precipitation / dissolution of minerals, ion-exchange reactions with the matrix, and the reaction of acidic components of the oil with bases in the aqueous solution.

A preprocessor called EQBATCH can be used for UTCHEM to calculate the initial equilibrium state of the reservoir. EQBATCH writes the output data in a format similar to the geochemical input data of UTCHEM, so it can be directly pasted into the input for UTCHEM. Formation brine composition and elemental concentration, pH, temperature, acid number of the crude oil and some knowledge about the rock and its

minerals are all important data for EQBATCH calculation. The UTCHEM geochemical input for current simulation model was kindly provided by Mr. Faiz Veedu and Mr. Abhinav Sharma from EQBATCH calculations.

B.1.4 Coreflood Simulation

As discussed in Section A, the ASP formulation was tested in coreflood experiments. About 92% of the waterflood residual oil was recovered. This coreflood was simulated to estimate various simulation parameters needed to simulate the ASP pilot. The UTCHEM model parameters for phase behavior data, surfactant, relative permeability (Figure B.6), capillary desaturation curve (Figure B.7), and polymer viscosity dependence on salinity / polymer concentration / shear rate are listed in Table B.3. The adsorption parameters for polymer were obtained by assuming a maximum polymer adsorption and using core properties. The adsorption parameters of surfactant were obtained by matching coreflood results using UTCHEM simulation.

Table B.2 Review of Core and Fluid Properties for GB-2 Coreflood.

Core & Fluid Properties (from Section A)	
Porosity	0.2014
Absolute Permeability (md)	491
Temperature (°F)	131
Length (cm)	29.067 (0.9536ft)
Diameter (cm)	2.54 (0.0833ft)
Residual Water Saturation, S_{wr}	0.36
Residual Oil Saturation, S_{orw}	0.314
Water Endpoint Relative Perm., k_{rw}^o	0.119
Oil Endpoint Relative Perm., k_{ro}^o	0.89
Water Viscosity (cP)	0.54
Oil Viscosity (cP)	28

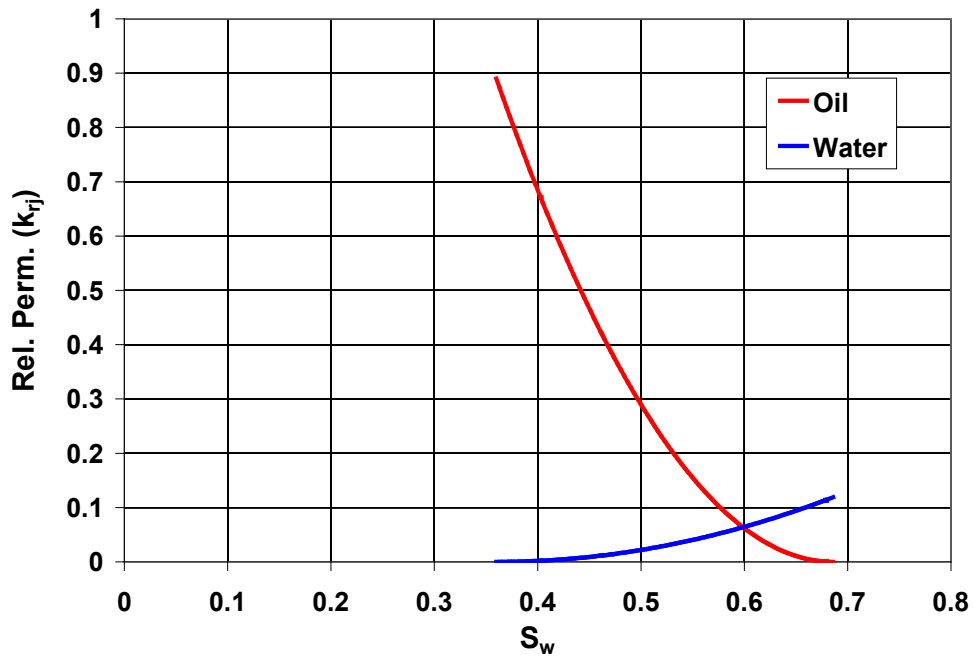


Figure B.6: Relative Permeability Curves used in UTCHEM Coreflood Simulation.

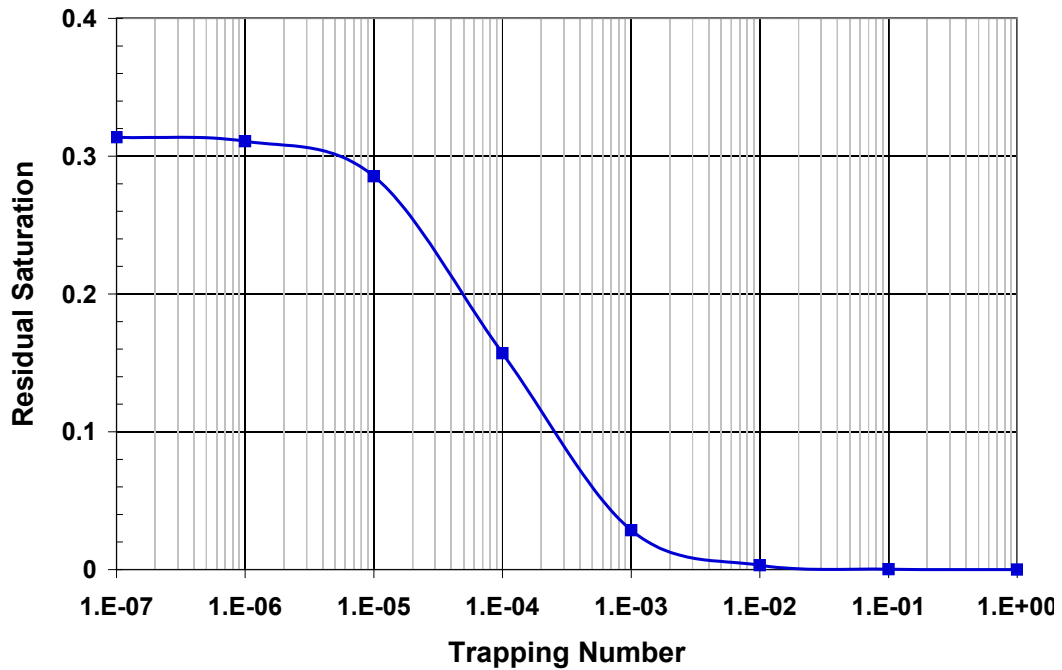


Figure B.7: Capillary Desaturation Curve for Oil in Simulation Model.

Table B.3 Summary of Simulation Inputs for GB-2 Coreflood.

Simulation Inputs	
Simulation Model Dimension (ft)	$0.9536 \times 0.07385 \times 0.07385$
Number of Grid Blocks in X, Y, Z	$100 \times 1 \times 1$
Capillary Desaturation Parameters for Water, Oil, ME	1865, 10000, 364.2
Intercept of Binodal Curve at Zero, OPT., and 2OPT. Salinities (HBNC70 – HBNC72)	0.007, 0.002, 0.007
CMC (volume fraction)	0.001
Type III Salinity Window (CSEL, CSEU, COPT)	0.25, 0.60, 0.31
Interfacial Tension Parameters for Huh's Model (CHUH, AHUH)	0.3, 10
Log10 of Oil/Water Interfacial Tension (XIFTW)	1.3
Compositional Phase Viscosity Parameters for ME (ALPHAV1 - ALPHAV5)	1.0, 2.0, 0.5, 0.5, 0.5
Parameters to Calculate Polymer Viscosity (AP1, AP2, AP3)	71.473, 2, 1630.083
Salinity Dependence of Polymer Viscosity (SSLOPE)	-0.5490
Shear Rate Dependence of Polymer Viscosity (GAMMAC, POWN, GAMHF)	4.0, 1.68, 46.86
Permeability Reduction Factors (BRK, CRK)	100, 0.015
Relative Perm. Exponent of Water	2.0
Relative Perm. Exponent of Oil	2.0
Physical Dispersion Coefficient for Water, Oil, ME (ALPHAL1-3, ALPHAT1-3)	0.02, 0.002
Surfactant Adsorption Parameters (AD31, AD32, B3D)	2.7, 0.1, 1000
Polymer Adsorption Parameters (AD41, AD42, B4D)	3.9, 0, 100

Figure B.8 through Figure B.10 show the match between the simulation and measured data for the GB-2 coreflood. As shown in Figure B.8, oil breakthrough occurs

at about 0.28PV with an oil cut of about 50%, which is in close agreement with experimental observations. The cumulative oil recovery was also satisfactorily matched.

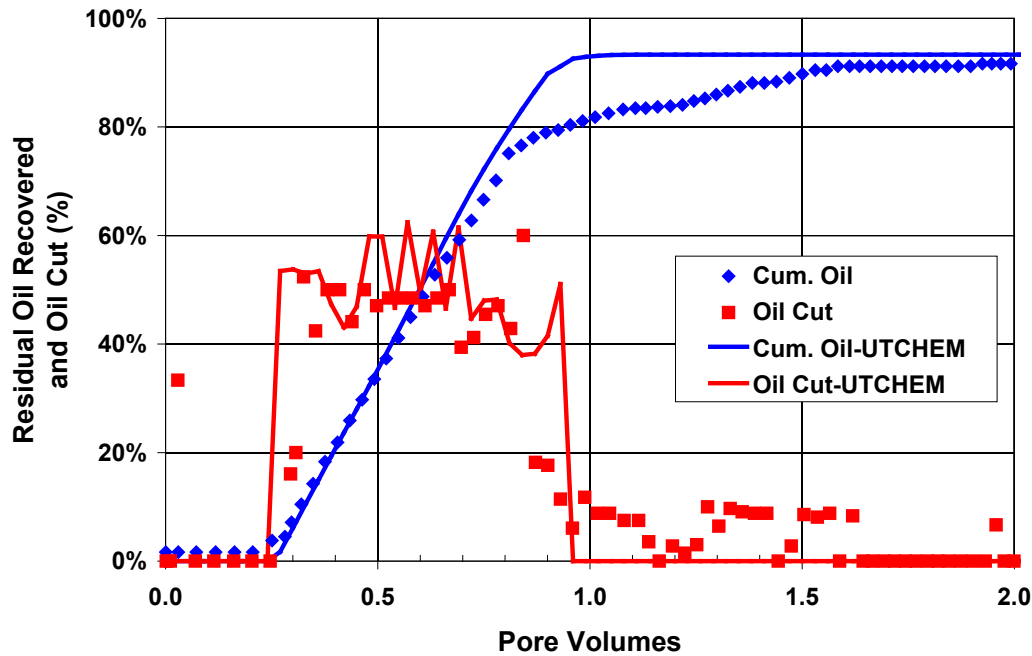


Figure B.8: Comparison of Simulated and Measured Oil Recovery and Oil Cut for GB-2 Coreflood.

Figure B.9 shows a good match between the simulation and measured data for the effluent pH. A Winsor Type III salinity region at 0.5PV of injection is shown in Figure B.10, which is bounded by CSEU and CSEL. This is a good illustration of how the Type III region is affected by the chemical propagation in the core. The effective salinity passes through the Type III region in the middle of the core and returns back to Type I, which gives a negative salinity gradient to the system (at least partially). An ultra-low interfacial tension (less than 0.001dyne/cm) is achieved when the salinity passes through the Type III region. Also shown in the plot is the oil concentration. It is clearly shown that a substantial oil bank is formed in the core.

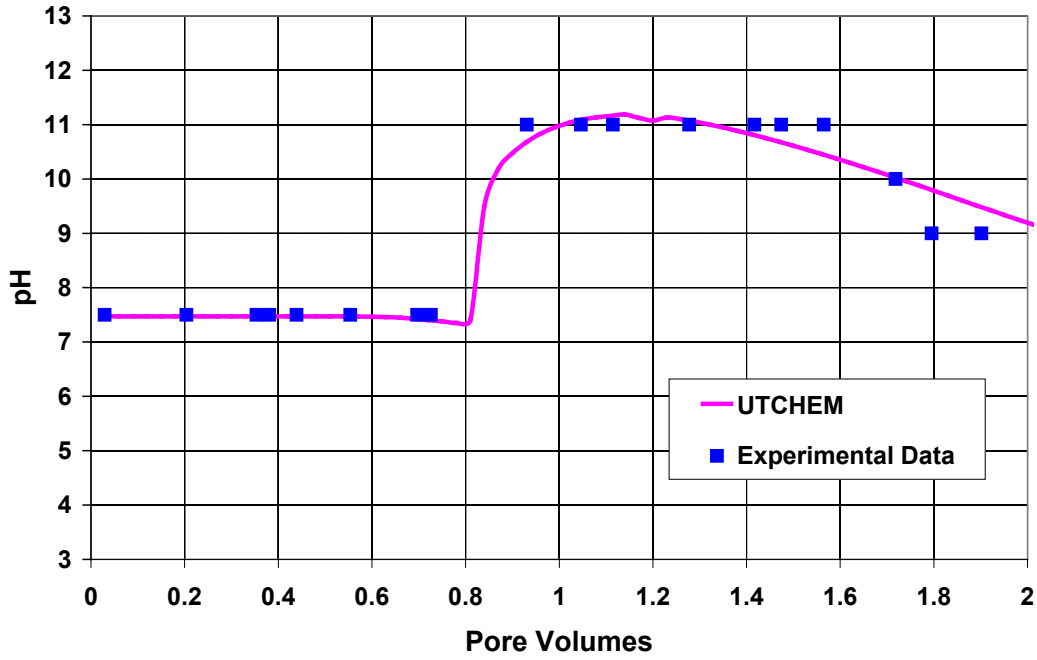


Figure B.9: Comparison of the Effluent pH between UTCHEM and Experimental Data for GB-2 Coreflood.

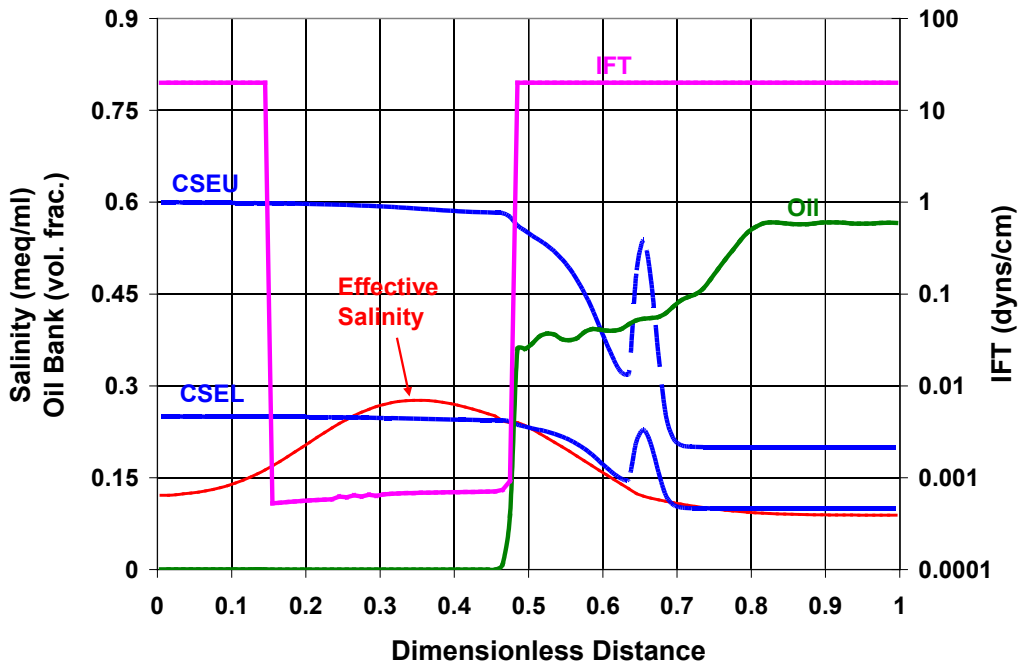


Figure B.10: Simulated Salinity, IFT and Oil Saturation for GB-2 at 0.5 PV.

B.2 PILOT SCALE SIMULATION STUDY

Before the simulation results are presented for this section, it is imperative to discuss the reservoir and the simulation model. A detailed geological model for the Catahoula sand was built using data from logs from each well and from data collected as a part of the pilot such as flowing spinner surveys and an inter-well tracer test program.

B.2.1 Simulation Model Setup

The inverted five-spot pattern and associated peripheral producers (shown as the red-boxed area in Figure B.11) represents the area of interest and is a part of ~ 50acre simulation model. In theory a direct five spot is preferable, as it enables a better fluid confinement. But too large a quantity of chemicals would probably be wasted outside the pattern and the success of the pilot would hinge heavily on the behavior of the center producer. To our knowledge, the pattern is not confined by any geological boundaries (at least not nearby). Field production history suggests a strong aquifer charge with a preferential flow direction of SW to NE (red arrows in Figure B.11).

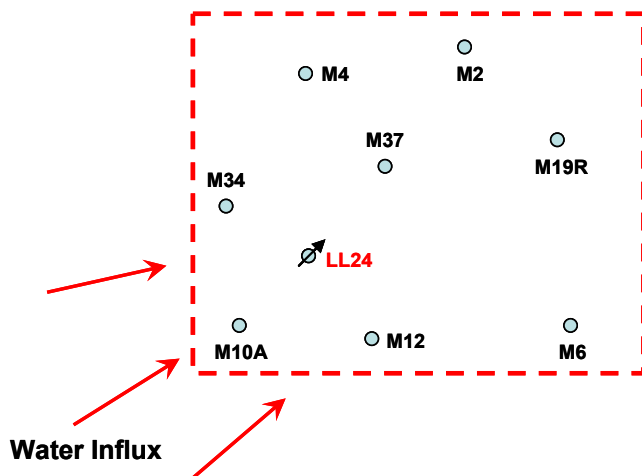


Figure B.11: Areal View of the Well Placement in the Simulation Model. The prefix M and LL refer to the Martin lease and Layline respectively.

Pattern Volume Calculation

A pattern volume calculation was conducted by geologists from Layline Petroleum. This calculation is a key piece of information for evaluating project economics, as well as interpreting pilot results later on. The pilot pattern was divided into 17 sub-polygons for area and volume calculations as shown in Figure B.4. Porosity was taken to be a constant of 0.33, and the original oil saturation in the reservoir was 0.75. A formation volume factor for oil of 1.05 was used. Volume averaged net pay thickness was 49.6 ft.

Table B.4 Areal and Volumetric Calculations for Pilot Pattern.

Polygon No.	Avg. Net Pay (ft)	Area (acre)	Pore Volume (bbl)	OOIP (STB)
1	48	0.004	519	371
2	48.5	0.074	9215	6582
3	49.5	0.181	22933	16381
4	50.5	0.113	14626	10447
5	51.5	0.120	15866	11333
6	52.5	0.105	14128	10092
7	53.5	0.085	11703	8359
8	54	0.025	3507	2505
9	53.5	0.012	1666	1190
10	54	0.008	1050	750
11	48.5	0.108	13437	9598
12	47.5	0.103	12585	8989
13	46.5	0.127	15107	10791
14	45.5	0.040	4712	3366
15	44.5	0.026	3005	2146
16	43.5	0.022	2442	1744
17	43	0.007	809	578
Total		1.16	147310	105222

Spinner Survey

A spinner survey was conducted by Layline Petroleum (the Operator) on the injector well (Martin 24). The perforated interval (72ft in total) runs from 2118ft down to 2190ft, as shown in Figure B.12 (left). With an average net pay thickness of 49.6ft, the average net-to-gross (NTG) is about 0.70. It appeared during the test that the injected fluid predominantly entered the reservoir through the top 12ft of perforations with less fluid going to the bottom layers. Based on the change in slope of the flow profile (fraction of flow going into each section of sand), it would be more realistic to further divide the perforation interval into thinner layers as shown in Figure B.12 (right). The top layers have higher permeability than the bottom layers. Furthermore, a water injectivity of 1.8bpd/psi was reported from the field during the tracer test injection. Based on this, an average (arithmetic) permeability of 125md was estimated with an assumed relative permeability value of 0.12 (same as Berea core data). Individual layer permeability was then estimated by using the spinner survey information with the overall estimated permeability.

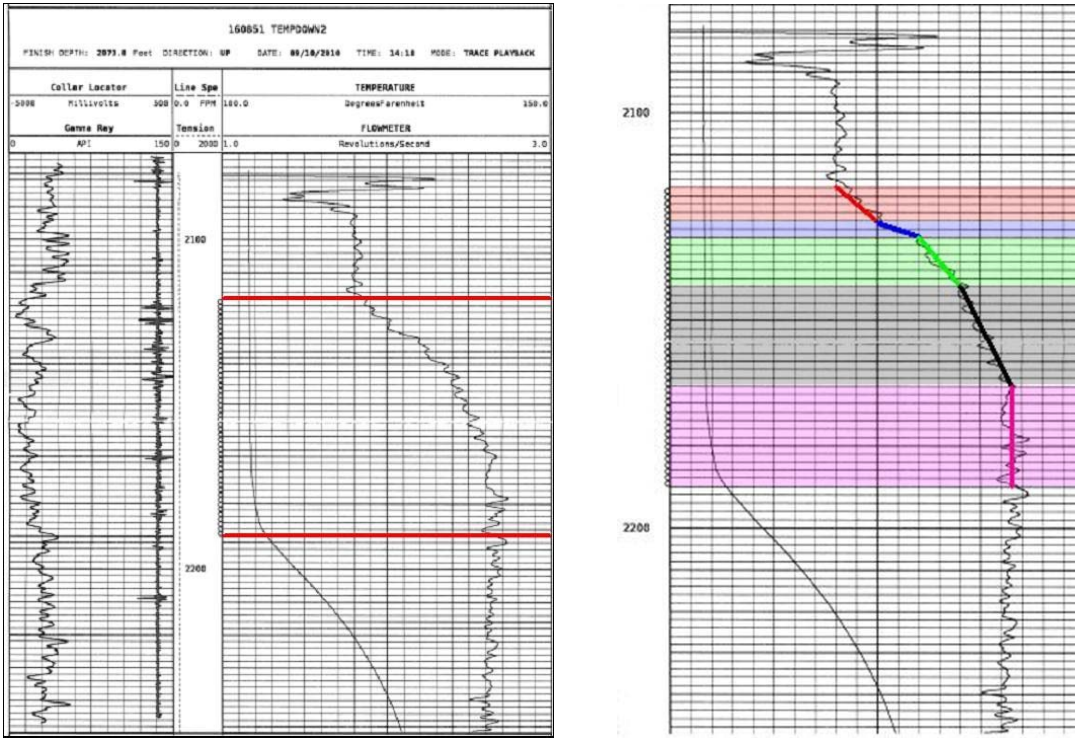


Figure B.12: Spinner Survey Results Provided by Weatherford.

Two different layering and gridding schemes were implemented in the study, the coarser (5-layer) and the refined (9-layer) grids. The layer division of the coarser model was based upon Figure B.12 (right). The individual layer properties, including thickness, x-direction permeability, total grid block number and cell dimensions in x, y, z directions of this model are listed in Table B.5 and Table B.6. For simplicity, the net pay thickness was used directly as layer thickness in the simulation. For both gridding schemes, we assume $k_y/k_x=1$, $k_z/k_x=0.2$, and $\phi=0.33$.

Table B.5 5-Layer Model: Individual Layer Properties.

Layer No.	Thickness (ft)			k_x (md)
	Gross	NTG	Net (model)	
1	8	0.7	5.6	250
2	4		2.8	500

3	12	8.4	167
4	24	16.8	100
5	24	16.8	20

Table B.6 5-Layer Model: Reservoir Size and Dimensions.

Simulation Model Volume (ft × ft × ft)	2010.86 × 1355.14 × 50.4
Number of Grid Blocks in x, y, z	61 × 43 × 5
Cell Dimensions in x (ft)	18 × 43.71; 30 × 21.855; 13 × 43.71
Cell Dimensions in y (ft)	8 × 43.71; 24 × 14.57; 11 × 43.71
Cell Dimensions in z (ft)	8, 4, 12, 24, 24
Pattern Pore Volume (bbl)	150097
Initial Oil Saturation, S_{oi}	0.75
Residual Oil Saturation to WF, S_{orw}	0.4

The more refined 9-layer model was used to investigate the layering effect on simulation results. As can be seen from Table B.8 and Table B.10, smaller cell dimension (in x-y plane) within the pattern area was also implemented in this model with the intention to better capture the near wellbore flow behavior.

Table B.7 9-Layer Model: Individual Layer Properties.

Layer No.	Thickness (ft)			k_x (md)
	Gross	NTG	Net (model)	
1	4		2.8	250
2	4		2.8	250
3	4		2.8	350
4	6		4.2	167
5	6	0.7	4.2	167
6	12		8.4	100
7	12		8.4	100
8	12		8.4	50
9	12		8.4	50

Table B.8 9-Layer Model: Reservoir Size and Dimensions.

Simulation Model Volume (ft × ft × ft)	2010.86 × 1355.14 × 50.4
Number of Grid Blocks in x, y, z	80 × 59 × 9
Cell Dimensions in x (ft)	17 × 43.71; 51 × 14.57; 12 × 43.71
Cell Dimensions in y (ft)	7 × 43.71; 42 × 14.57; 10 × 43.71
Cell Dimensions in z (ft)	3 × 2.8; 2 × 4.2; 4 × 8.4
Pattern Pore Volume (bbl)	150097
Initial Oil Saturation, S_{oi}	0.75
Residual Oil Saturation to WF, S_{orw}	0.4

Multi-well Tracer Test

A multi-well bromide tracer study was conducted in the pilot area for a better understanding of inter-well communication in the reservoir. As mentioned earlier, a strong aquifer charge exists in the pilot area. In the simulation model, influx and efflux due to the aquifer were modeled by SW water injection (4 additional injectors) and NE production wells (5 additional producers). It was hoped that tracer test results could also help better quantify the influence of the aquifer.

In the field, 54 barrels of sodium bromide tracer were introduced at a concentration of ~50,000ppm and rate of ~1500bpd into the injector, Martin 24. After this initial injection, liquid samples were collected for 70 days from eight offset producing wells and sent to TIORCO laboratory for bromide concentration analysis by ion chromatography. The production wells represented in this study include Martin 2, 4, 6, 10A, 12, 19, 34, and 37 (see Figure 8.1 and Figure B.11). In general, wells with consistent bromide concentrations 5ppm over baseline are considered to have obvious breakthrough, while wells with 1-4ppm over baseline must be investigated further for other variables before breakthrough can be determined. Figure B.13 shows the tracer breakthrough profiles on all the monitoring wells.

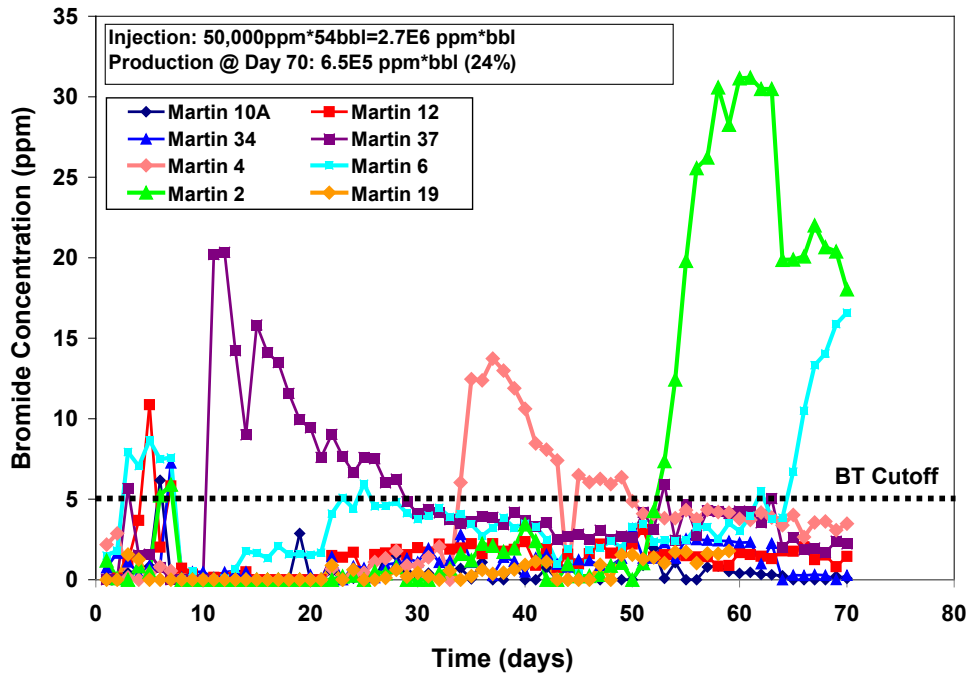


Figure B.13: Detailed Bromide Tracer Response for All Monitoring Wells 70 Days after Injection.

The field data is quite noisy. Bromide breakthrough was initially observed in production well Martin 37 about 10 days after injection. Tracer breakthrough occurred 35 days after injection in Martin 4, 50 days in Martin 2, and 65 days in Martin 6. Breakthrough was not observed in production wells Martin 10A, 12, 19, or 34 until 70 days after injection. Recalling the well locations in the field from Figure B.11, it would appear that tracer tends to break through earlier in producers (Martin 37, 4, and 2) to the north of the injector (Martin 24), clearly demonstrating the influence of the aquifer influx. The breakthrough of Martin 6 right after these wells is quite puzzling and seems to suggest the existence of a high-perm conduit between the injector and Martin 6. On day 70, the tracer recovery was only about 24%. Although the final recovery would definitely be higher since bromide was still being produced on Martin 2 and 6 at that time, such a

low recovery could possibly be attributed to the poor chemical confinement in the pilot area.

Due to the complexity of the breakthrough profile, it was decided to focus the matching effort on the breakthrough time and concentration of the Martin 37 well, which is the nearest producer to the injector. The locations and constraints (rate or pressure) of the auxiliary wells (for simulating the aquifer influx) were adjusted to obtain the match shown in Figure B.14 below. The match was obtained using a 5-layer model. No substantial improvement can be obtained with the 9-layer model. Tracer breakthrough occurred on Martin 37 after 10 days and reached a peak concentration of 20ppm, which is in good agreement with field data considering the simplicity of the current layer cake model. Martin 4 and 2 also exhibited breakthrough fairly early, but the peak concentrations were quite different than the field measurements. A few of the possible reasons for the inconsistency between the field data and simulated results may be fractures, behind pipe flow, thief zones, and other reservoir characterization uncertainties. Nonetheless, a decision was made at this point to move forward with the simplified layer-cake model for pilot-scale waterflood and ASP flood simulations.

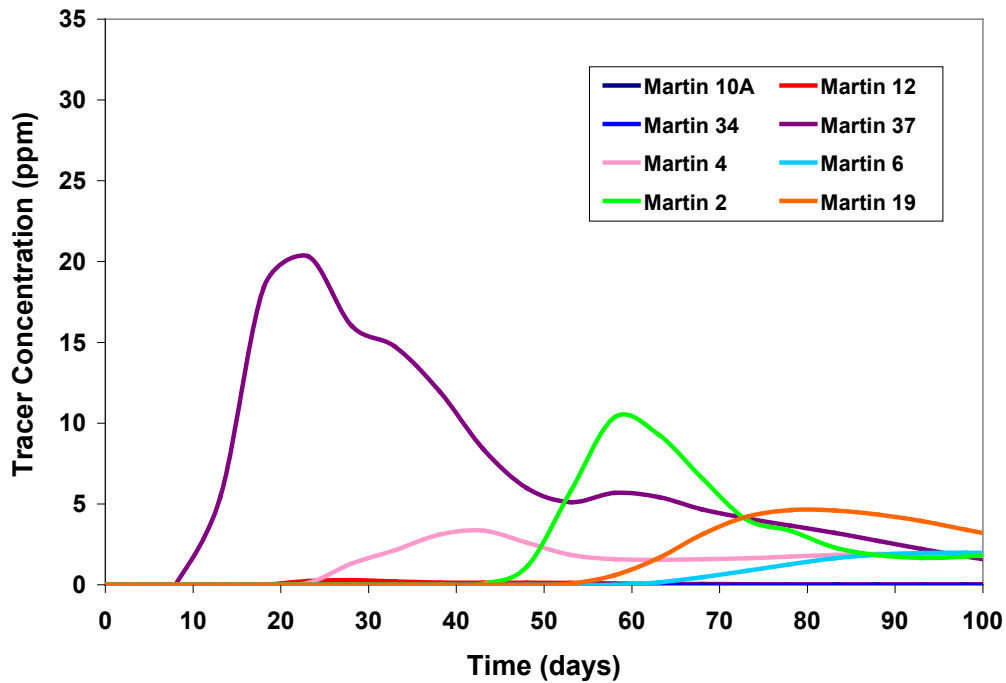


Figure B.14: Tracer Concentration Response Simulated using UTCHEM.

B.2.2 Waterflood

Brookshire Dome field was discovered in 1996 and has been water flooded for about 15 years prior to the ASP pilot implementation. Due to the reservoir layering, the oil saturation is probably very non-uniform, with some of the layers potentially at residual oil saturation, especially the top high-perm layers. Since no detailed oil distribution information was available, a 15-year waterflood was simulated prior to chemical flooding to establish initial oil saturation in the reservoir. The very limited information regarding reservoir rock properties forced us to use relevant data from the Berea coreflood model.

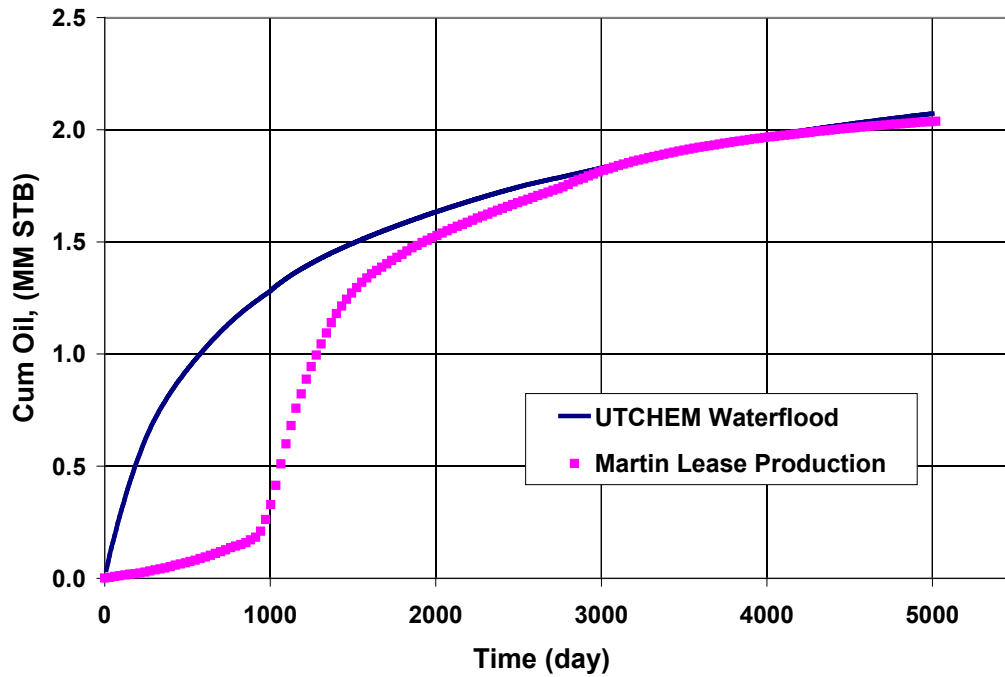


Figure B.15: Tracer Concentration Response Simulated using UTCHEM. Note that the simulation assumes all the wells produce from day 1 while in reality the wells were drilled over a period of time.

Figure B.15 shows a cumulative oil production comparison between UTCHEM waterflood simulation and field production data. The model was able to predict the cumulative oil production of about 2 million STB from all producers in the model, which is well in line with the field production data. The rapid increase of oil production was due to extensive field development during that period of time, whereas the simulation model already has all the wells in place from the very beginning. After 15 years of production, all the wells in the pilot area are producing at very high water cut (>99%). The average oil saturations within each layer for both models are listed in Table B.9 and Table B.10.

Table B.9 5-Layer Model: S_o and Oil in Place after 5000 Days of Waterflood.

Layer No.	S_o After WF	H (ft)	PV (bbl)	Oil Present after WF (bbl)
1	0.4466	5.6	16677	7403
2	0.4380	2.8	8339	3611
3	0.4289	8.4	25016	11452
4	0.4427	16.8	50032	24831
5	0.4515	16.8	50032	29739
Sum (bbl)		50.4	150097	77036

Table B.10 9-Layer Model: S_o and Oil in Place after 5000 Days of Waterflood.

Layer No.	S_o After WF	H (ft)	PV (bbl)	Oil Present after WF (bbl)
1	0.4466	2.8	8339	3724
2	0.4380	2.8	8339	3652
3	0.4289	2.8	8339	3576
4	0.4427	4.2	12508	5537
5	0.4515	4.2	12508	5647
6	0.4818	8.4	25016	12053
7	0.5057	8.4	25016	12651
8	0.5933	8.4	25016	14842
9	0.6030	8.4	25016	15085
Sum (bbl)		50.4	150097	76768

The post-waterflood S_o distributions in different layers are shown in Figure B.16 for the 5-layer model. Clearly the top layers have lower oil saturation, whereas the bottom low-perm layers have more mobile oil left due to poor sweep. Permeability contrast determines that top layers would be preferentially water flooded. Notice for wells M2, 19, and 6, the bottom layer oil saturation is still quite high even after extensive waterflooding. Aside from the poor sweep just mentioned, the fact that these wells are relatively closer to the closed simulation boundary may also contribute to the possibly ‘false’ oil accumulation, although this affect has been partially alleviated by five other

producers (for simulating aquifer influx) placed near the model boundary. Based on this consideration, the production from the peripheral producers will not be counted as cumulative oil produced in the following sections. Only production from the in-pattern producers, namely M34, 37, 10A, and 12, will be counted and presented. This is likely to underestimate the total production from lease area, but provides unambiguous evaluation of the pilot performance, since all the area and volume calculations are made based upon the pilot pattern.

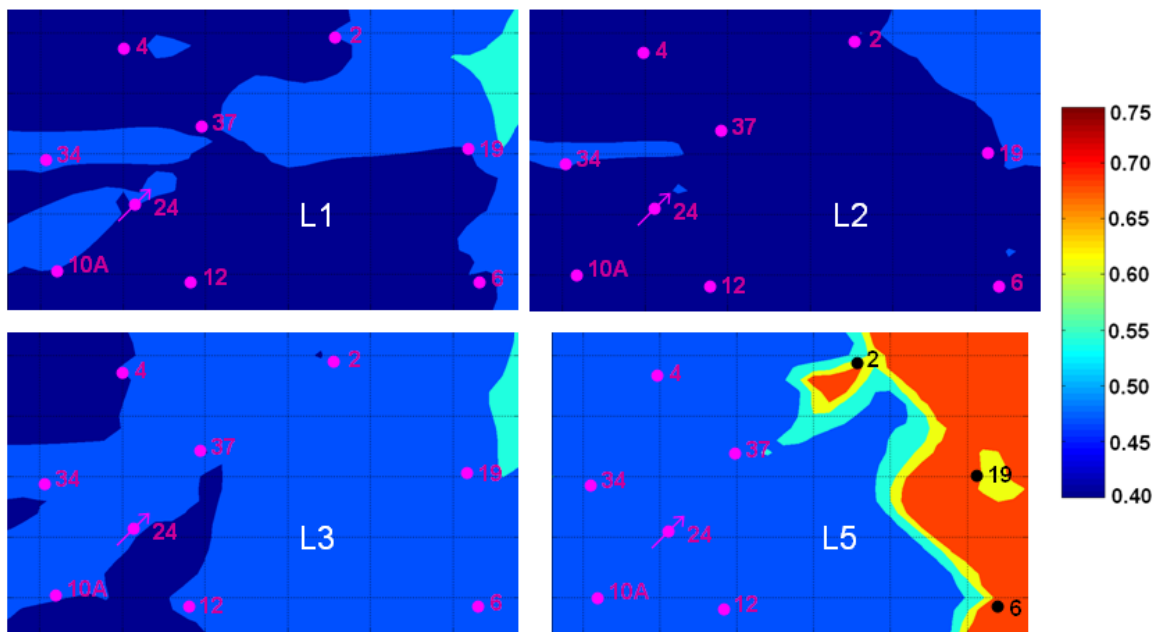


Figure B.16: Areal View of Post-Waterflood Oil Saturation of Layer 1, 2, 3, and 5 for Coarser Model (5-layer).

B.2.3 General Operating Strategy Comparison (w/ 5-Layer Model)

Unless otherwise specified, all the wells within the pattern are rate constrained. And the rates are specified based on tracer test conditions. Martin 24 is injecting at 1500bpd and the producers are producing at rates specified in the table below. Wells

located on the south side of the pattern, namely M10A and M12 are producing at higher rates to counterbalance the influence of the aquifer influx.

Table B.11 Producer Rates for Base Case Simulation (from tracer test).

Well No.	Rate (bpd)	Well No.	Rate (bpd)
M4	266	M34	260
M2	308	M37	290
M19	600	M10A	500
M6	442	M12	600

The ASP slug injection (started after waterflooding) lasts for 0.3PV or about 30 days. The formulation injected is the same as in coreflood experiments and simulations. About 0.7PV polymer drive was injected after the ASP slug and this period of injection lasts for 100 days. Water post-flush was conducted after the polymer drive and this lasts for 500 days. Sensitivity simulation runs (see later section) showed that 2000ppm polymer can only provide marginal mobility control. For all later studies, the concentration was raised to 4000ppm 3330S. In the field (see Section C), higher MW polymer FP 3430S was used to maintain high viscosity but at a lower concentration. Table B.12 lists various operating strategies evaluated in this section using the 5-layer model.

Table B.12 Different Strategies Investigated in this Section.

Case #	Description
1	Base case ASP flood (30 days ASP slug + 70 days polymer drive)
2	2X ASP injection (doubling the size of slug and drive, 60+140)
3	ASP bottom injection (injecting into bottom layer)
4	Polymer pre-flush + ASP (100 days of polymer first, then ASP)
5	ASP double production rates (doubling the rates on all producers)

Case 1: Base Case ASP Flood

The cumulative oil recovery and oil production rate of Case 1 (base case ASP) is shown in Figure B.17. The cumulative oil recovery after 500 days is 21,085bbl. The maximum total oil production rate predicted by UTCHEM is about 235bpd. Due to the close well spacing in the pattern, oil bank breakthrough occurs in all the wells within 30 days. The maximum oil rate occurs at about 80 days. It can be seen that the oil bank is still being produced even after the polymer drive is injected (100 days). After about 290 days since the start of the slug injection, the water cut goes back to 99%. Hence, no more incremental oil recovery is counted after that. Chemical cost per barrel of oil produced in this case is about \$21.35/bbl (assuming \$2/lb surfactant, \$1.45/lb co-solvent, \$1.48/lb polymer, \$0.15/lb alkali, and \$1.5/lb EDTA).

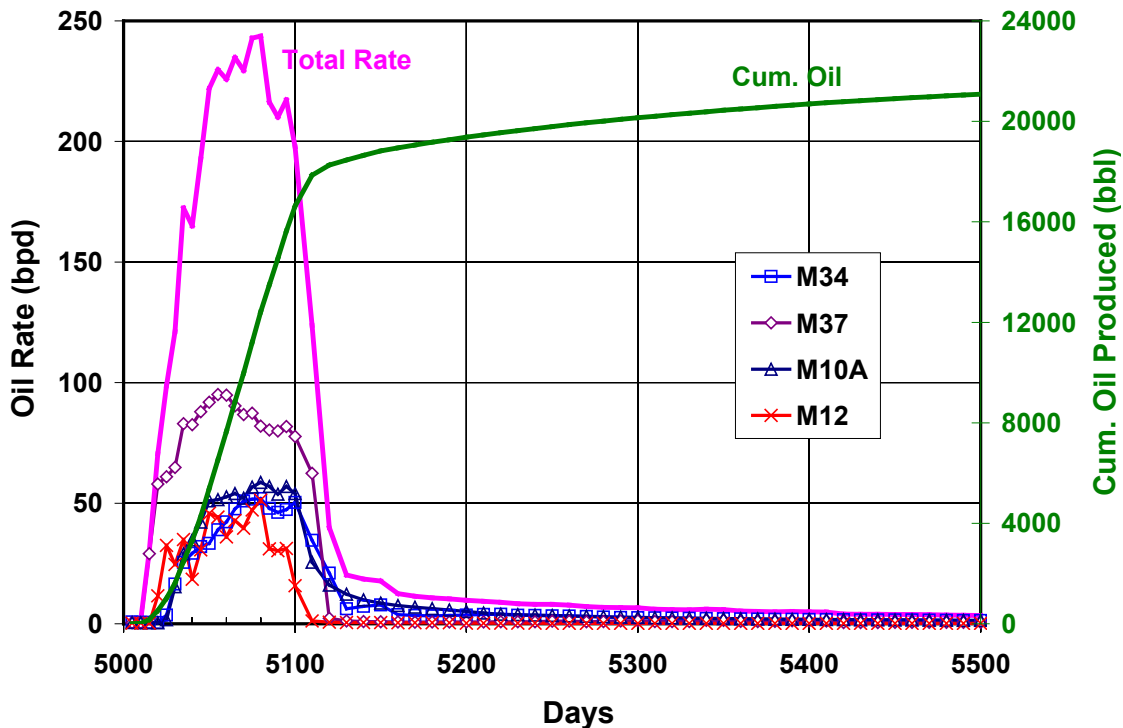


Figure B.17: Cumulative Oil Recovery and Oil Production Rate for Case 1 (base case ASP injection).

Oil saturation distribution at the end of the ASP flood is shown in Figure B.18 below. In the top three layers (high-perm), waterflood residual oil has been effectively recovered inside the pilot pattern, resulting in near zero residual oil saturation. Due to the permeability contrast, however, most chemicals only go into the high-perm top layers, leaving the bottom layer essentially untouched by chemicals, and at high oil saturation.

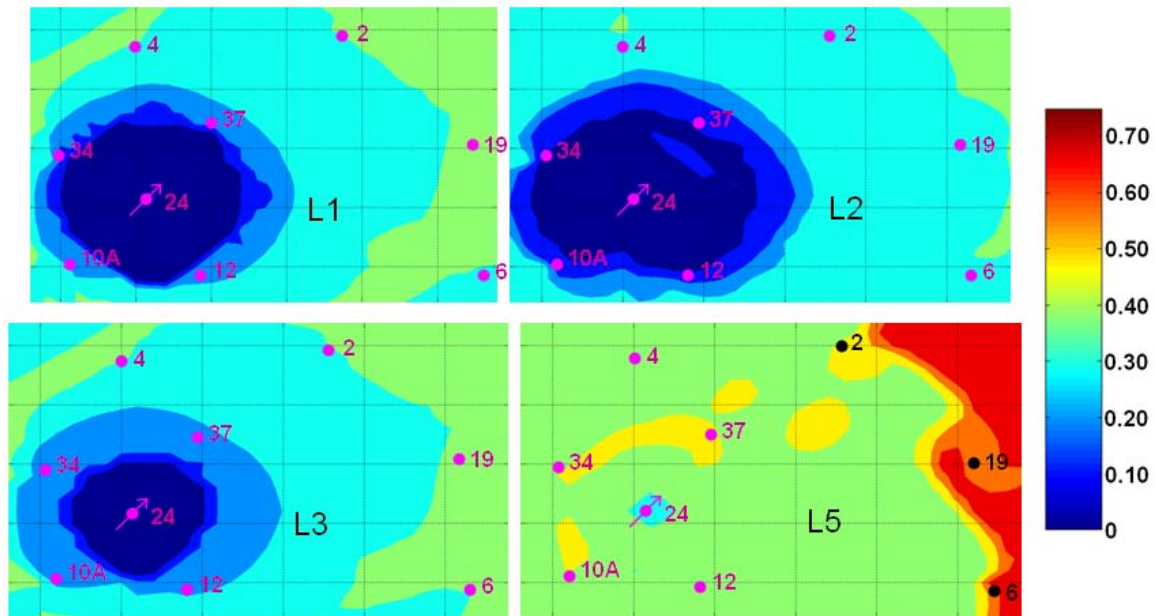


Figure B.18: Areal View of Post Chemical Flood Oil Saturation of Layer 1, 2, 3, and 5 for Case 1 (base case ASP injection).

Case 2: 2X ASP Injection

Chemical cost accounts for a major part of the expense during a chemical flood; hence, optimizing the injected chemical mass is crucial. In Case 2, the injected chemical mass is doubled (denoted as 2X ASP) for comparison with the base case. The cumulative oil recovery and oil production rate curves are shown in Figure B.19. The cumulative oil recovery after 500 days is 34,252 bbl due to more chemical mass injected. The maximum total oil production rate predicted by UTCHEM is about 270bpd. Similar

to Case 1, oil bank breakthrough occurs in all the wells within 30 days. The maximum oil rate occurs at about 70 days. After about 260 days since the start of the slug injection, the water cut goes back to 99%. Both chemical cost and oil production for this case are different from Case 1. Cost per barrel of oil produced is probably a better metric for economic comparison. For Case 2, this number is \$26.30/bbl, which is higher than Case 1. In the meantime however, significantly more oil has been produced; with high oil prices, the economics of this scenario could still be quite attractive. In the field execution phase, the decision was made to stick to the original 1X ASP injection plan due to project economics; and depending on field performance, further expansion of the project can be carried out accordingly.

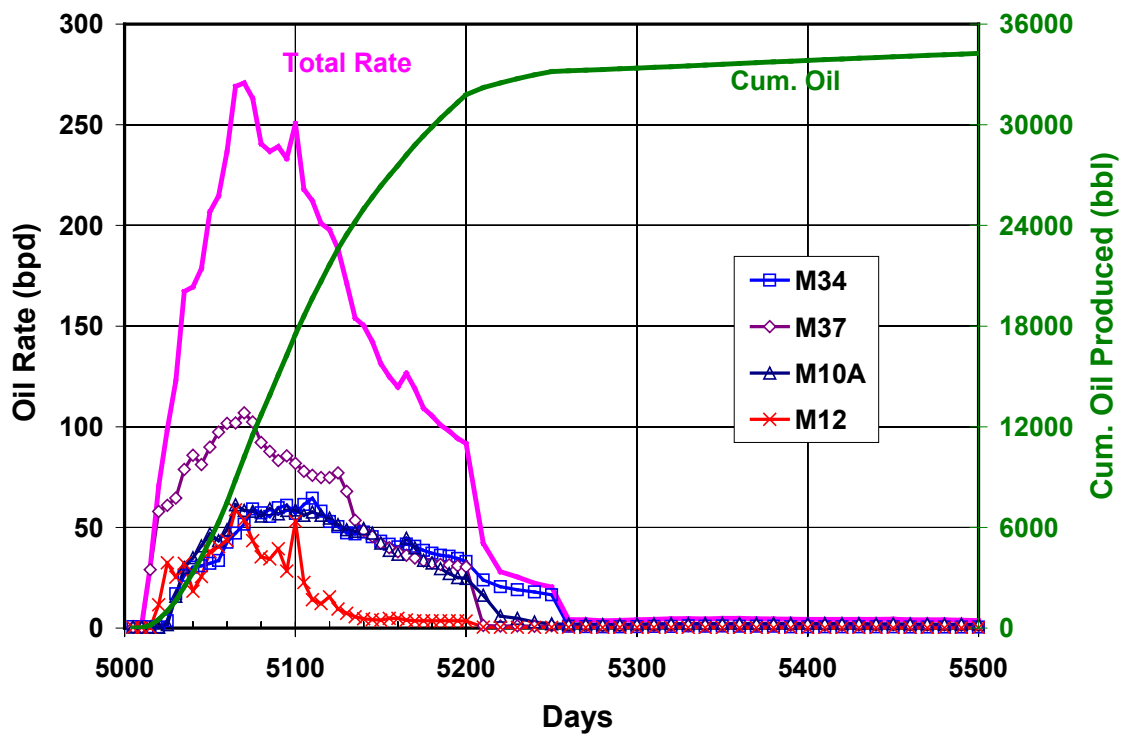


Figure B.19: Cumulative Oil Recovery and Oil Production Rate for Case 2 (2X ASP injection).

Oil saturation distribution at the end of the ASP flood is shown in Figure B.20 below. In the top three layers (high-perm), near zero residual oil zone is further expanded in this case due to more chemical injection. And chemicals start to penetrate into the low-perm bottom layer. The oil saturation of the near injector region has been effectively reduced.

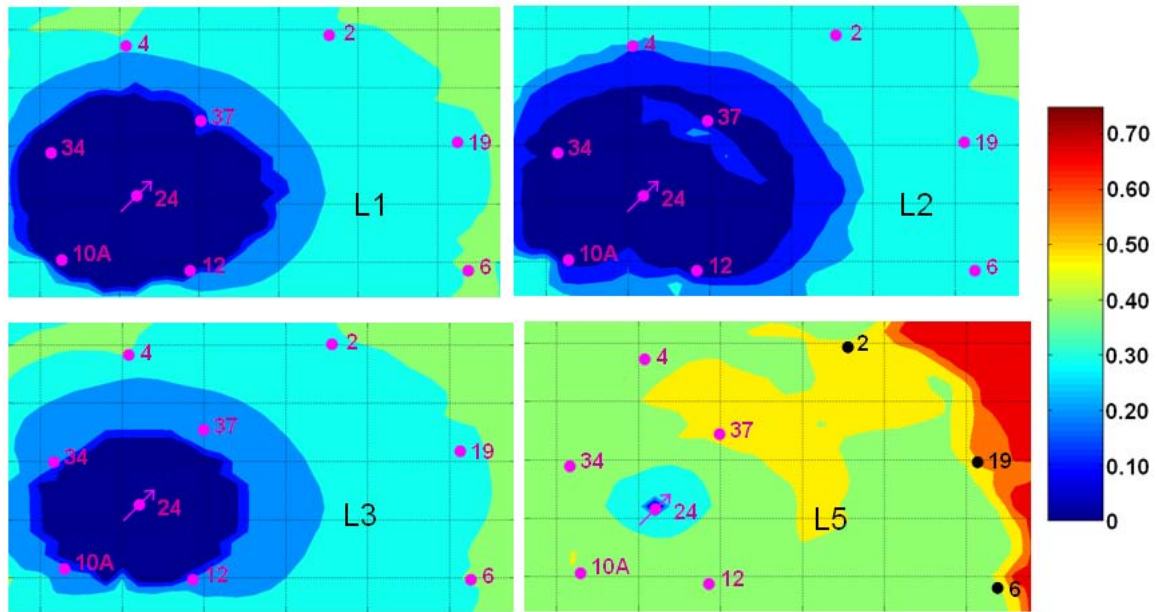


Figure B.20: Areal View of Post Chemical Flood Oil Saturation of Layer 1, 2, 3, and 5 for Case 2 (2X ASP injection).

Case 3: ASP Bottom Injection

As discussed before, oil saturations in the bottom layers are much higher than the top layers after the waterflood due to unfavorable permeability contrast. If more chemicals can be directed into the bottom layers, higher recovery can be expected. Two possible solutions are proposed: 1) injecting chemicals only into the bottom layer by blocking out the rest of the perforation interval, as discussed in this section; 2) injecting a small portion of polymer before the ASP slug for conformance control and enhancing

cross flow in the vertical direction. The cumulative oil recovery and oil production rate of Case 1 (base case ASP) is shown in Figure B.21.

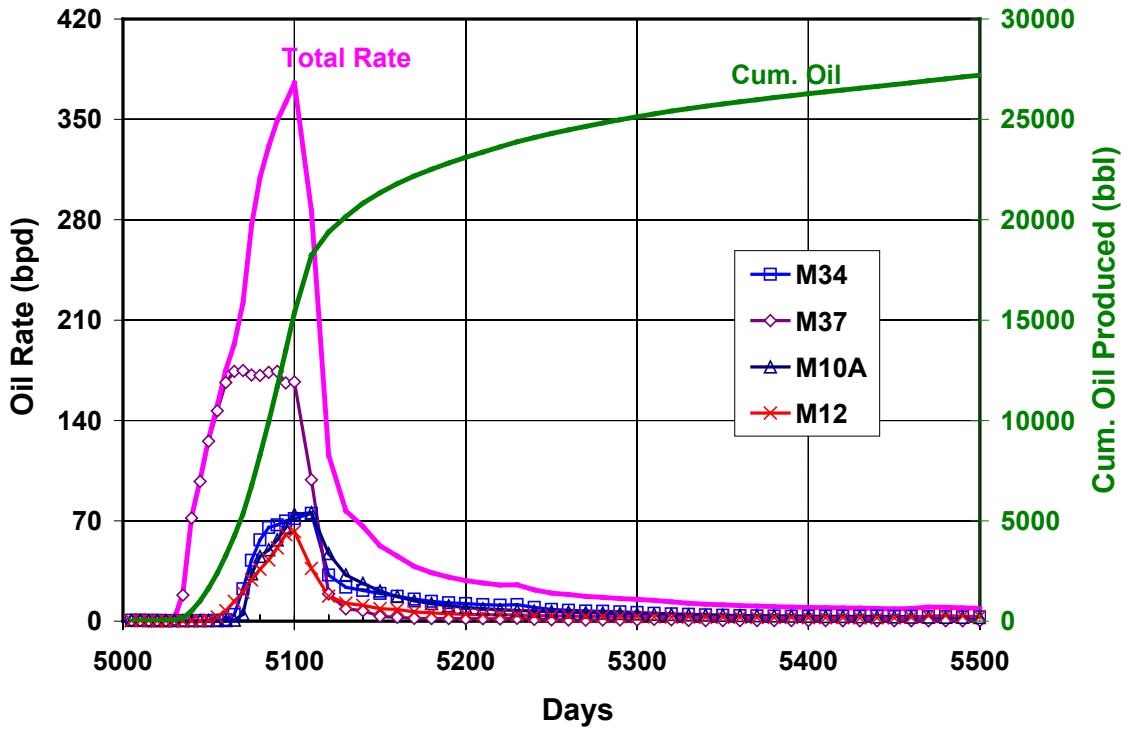


Figure B.21: Cumulative Oil Recovery and Oil Production Rate for Case 3 (ASP bottom layer injection).

The cumulative oil recovery after 500 days is 27,203 bbl. The maximum total oil production rate predicted by UTCHEM is about 375 bpd. Oil bank breakthrough at M37 occurs after about 35 days of injection. After 70 days, all the other wells show substantial oil production. The maximum oil rate occurs at about 100 days. After about 320 days since the start of the slug injection, the water cut goes back to 99%. Chemical cost per barrel of oil produced in this case is about \$16.55/bbl, which is much more attractive than Case 1 and Case 2. However, a practical concern for this scenario would be the fluid injectivity, considering the low permeability in the bottom layer. The simulation result

suggests an injection pressure way above formation parting pressure if this scheme were to be implemented in the field. Therefore, this bottom injection scenario was abandoned. Figure B.22 shows the effectiveness of this approach in recovering residual oil in low-perm bottom layers.

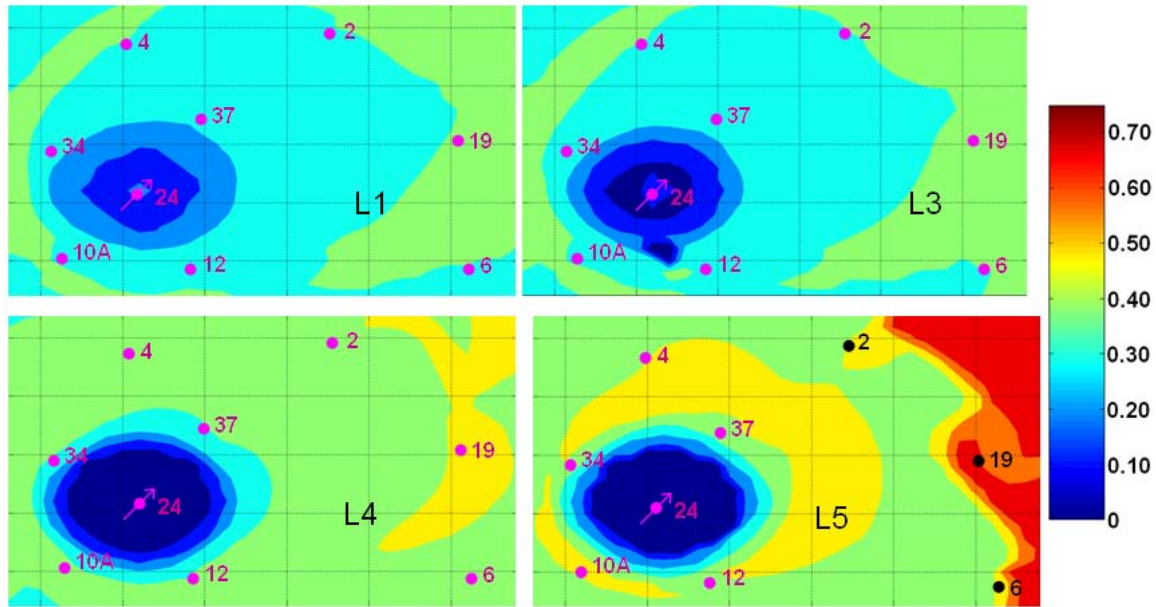


Figure B.22: Areal View of Post Chemical Flood Oil Saturation of Layer 1, 3, 4, and 5 for Case 3 (ASP bottom layer injection).

Case 4: Polymer Pre-Flush + ASP

As discussed above, another way to possibly modify the injection profile is to utilize a polymer pre-flush. In this case, 70 days of polymer is injected before the ASP slug. The cumulative oil recovery and oil production rate are shown in Figure B.23. The cumulative oil recovery after 500 days is 27,586 bbl. The maximum total oil production rate predicted by UTCHEM is about 565 bpd. Oil bank breakthrough occurs in all the wells after about 100 days of injection. The maximum oil rate occurs at about 120 days. After about 300 days since the start of the slug injection, the water cut goes back to 99%.

Chemical cost per barrel of oil produced in this case is about \$21.48/bbl, which is comparable to base case ASP flood. In the meantime, since quite a bit more oil (~ 6500bbls) are produced with the injection of pre-flush. The overall economics for this case is better than the base case.

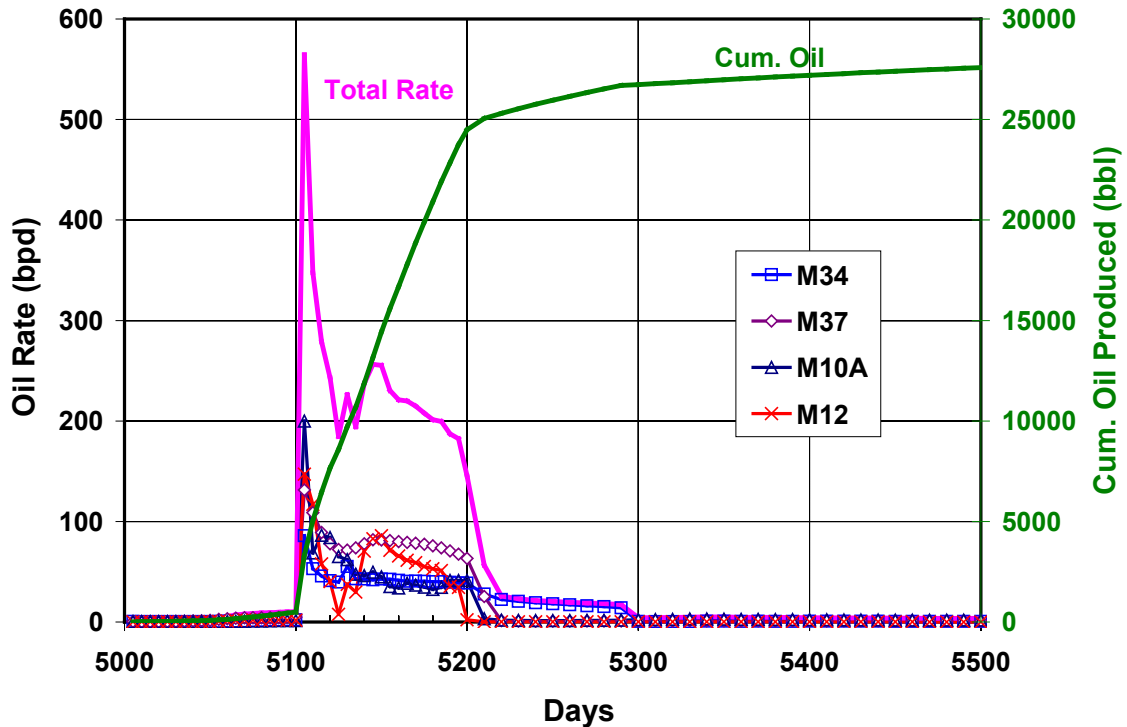


Figure B.23: Cumulative Oil Recovery and Oil Production Rate for Case 4 (Polymer Pre-flush and ASP flood).

Figure B.24 below shows the impact of the polymer pre-flush on sweep efficiency, especially on the bottom low-perm layer. Apparently more of the surfactant slug has been directed into the low-perm layers due to the enhanced cross flow between different layers. Hence we observe in Figure B.23 that substantial enhancement of oil recovery is achieved with this polymer pre-flush injection scheme.

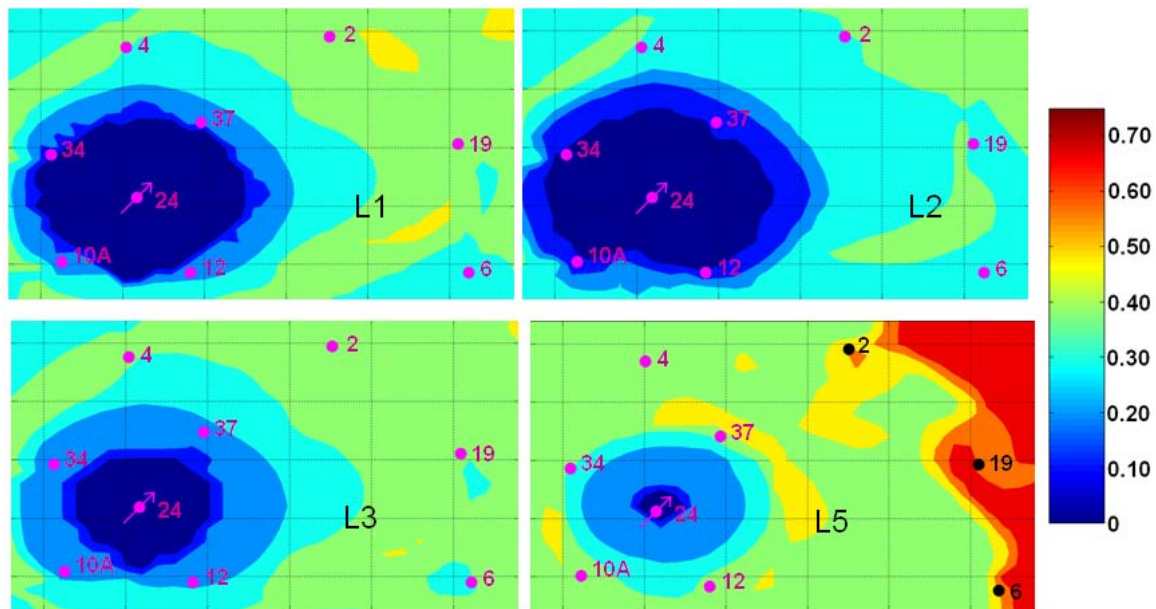


Figure B.24: Areal View of Post Chemical Flood Oil Saturation of Layer 1, 2, 3, and 5 for Case 4 (Polymer Pre-flush and ASP flood).

Case 5: ASP with Doubled Production Rates

Considering the active aquifer influx in the pilot area, one of the concerns is the dilution of chemicals once they are injected. By producing at higher rates on the pilot producers, it is hoped that this dilution effect can be mitigated. In case 5, all the producers now are set to produce at double rates (two times the rates specified in Table B.11). The cumulative oil recovery and oil production rate are shown in Figure B.25. The cumulative oil recovery after 500 days is 31,400 bbl. The maximum total oil production rate predicted by UTCHEM is about 345 bpd. Oil bank breakthrough occurs in all the wells after about 30 days of injection. The maximum oil rate occurs at about 70 days. After about 230 days since the start of the slug injection, the water cut goes back to 99%. Chemical cost per barrel of oil produced in this case is about \$14.33/bbl, which is apparently the best of all cases studied so far. In practice, however, there is a maximum production rate for the pumping unit used in the field. For this project, this upper limit is

600bpd. Figure B.26 below shows the oil distribution after the ASP flood. Although producing at much higher rates in this case, the total chemicals injected remain the same as the base case, therefore, the areal impact of the slug injection is about the same as the base case.

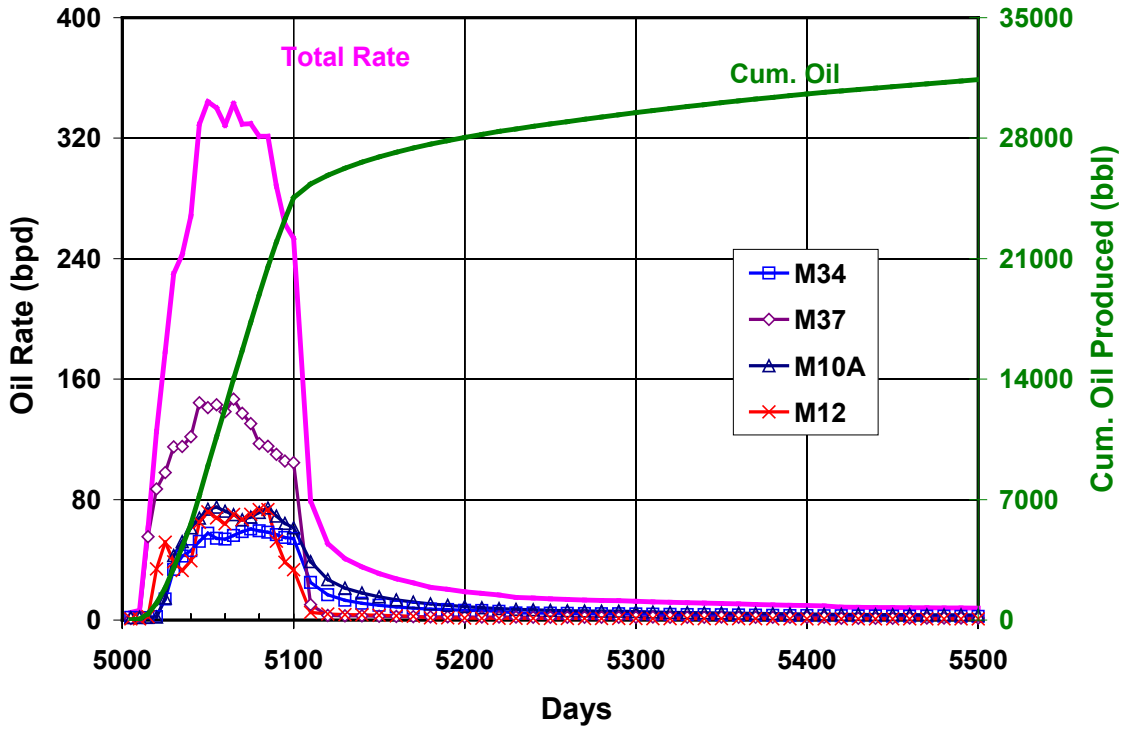


Figure B.25: Cumulative Oil Recovery and Oil Production Rate for Case 5 (ASP with doubled production rates).

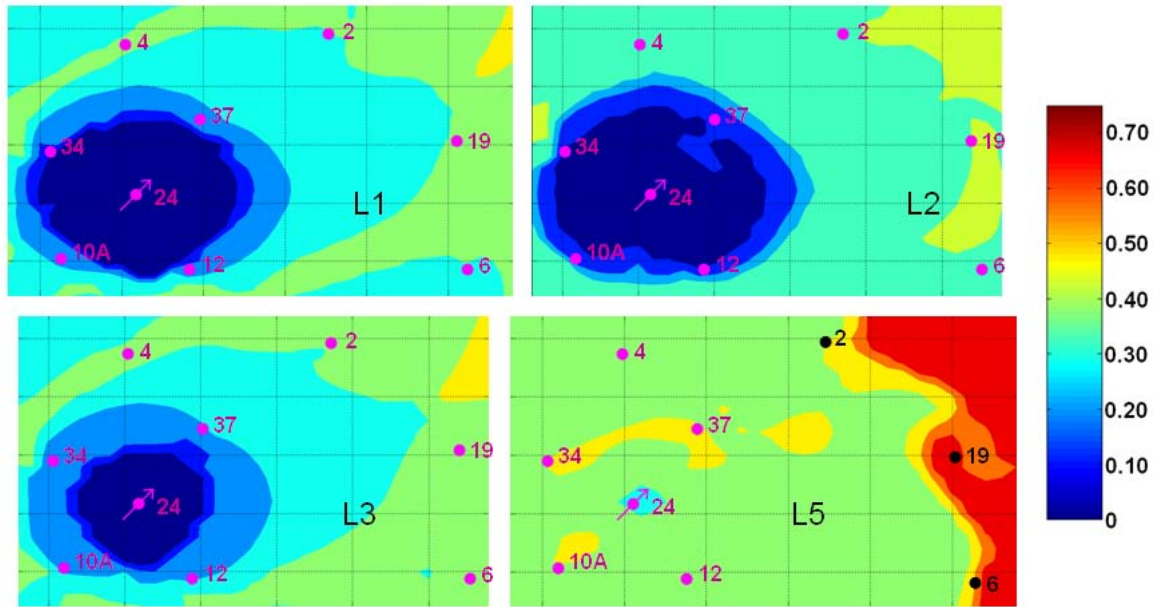


Figure B.26: Areal View of Post Chemical Flood Oil Saturation of Layer 1, 2, 3, and 5 for Case 5 (ASP with doubled production rates).

Summary

Table B.13 below summarizes the simulation results for all five cases studied in this section. Figure B.27 shows the cumulative oil recovery history for these scenarios.

Table B.13 Simulation Results Summary for Different Operating Strategies.

Case #	Brief Description	Oil Recovered (bbl)	Max. Rate (bpd)	Time to Reach 1% Water Cut (days)	Cost (\$bbl)
1	ASP base case	21085	235	290	21.35
2	2X ASP	34252	270	260	26.30
3	ASP bottom inj.	27203	375	320	16.55
4	Pre-flush + ASP	27586	565	300	21.48
5	2X prod. rates	31400	345	230	14.33

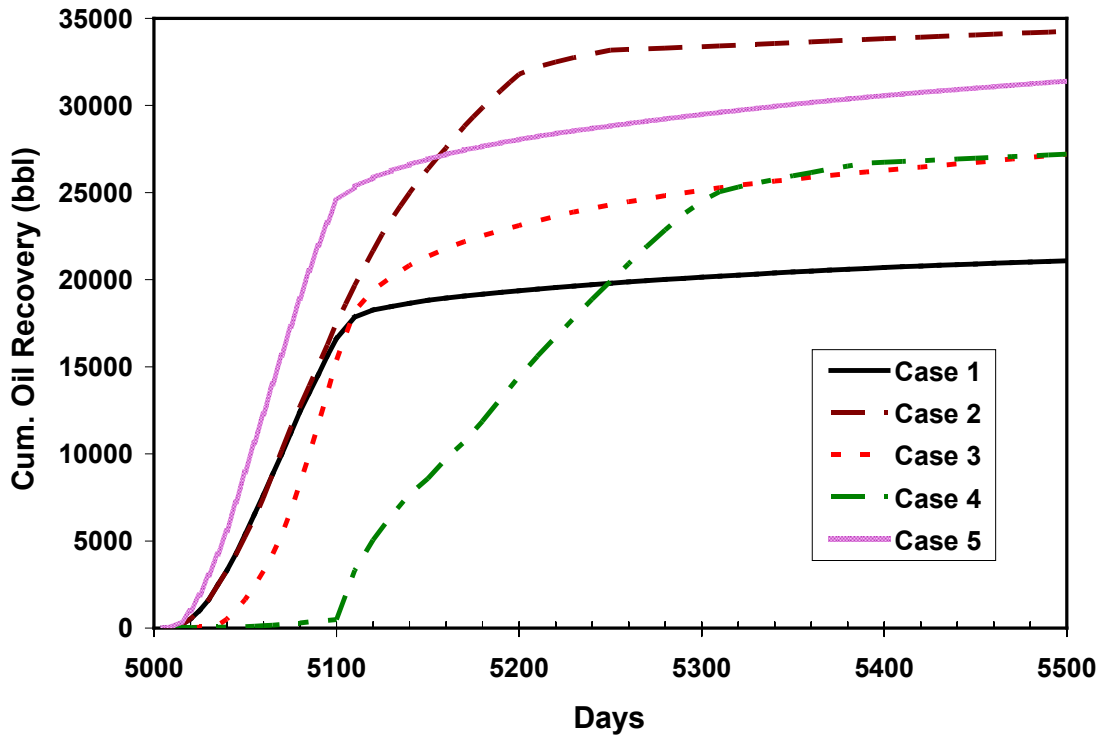


Figure B.27: Cum. Oil Production Comparison between 5 Cases Studied.

The 5-layer pilot-scale model has been used to studied different possible operating strategies in the field. The simulation results can be used to guide field execution and some of the general observations can be summarized below:

- 1). The originally planned amount of chemicals should be injected as the initial phase of the project, and depending on field performance, the injection can be expanded to larger volumes;
- 2). A polymer pre-flush will be helpful in getting the injection profile more uniform and help recover oil in the bottom layers;
- 3). Higher production rates will help counterbalance the influence of the aquifer influx, and thus should be implemented in the field when possible;

- 4). Injectivity might be an issue for chemical injection and will need careful monitoring in the field.

B.2.4 Sensitivity Simulations for ASP Flood (w/ 9-Layer Model)

The previous section's simulations using a 5-layer model provided some general guidelines for field. To further refine the work from the pilot-scale 5-layer study, a 9-layer model was employed and various sensitivity cases were simulated with different polymer concentration, total chemical mass, and alkali consumption.

Polymer Concentration Sensitivity

The importance of polymer in the ASP flood can never be overstated. Sufficient polymer in the flood provides good mobility control and decreases the chances of fingering and bypassing mobilized oil. Moreover, in the polymer drive phase, the typically lowered salinity provides a salinity gradient for the surfactant slug.

The sensitivity of oil recovery to polymer concentration is studied through a comparison with the base case ASP simulations. The base case here is the same as Case 1 investigated in the previous section, where a concentration of 4000ppm 3330S was used in the flood. Before going into details of the sensitivity study, the results of the simulations with the 5-layer and 9-layer grid models are presented in Figure B.28 below. The refined 9-layer model shows a higher oil production of 23,756bbbls, or 2700bbbls more oil in comparison with the coarser 5-layer model. The oil recovery and daily production rate decreased with an increase in the size of the grid block. The reason for the difference in recovery as discussed by Veedu (Veedu, 2010), was the surfactant and sodium carbonate dilution in large grid blocks. The following sensitivities were based on the 9-layer base case ASP simulation, with only changes made on polymer concentration, to 2000ppm and 3000ppm.

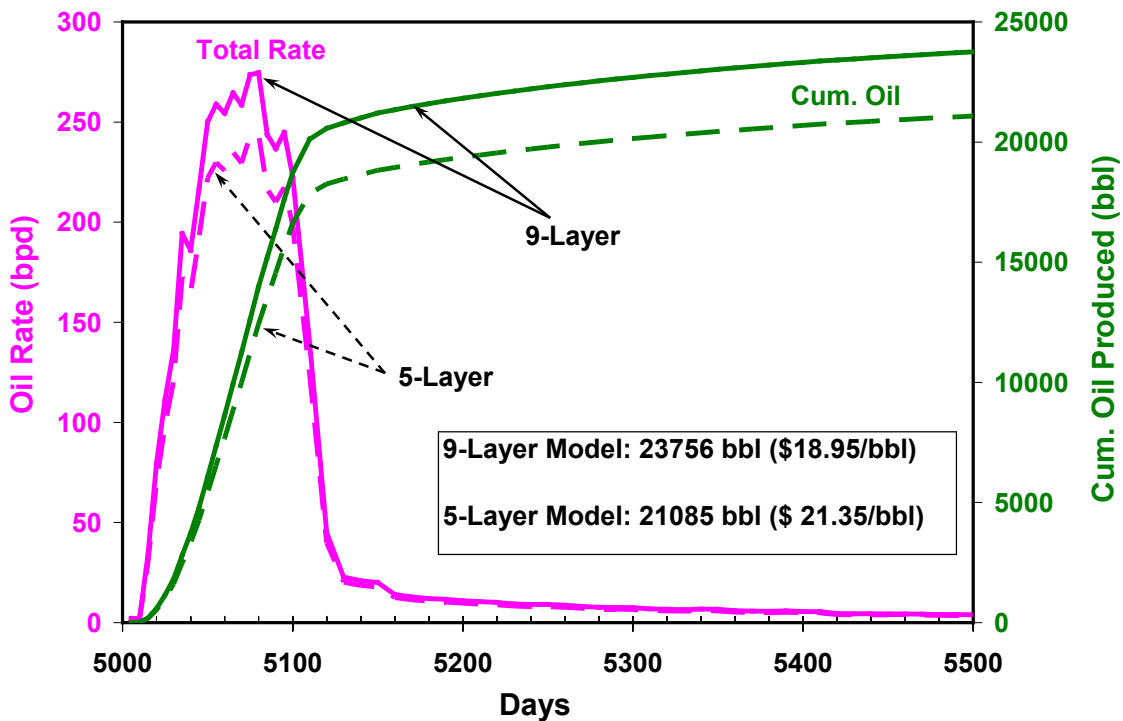


Figure B.28: Cum. Oil Production and Total Oil Rate Comparison between 5-Layer and 9-Layer Models.

The cumulative oil recovery and oil production rate plots for these two cases are shown in Figure B.29 to Figure B.31. Figure B.31 presents the cumulative oil recovery comparison for all the sensitivity cases. Clearly, as the polymer concentration is increased, the recovery increases. This can be attributed to the better mobility control due to the higher computed grid-block concentration of polymer. Recall from the linear coreflood experiment and simulation results, where 2000ppm polymer was able to provide sufficient mobility control in a homogeneous coreflood setting. The mobility ratio during a core flood can be estimated by taking the ratio of pressure gradients in the oil bank and surfactant slug (Yang *et al.*, 2010). Judging from Figure A.27, this ratio was very close to 1, thus the mobility control was only marginally achieved in the 1D linear

core flood. In a more realistic heterogeneous pilot model (although still a much simplified one), this marginal mobility control was no longer sufficient. Therefore, 4000ppm 3330S concentration was used in all the simulation cases in the previous section to ensure an adequate mobility control. In the field, however, a higher molecular weight 3430S polymer was chosen to provide an equivalent viscosity but at a lower concentration.

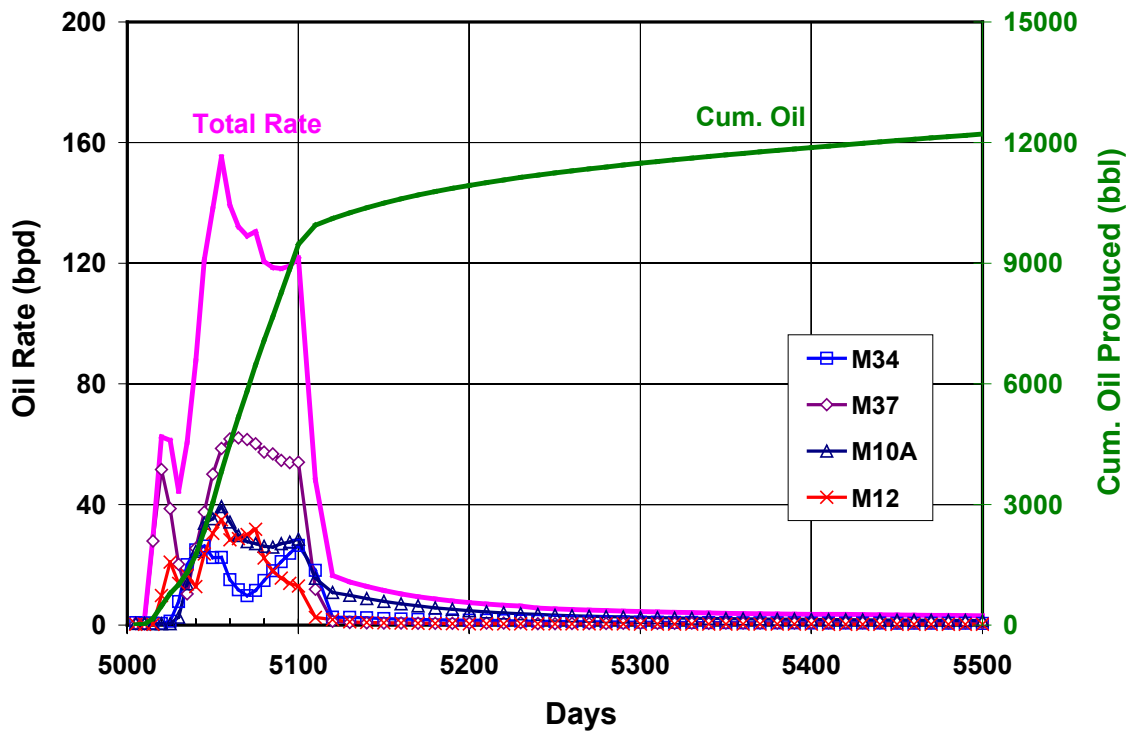


Figure B.29: Cumulative Oil Recovery and Oil Production Rate for ASP Simulation with 2000 ppm Polymer.

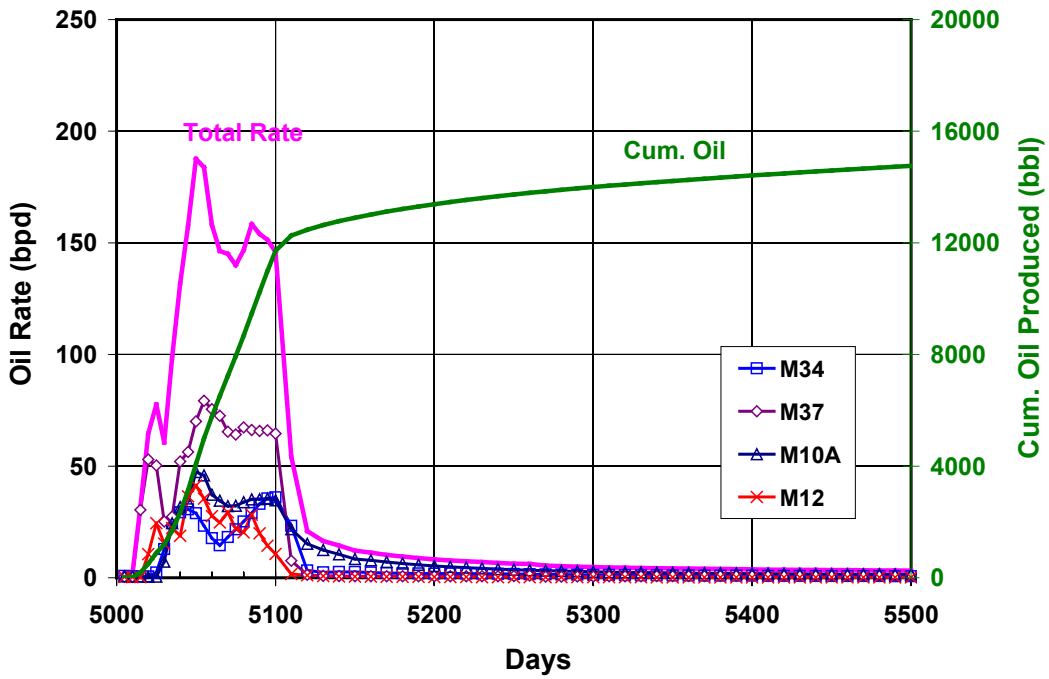


Figure B.30: Cumulative Oil Recovery and Oil Production Rate for ASP Simulation with 3000 ppm Polymer.

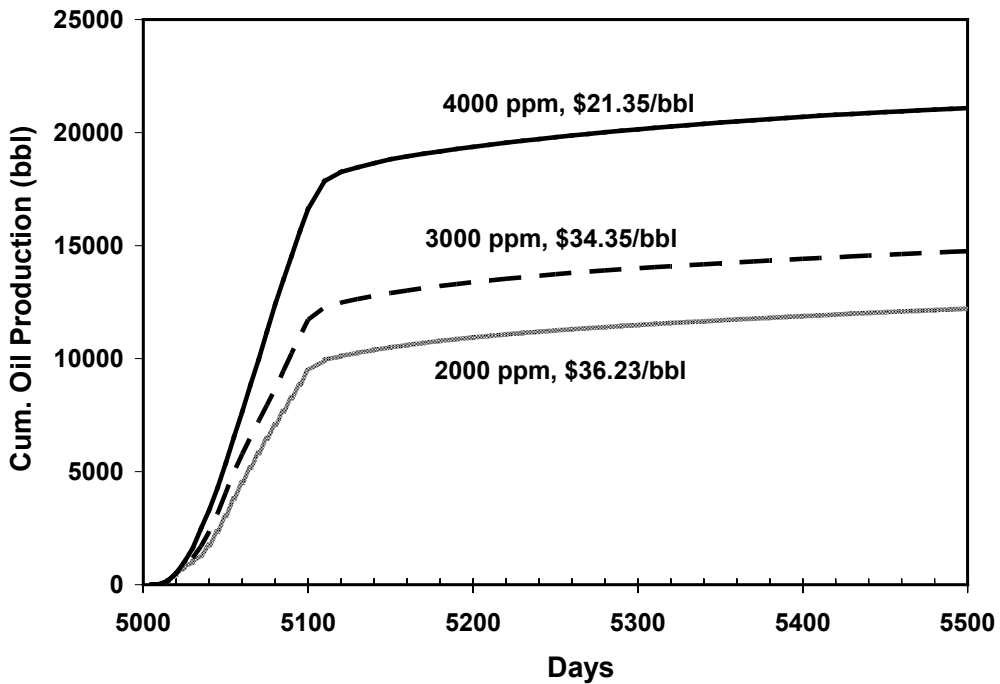


Figure B.31: Effect of Polymer Concentration on the Recovery Results of ASP Flood.

Total Chemical Mass Sensitivity

It is important in a surfactant flood to have a sufficient amount of chemicals injected to sweep the designed pilot pore volume. However, the existence of fractures near an injector, and thief zones in a pilot pattern, as well as poor fluid confinement within the pattern, result in big uncertainties in the chemical mass estimation. In this sensitivity study, the injected chemical mass is varied around that of a base case (which is equivalent to changing the swept pore volume), and the impact of this change is examined.

The base case scenario includes a 70-day polymer pre-flush, 200-day of surfactant slug (at a rate of 300 bpd), 250-day polymer drive and chase water injection till 1000 days. The injection rate in this sensitivity study was reduced to 300 bpd due to the practical concerns on polymer injectivity. All the producers were set to produce at maximum rate of 600 bpd to counteract the dilution of aquifer influx. Different cases studied includes: 1) base case; 2) 15% less total chemical (or equivalently 15% more-than-expected swept pore volume); 3) 15% more total chemical; and 4) 30% less total chemical.

The cumulative oil recovery and oil production rate plots for these four cases are shown in Figure B.32 to Figure B.35. The production profiles for different cases are quite similar in terms of peak and average production rates. The main difference is the duration of the active production period.

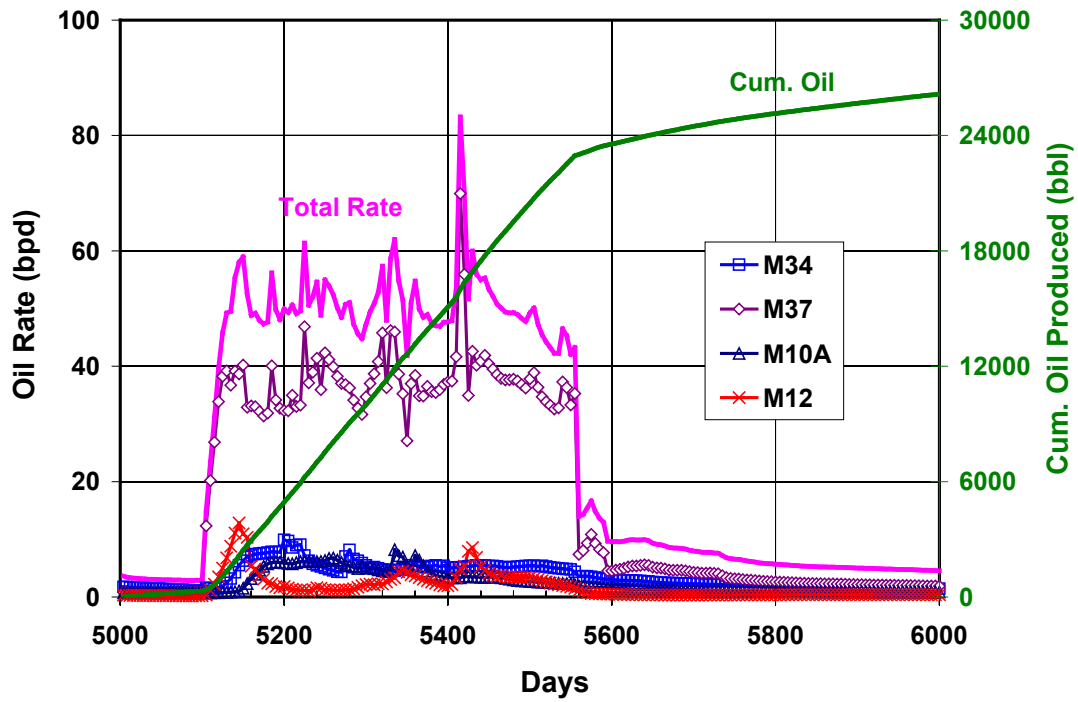


Figure B.32: Chemical Mass Sensitivity Study: Base Case.

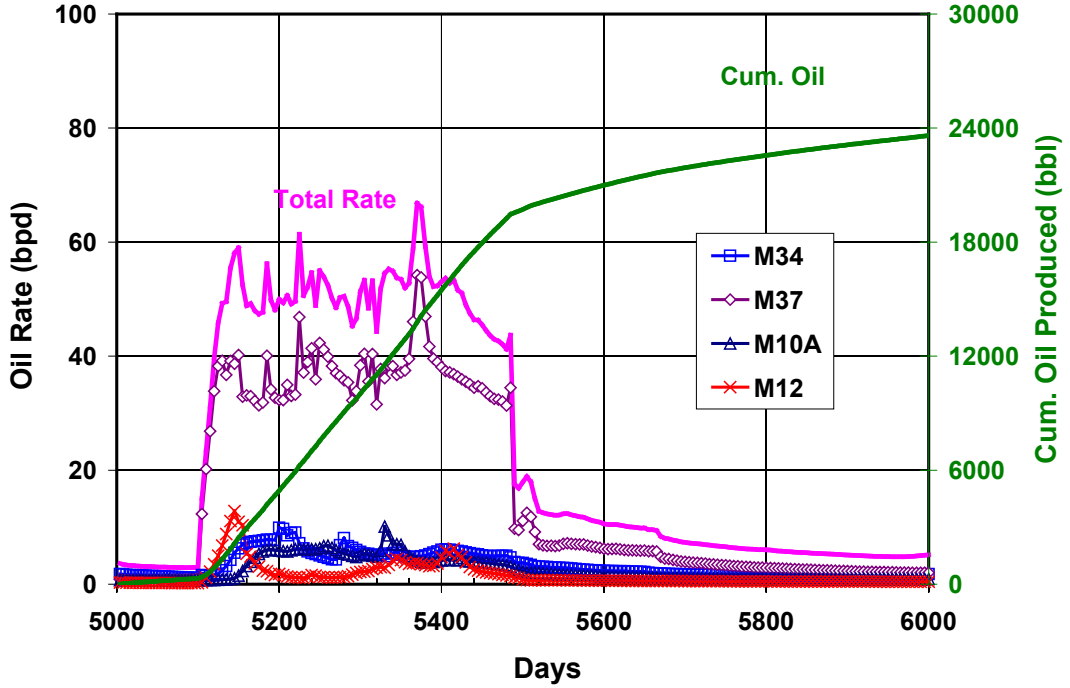


Figure B.33: Chemical Mass Sensitivity Study: 15% Less Chemical Mass.

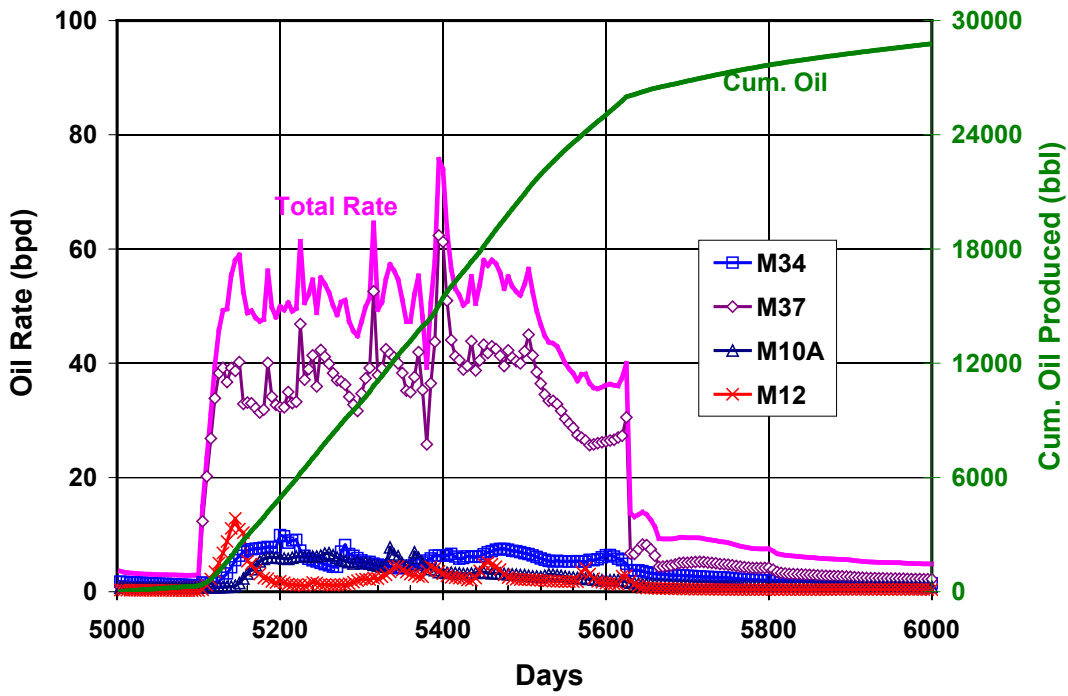


Figure B.34: Chemical Mass Sensitivity Study: 15% More Chemical Mass.

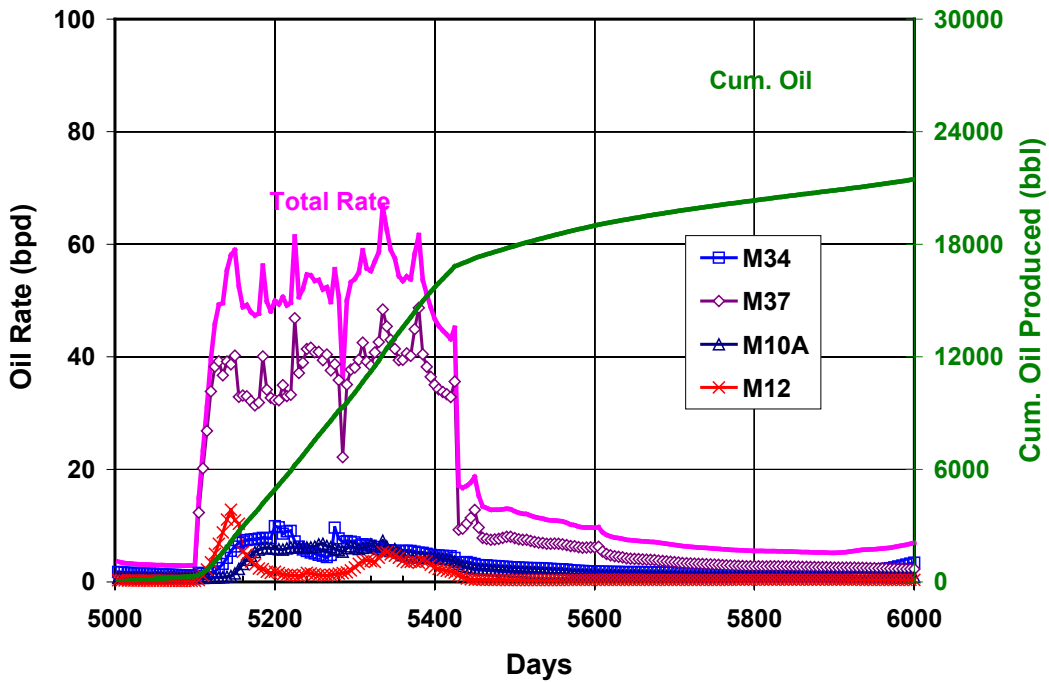


Figure B.35: Chemical Mass Sensitivity Study: 30% Less Chemical Mass.

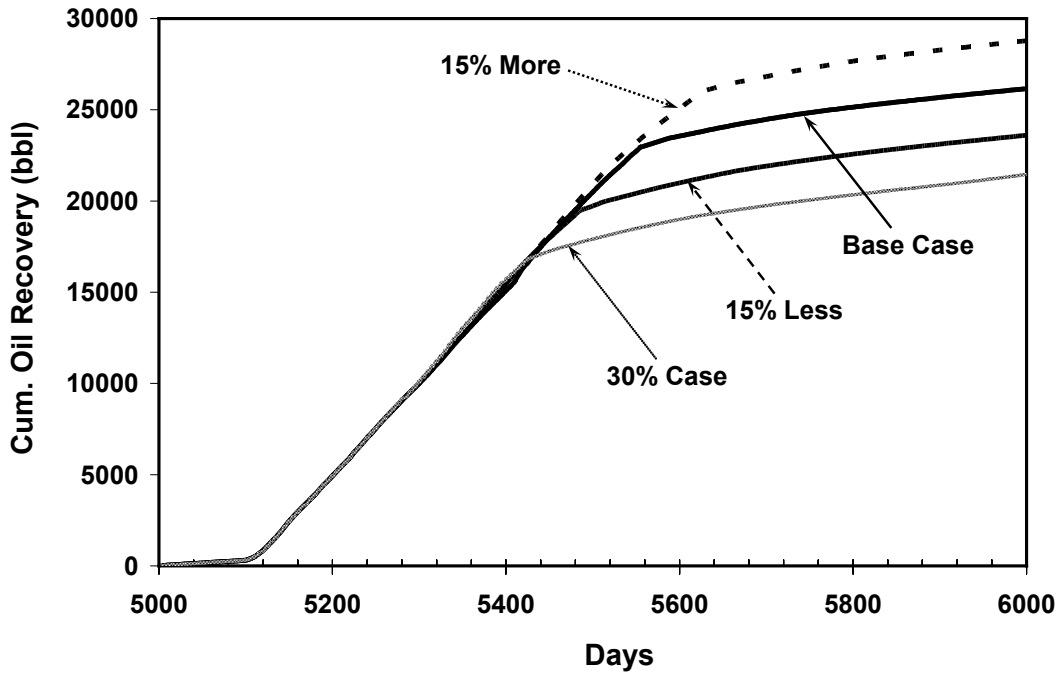


Figure B.36: Cum. Oil Production Comparison between the Chemical Mass Sensitivity Cases.

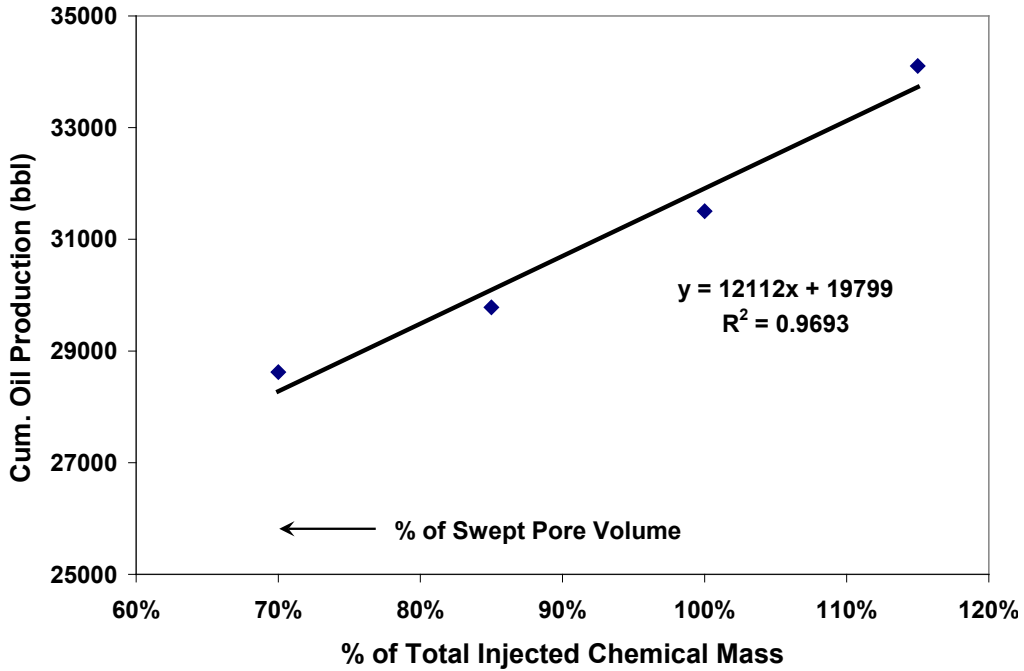


Figure B.37: Dependence of Cum. Production on Total Injected Chemical Mass (or Swept Pore Volume).

Figure B.36 presents the oil recovery comparison for all the simulated cases. As the total injected chemical mass is increased, the simulated oil recovery increases. The cumulative oil production shows a linear increase with total injected mass (Figure B.37), which again is equivalent to a decrease in swept pore volume. In a case where the true swept pore volume is larger than expected, the designed injection mass would be smaller than needed which results in less oil recovery. Depending on how well the swept pore volume is estimated, this impact could be quite substantial, and the associated risk should be carefully evaluated.

Alkali Consumption Sensitivity

During an ASP flood, the high pH front is retarded by geochemical reactions in the reservoir. When alkali is injected in the slug with surfactant and polymer, the concentration of alkali must be high enough to satisfy alkali consumption and still transport with the surfactant. It is therefore very important that ASP pilots be designed taking into account the consumption of alkali in the reservoir. When there is a high level of alkali consumption, the pH front cannot be propagated at the same rate as the synthetic surfactant, thereby reducing the slug effectiveness. Large consumption of alkali also causes adverse changes in total salinity if most of the alkali is consumed. Various alkali consumption/retardation mechanisms (Dean, 2011) include mixing with hard formation water in front of the slug, mixing with cations from ion exchange with clay, sodium/hydrogen base exchange, and reaction with minerals that dissolve at high pH.

Novosad (1984) carried out experiments to measure the alkalinity loss resulting from cation exchange capacity (CEC) in Berea cores. They found out the CEC is between 0.1 and 0.4meq/100g rock. They noted that the cation exchange capacity was about half of the total exchange capacity. Cation exchange reactions are much more significant for

large-surface-area clay contents (Mohnot *et al.*, 1987). Another cause of alkali consumption lies in the reaction of alkali with rock minerals (Sydansk, 1982). It is generally recognized (Mohammadi, 2008) that the increase of pH, temperature, and contact time with minerals increases the alkali consumption. It is, therefore, of key importance to load the ASP slug with sufficient amount of alkali for contingency, especially when the CEC condition in the reservoir is uncertain. This way the performance of the slug can be ensured even when the consumption is higher than expected. In the meantime, however, the impact of high alkali concentration on phase behavior should also be carefully evaluated. Dean (2011) performed core flood experiments on a Bentheimer sandstone of high clay content (CEC = 2meq/100g rock). For a non-reactive crude at 86°C, a 0.3 PV slug of 0.7% Na₂CO₃ is more than minimum required mass and concentration at a reasonable field flux of 0.33ft/D. When the crude oil is reactive however, alkali will also be consumed to generate soap (Hourshad, 2008).

Different alkali consumption scenarios are examined in this sensitivity study by adjusting the cation exchange capacities in the simulation model. The CEC value was changed from virtually zero to 0.15meq/ml of PV (2.8meq/100g rock, $\phi = 0.33$, $\rho_s = 2.65$ g/cc). The injection sequence consisted of 10 days of polymer pre-flush, followed by ASP slug injection. Figure B.38 demonstrates the effect of CEC on effluent pH on two producers, M37 and M34. The fact that M37 well is closer to the injector M24 than M34 results in an earlier pH breakthrough on M37. As the CEC value becomes higher, more alkali will be consumed in the reservoir, which translates to slower propagation of the pH front, or later pH breakthrough on the producers.

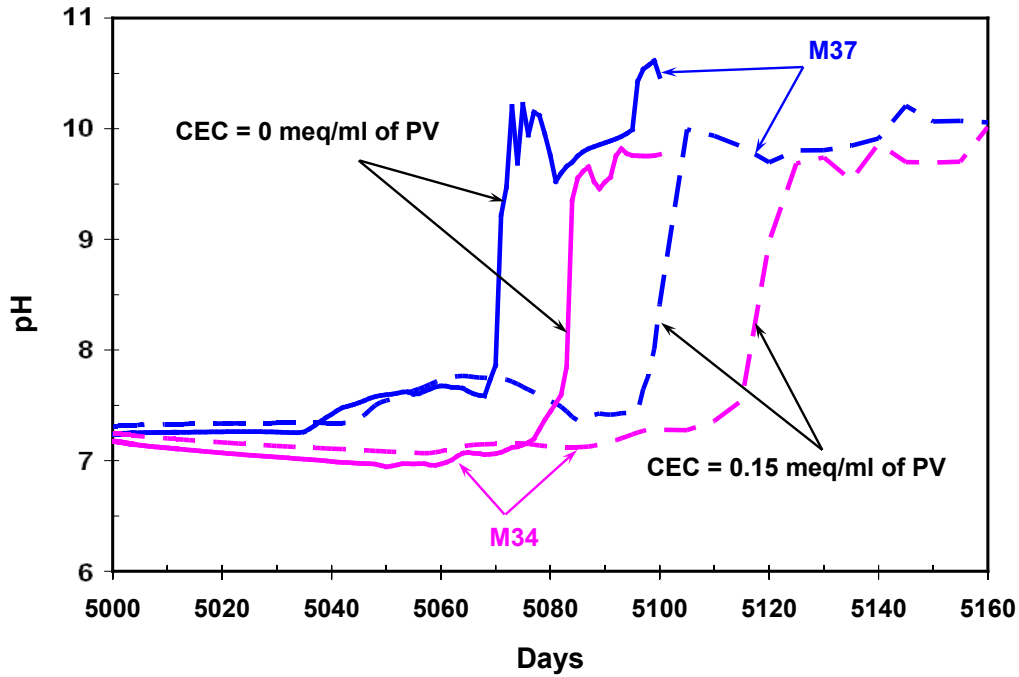


Figure B.38: pH Breakthrough Profiles on M37 and M34 with Two Different Cation Exchange Capacities.

Hourshad (2008) performed a 1D core flood simulation to study the alkali consumption and resulted pH front retardation in a sandstone reservoir rock. A relatively large CEC value of 1.8meq/100g rock was used to account for high clay content in the rock. At 1PV injection volume, a spatial separation of $X_D=0.4$ between the pH and surfactant fronts was clearly shown from her study. Figure B.39 above delivers the same idea for current 3D simulation, only from a temporal viewpoint. The impact of a high CEC value on the propagation of pH and surfactant fronts was evident. As the CEC value gets larger, alkali consumption goes up in the reservoir, and thus the pH front starts to lag behind the surfactant concentration front. With a CEC value of 0.15meq/ml of PV, it takes much more time for the pH to break through after the surfactant front reached the producer. This is very likely to be caused by the high CEC and a slower pH front.

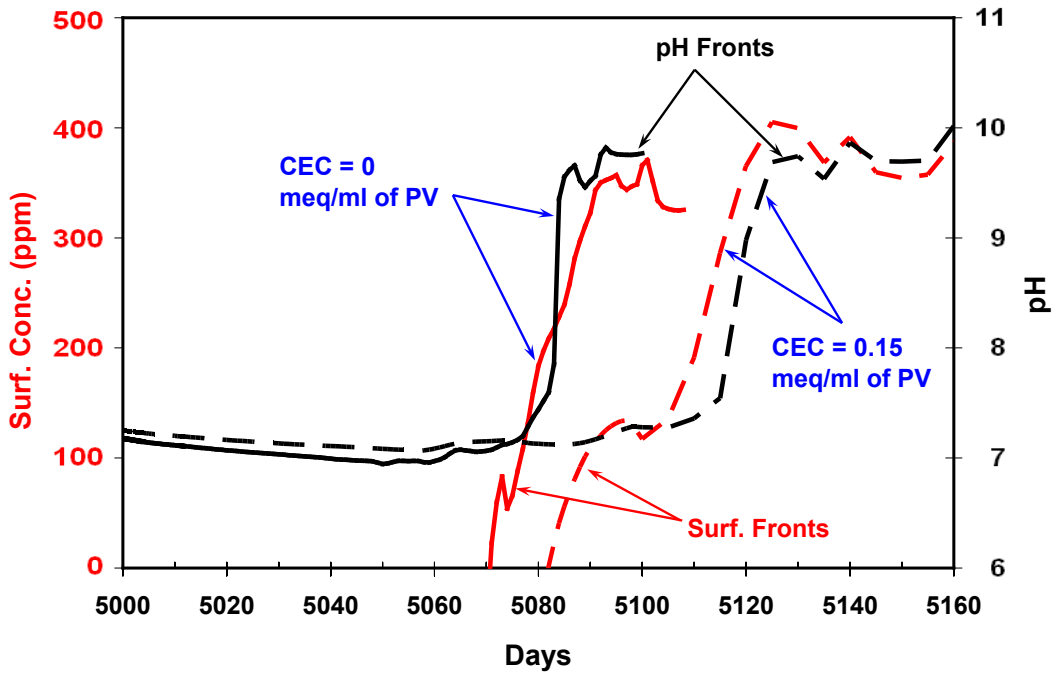


Figure B.39: pH and Surfactant Breakthrough Profiles on M34 with Two Different Cation Exchange Capacities.

For zero or low CEC for Berea (Novosad *et al.*, 1984)), we would not expect to see significant separation between the pH and surfactant fronts with Berea sandstone, which apparently agrees with what we have seen from the Berea core flood experiment. However, the mineralogy and lithology of the Brookshire field Catahoula sand is quite different from Berea sample used in the lab, and the reservoir rock may contain high clay content, which in turn would dramatically change the phase behavior and optimum condition of the system. It is probably worth mentioning that pH front always breaks through in all simulation runs, even though it might take much longer time to happen. In the field (see next chapter), however, pH breakthrough has yet to be observed, even on the nearest producer.

B.3 SECTION SUMMARY

The Brookshire Dome ASP pilot flood was simulated using UTCHEM. The pilot model was built upon the success of history matching lab-scale coreflood experiments. Geologic uncertainties still remain a challenge. Field inputs, including well logs, an injection well spinner survey, an inter-well tracer test, and waterflood production data, were used for setting up the pilot-scale model. Different possible operating strategies were simulated and compared with a base case scenario where a surfactant slug with a chase polymer drive was injected as done in the coreflood. Various sensitivity runs were performed on different factors impacting the project performance. Some of the more general conclusions and directions for improvement are as follows:

1. A polymer pre-flush will be helpful in getting the injection profile more uniform and thus recover oil from the bottom low-perm layers; higher production rates will help counterbalance the influence of the aquifer influx, and thus should be implemented in the field when possible; injectivity might be an issue for chemical injections and will need careful monitoring in the field; chemical injection should be carried out following the original plan, and depending on field performance, the project can be expanded to a larger scale.
2. A pilot project is always challenged by unexpected problems and potential risks. A sensitivity study on different factors is thus very helpful and useful for project design. Mobility control is crucial to ensure the integrity of the ASP slug and the successful recovery of the mobilized oil. It is also important to recognize and be fully aware of the impact of various uncertainties on the pilot performance. Two among many others are swept pore volume estimation and alkali consumption in the pilot pattern. Sensitivity studies conducted in this section clearly shows how big a difference they can make.

3. The current pilot-scale geological model is over-simplified. The poor match to the field tracer test and our inability to predict chemical injectivity pose serious questions about the accuracy of the results obtained from the model and they need to be interpreted and evaluated with caution.

C. Field Implementation and Performance Update

A tertiary alkaline / surfactant / polymer flood was implemented From September 2011 to March 2012 in the Brookshire Dome field, Texas. Production monitoring and data collection are continuing at this time. With initial discovery of the Catahoula sand formation in 1996 and over 15 years of waterflooding and infill drilling, oil cuts are less than one percent, suggesting that the reservoir is approaching residual oil saturation to waterflood. The mature stage of the field makes it a typical candidate for the application of a chemical EOR process.

As discussed in previous sections, laboratory phase behavior and coreflood experiments were conducted to determine the optimal chemical formulation for the field crude oil and to provide essential parameters for a numerical simulation model. Spinner survey and an inter-well tracer test program were conducted to collect reservoir information and understand well connectivity, as well as support the interpretation of the pilot results. A field laboratory was set up onsite to monitor the quality of injected and produced fluids. We discuss in this section the field implementation, results of the pilot to date, major risks and uncertainties encountered during field execution, and the important lessons learnt from the project.

C.1 FIELD IMPLEMENTATION

C.1.1 Field Injection Plan

The original injection plan was to inject 0.3PV of an ASP slug followed by 0.7PV of a polymer drive. The surfactant formulation contained 0.3wt% Petrostep S-13C, 0.2wt% of Tomadol 15-12 (field substitute for Neodol 25-12), and 0.8wt% of Na_2CO_3 . Notice that the co-solvent concentration was raised (from 0.1wt% in the lab) to ensure

aqueous stability of the injected slug. And the alkali concentration was reduced by 0.2wt% (from 1wt% in the lab) to account for the downshift of optimum salinity observed during QC on the field surfactant batch. This decrease in alkali concentration, however, caused a possible risk of insufficient alkali injection due to high consumption. To ensure a stringent mobility control, the higher molecular weight 3430S polymer (EOR 90) was used at an average concentration (over the entire injection period) of 2700ppm. Even higher concentration of polymer was actually used due to viscosity loss when switching to new polymer batches.

In view of severe layering of the reservoir and unfavorable oil distribution (high oil saturation in bottom layers of low permeability), a polymer pre-flush was designed for conformance control and was injected in the field before the ASP slug. The polymer concentration was tapered off in the drive phase and chase water was injected at the tail end. Table C.1 below lists the final chemical injection schedule, in terms of pore volume of fluid injected and nominal concentration of chemicals.

Table C.1 ASP Pilot Final Injection Schedule.

Injection Phase	Pore Volume	Nominal Concentration (%)		
		Alkali	Surfactant + Co-solvent	Polymer
Polymer Pre-Flush (PPF)	0.05	---	---	0.24
ASP Slug (ASP)	0.3	0.8	0.5 (w/ EDTA)	0.28
Polymer Drive (PD)	0.7	---	---	Tapered
Chase Water (CW)	continuous	---	---	---

C.1.2 Project Timeline

Table C.2 shows the overall timeline of the project. Since the start of the project, Layline Petroleum has been proactive in executing the pilot. Laboratory experiments to select the ASP formulation and test it in corefloods were concluded in April, 2011, at the

University of Texas. Numerical simulations were also done afterwards at the University of Texas (Section B). Based on these test results, the chemicals were ordered. In parallel to ordering chemicals, an inter-well tracer test program was implemented in June, 2011 with the primary purpose of using tracer breakthrough data to identify communication and reservoir continuity between injection and production wells as well as quantify the impact of groundwater flow on the transport of the chemicals. Field preparation, including drilling a new producer, was completed in July, 2011 (Well 19R). EOR equipment was delivered in August and onsite facility installation and testing started right away. Chemicals were received from TIORCO in the same month.

Table C.2 Brookshire Dome Field ASP Pilot Timeline.

February, 2011	Surfactant Formulation Identified
April, 2011	Coreflood Test Completed
June, 2011	Field Tracer Test Completed
July, 2011	Field Preparation Completed
August, 2011	EOR Equipment Delivered
August, 2011	Chemicals Received in the Field
Sept. 2nd, 2011	Polymer Pre-Flush (PPF) Injection Started
Sept. 13th, 2011	ASP Slug (ASP) Injection Started
Jan. 3rd, 2012	Polymer Drive (PD) Injection Started
Feb. 24th, 2012	Polymer Drive Completed
April 6th, 2012	ESP Pump Installed for Production Enhancement

Chemical injection was initiated on September 2nd 2011 with a polymer pre-flush for conformance control. ASP slug injection started on September 13th after completion of the preflush for 11 days. On January 3rd 2012, polymer drive injection was initiated and lasted till February 24th, which concluded the entire chemical injection sequence in the pilot. On April 6th 2012, an ESP pump was installed to bump up the production rate and thus daily oil production.

C.2 FIELD OPERATION

C.2.1 Injection and Production Facilities

The produced water was processed by the water treatment facilities onsite. The treated water was mixed with soda ash stock solution (delivered at 10% concentration). Surfactant, co-solvent and EDTA were added into the flow line through a chemical injection calibration system where the concentrations of each component could be carefully controlled. Polymer was delivered as sacks of powders, which were added into the polymer hopper and mixed with treated water in the mixing tank. The solution was continuously mixed for proper hydration of the polymer molecules. Finally the surfactant and polymer flow lines merged and went through a static mixer and filtration system before being injected through a triplex pump. The chemical injection calibration system and polymer mixing unit were situated in a dedicated work unit, where the ambient environment was controlled. Such a controlled environment helps prevent phase separation of the surfactant slug and ensure proper polymer mixing. The entire pumping and mixing system was designed to be easily monitored and adjusted through the central control panel. Figure C.1 shows some of the surface facilities installed onsite. The EOR skid was built and installed by TIORCO based on specifications provided by Layline Petroleum and the University of Texas.

All the wells in the field are produced by rod pumps, with a pumping schedule based on predetermined production rates. The produced fluid from all the wells is connected to the production facilities. As the concentration of polymer increased, the importance of maximizing retention time became important. Emulsion breakers were used for faster separation of oil and produced fluid.

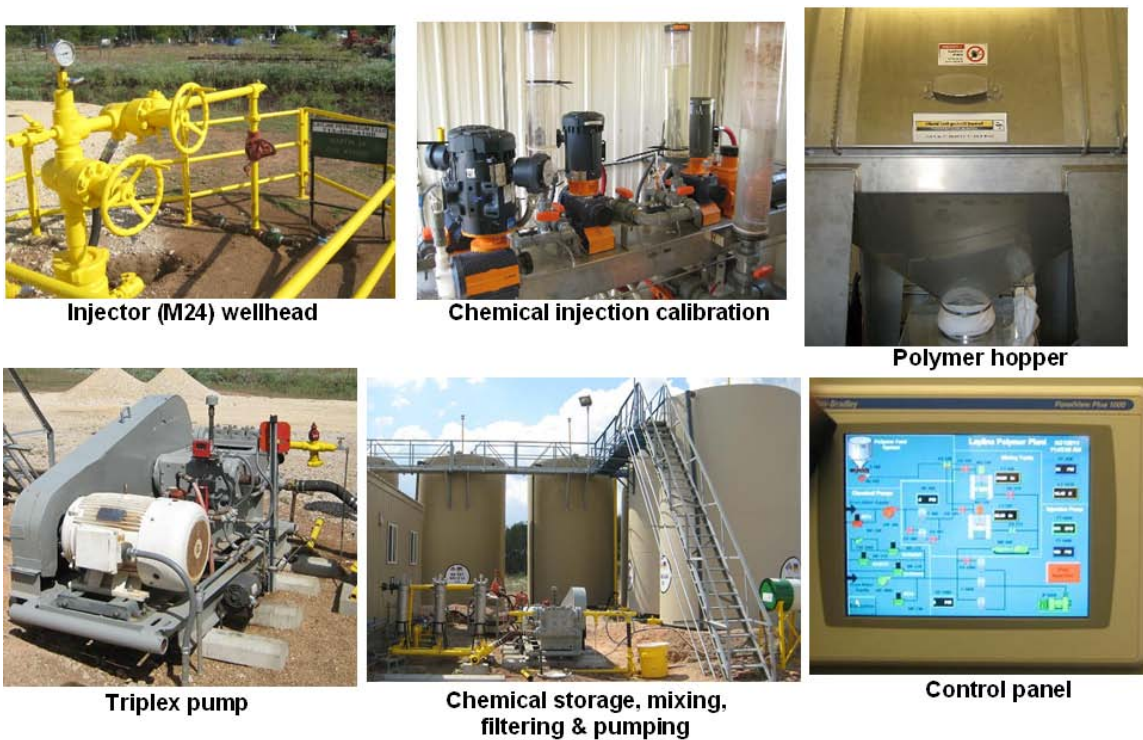


Figure C.1 Surface Facilities Installed at Pilot Location.

C.2.2 Field Laboratory Testing

Good quality control is essential for a successful pilot. There are four series of quality control checks that need to be put in place for a chemical flood pilot (Dean, 2011):

- 1). Periodically check surfactant phase behavior to make sure the optimum salinity and solubilization ratio are within acceptable range;
- 2). Polymer solution viscosity and filtration ratio should be checked frequently to ensure adequate mobility control;
- 3). Brine salinity and pH should also be checked for phase behavior and mobility control;

- 4). The aqueous stability of the ASP formulation needs to be verified to make sure that all components are soluble and form one single, stable, and clear phase.

A field laboratory was established and built on location with capabilities of testing fluid samples that were collected from injection and production wells. Samples off the injection line were collected every four hours and pH and conductivity (salinity) were recorded. Polymer concentration and viscosity were also recorded on samples taken from the mixing tank. The filtration ratio of the injected polymer solutions was also checked periodically (typically twice a day). The surfactant and co-solvent delivered to the field were tested in the research lab at the University of Texas for pre-pilot quality control. The performance of the field batch (surfactant and co-solvent) was consistent with the one used previously in lab screening, except for a slight shift of optimum salinity from 1% to 0.8% Na₂CO₃ (see solubilization plot in Figure C.2). Polymer samples were also frequently sent to research lab for rheology checks using a state-of-the-art rheometer. Inconsistency of viscosity at target concentration (Figure C.3) was indeed observed, and adjustments were made in the field. Chemical injection quantity and pressure was also monitored and recorded on a daily basis. On the producer side, produced fluid was monitored by collecting wellhead samples from all the pilot wells. These samples were analyzed for oil cuts, the presence of surfactant and polymer and pH. Wells outside the pilot area were also monitored for chemical breakthrough.

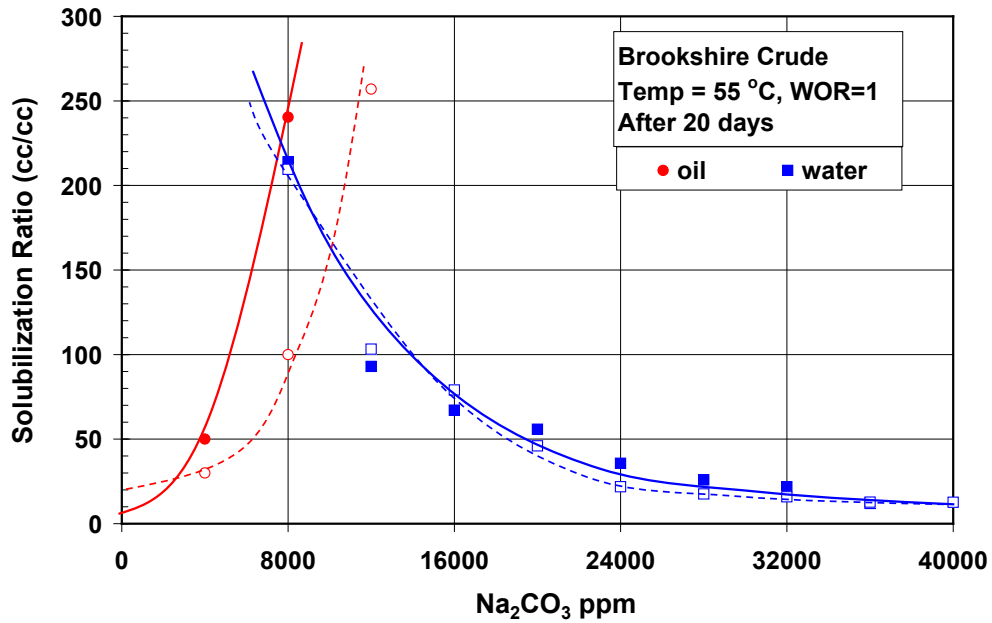


Figure C.2 Solubilization Plot Comparison between Field QC Test (solid lines & filled symbols) and Original Lab Results (dash lines & open symbols) (0.3wt% Petrostep S13-C + 0.1 wt% Neodol 25-12).

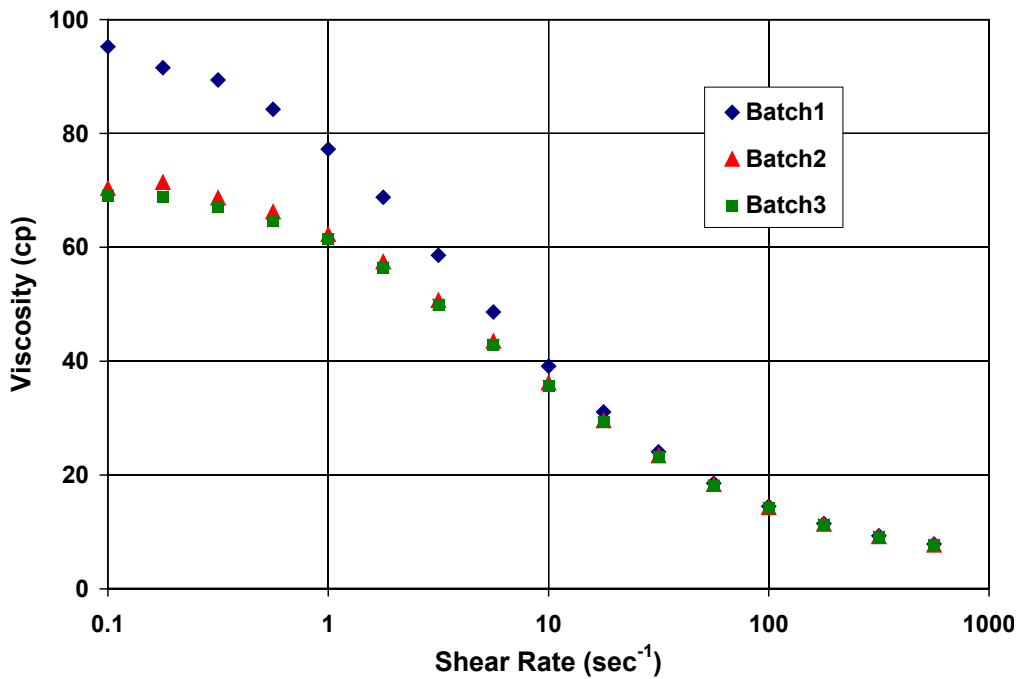


Figure C.3 QC Viscosity Measurements of Different 3430S Polymer (EOR90) Batches (@ 2500 ppm & 55°C).

C.3 FIELD OBSERVATIONS AND RESULTS

C.3.1 Injection Data

Prior to chemical injection, one of the major concerns in the field was the injectivity reduction due to viscous fluid injection, which is a potential problem in EOR operations (Qu, 1998; Jain, 2012; Sharma, 2012). The field injection permit was specified at 1055 psi maximum wellhead pressure to prevent fracturing the formation. Both theoretical and numerical calculations suggested a low injectivity of ~ 0.2 bpd/psi under this pressure if 2000ppm polymer were to be injected. The plot shown in Figure C.4 was based on a theoretical calculation conducted using equation (8.3-9) in Lake (1989). Any injection rate greater than 500 bpd was expected to result in injection above this pressure limit.

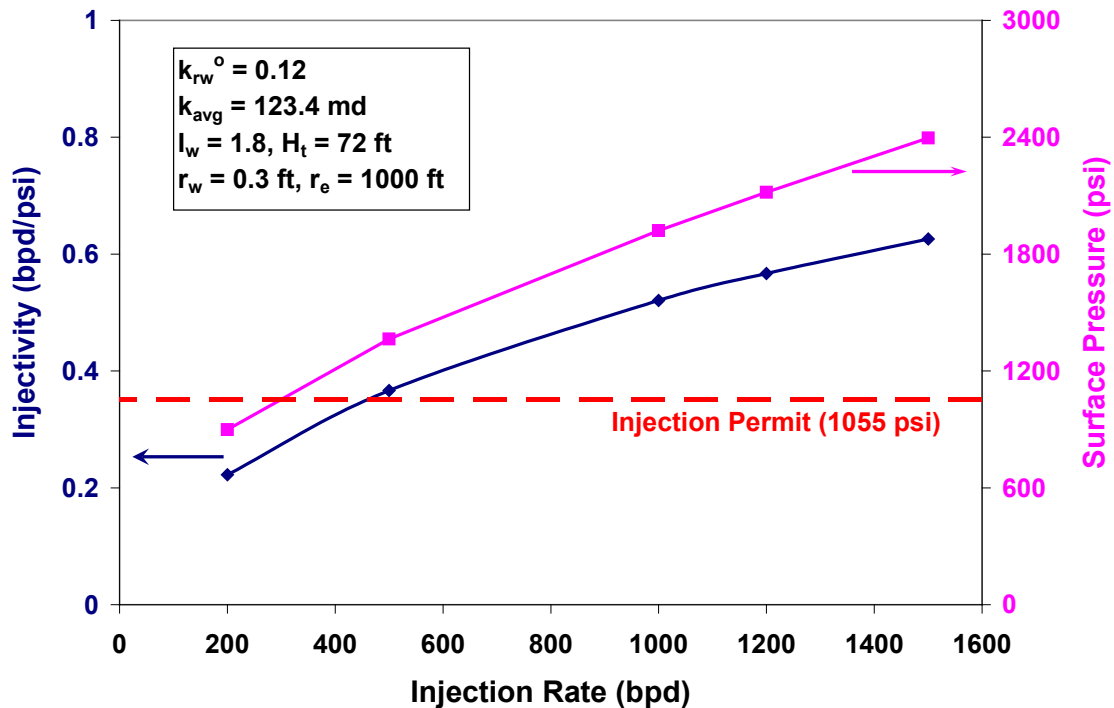


Figure C.4 Theoretical Calculation of Polymer Injectivity and Surface Pressure.

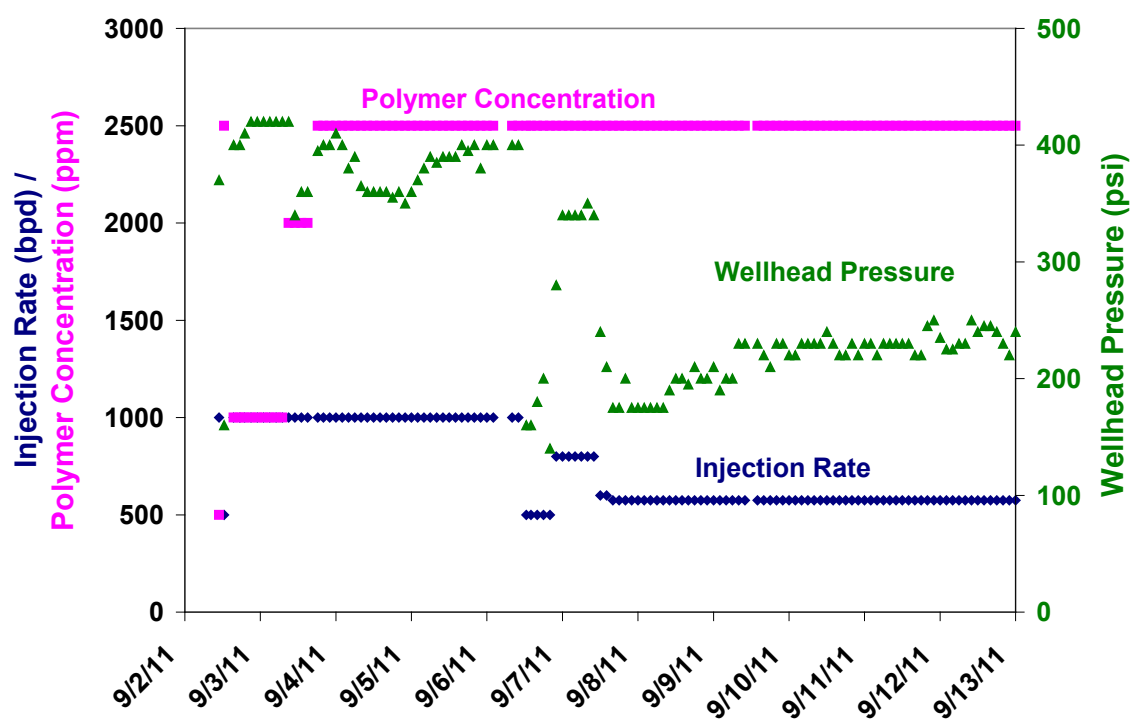


Figure C.5 Polymer Pre-Flush (PPF) Injection Data.

As a result of this calculation, at the onset of polymer pre-flush (PPF), as shown in Figure C.5 (the first data point), low concentration of polymer (1000ppm, ~ 12 cP at surface temperature) was injected at a fairly low rate (500bpd), with the intention to carefully monitor the injectivity and identify any associated issues. The surface pressure was found to be ~ 370 psi, resulting in a high injectivity of 2.7bpd/psi. With this surprisingly high injectivity, the polymer concentration was steadily increased to 2500ppm (~ 70 cP measured at the surface), and the injection rate was increased to 500bpd. As shown in Figure C.5, throughout the polymer pre-flush, the injection pressure remained well below the permitted injection pressure. The corresponding change of pressure with rate rendered an almost constant injectivity, despite the fact that polymer concentration and injection rate were both frequently adjusted. Since the injection was

done considerably below parting pressure, pre-existing fractures were suspected to be present in the injector and were likely responsible for this very high injectivity.

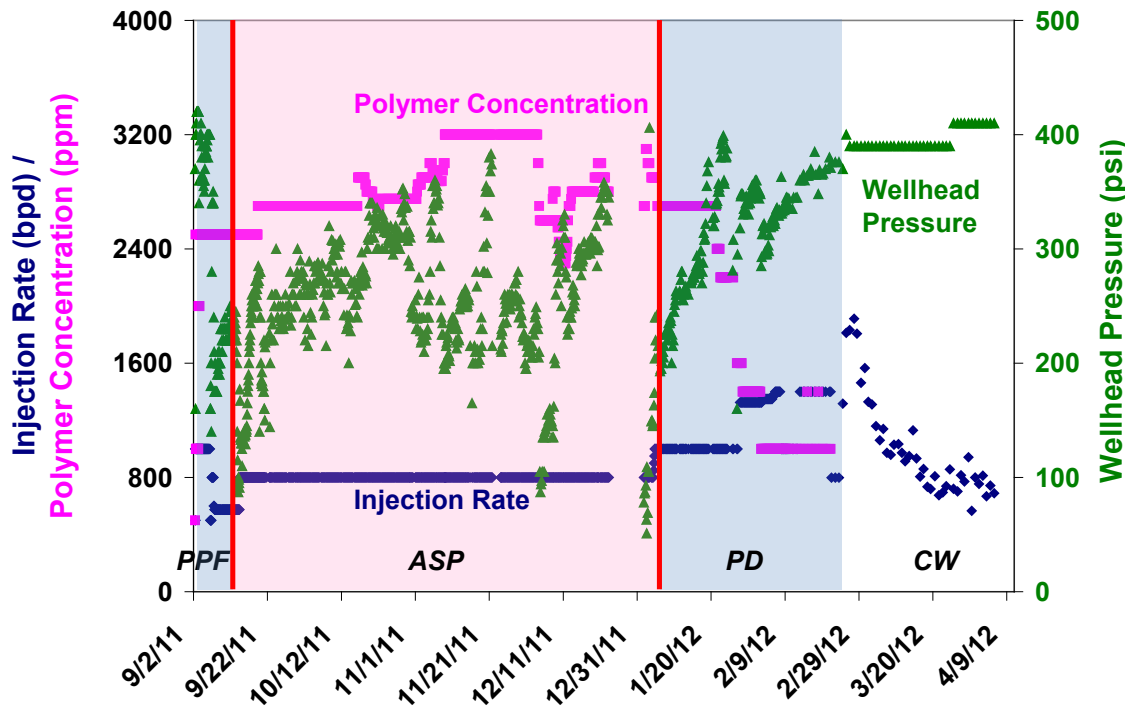


Figure C.6 Injection Data throughout the Entire Chemical Injection Sequence (PPF: polymer pre-flush; ASP: surfactant slug; PD: polymer drive; CW: chase water).

This lower-than-expected wellhead pressure was maintained throughout the entire injection sequence, as shown in Figure C.6. This abnormal injectivity response was recently studied numerically in our group (Lee, 2012). Various factors, including perforation density, shear rate coefficient (in rheological model), sand layer thickness (out-of-zone injection), near wellbore grid block size, and fracture growth, were investigated for effects on injectivity. While improvement on matching field data was achieved by adjusting certain parameters, the agreement was still not satisfactory,

indicating a more complicated mechanism controlling the process. This aspect will need a more in-depth study and may never be completely resolved.

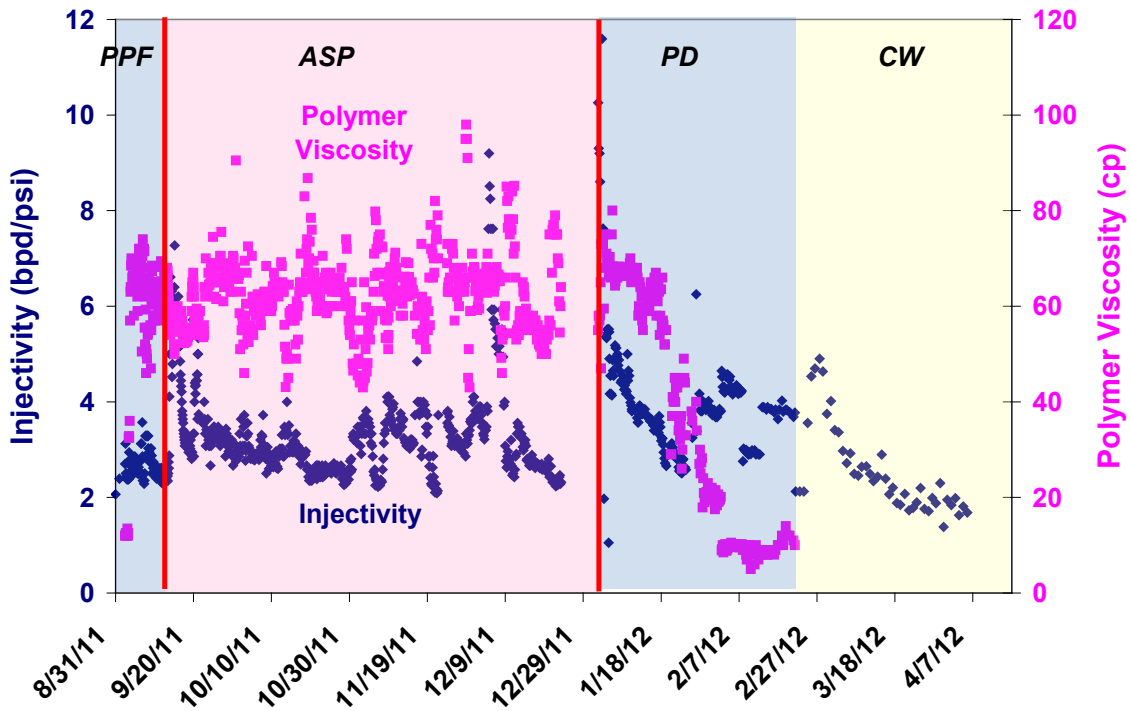


Figure C.7 Injectivity and Polymer Viscosity Profiles throughout the Chemical Injection Sequence.

Figure C.7 shows the corresponding injectivity and polymer viscosity data throughout the same time period. The injectivity here is calculated by simply dividing the wellhead pressure from the injection rate (assuming a hydrostatic reservoir pressure and neglecting frictional loss). The polymer viscosity reported here was measured on samples taken from the polymer mixing tank (before blending with surfactant, co-solvent and alkali) at surface temperature. For the ASP slug due to higher total salinity (1% Na_2CO_3 + brine salinity), the actually injected fluid viscosity will be lower, roughly two thirds of the reported polymer viscosity based on results from Section A. The polymer viscosity

was maintained throughout the pre-flush and ASP slug injection, and was gradually tapered down in the final polymer drive. The injectivity remained almost constant around 2.5 bpd/psi, for most of the injection period except when the ASP was initiated.

C.3.2 Residual Oil Mobilization

Upon contact with the residual oil, the synthetic surfactant and in-situ generated soap work together and start to solubilize the oil and dramatically bring down interfacial tension. The residual oil can then be mobilized and removed from pore space. This process was observed as evidenced by a sharp increase in fluid injectivity observed at the onset of surfactant slug injection, as shown in Figure C.8 (well injectivity and polymer viscosity).

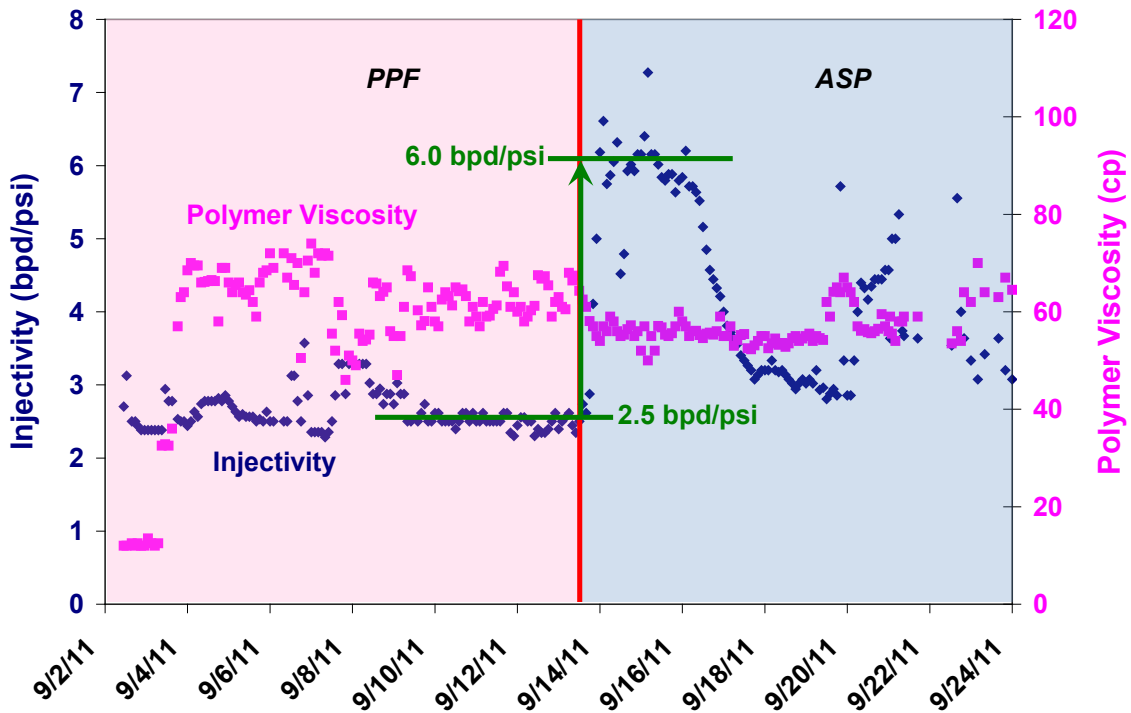


Figure C.8 Field Injectivity Response at the Onset of ASP Slug Injection: Indication of Oil Mobilization.

ASP slug injection was initiated at 14:00 hours on September 13th. As can be seen from figure above, almost right after the surfactant injection, the injectivity increased from 2.5bpd/psi to roughly 6 bpd/psi, and actually peaked at 7.5bpd/psi at one point. Although this may be partly due to a viscosity drop when switching from polymer pre-flush to the ASP slug, this decrease was not sufficient to explain the 2.4 times injectivity increase. Recalling the injectivity equation, one other variable that could potentially change injectivity is the relative permeability of the aqueous phase. Due to the mobilization of residual oil by slug injection, the residual oil saturation was reduced. This resulted in an increase in the aqueous phase saturation and led to a higher relative permeability to the ASP slug, which showed up as a sharp drop of injection pressure (Figure C.6), and as a sudden jump on the injectivity plot. Figure C.8 unambiguously shows the oil mobilization capability of the injected surfactant formulation.

C.3.3 Chemical Detection

Chemical detection from the produced fluids is also important for pilot interpretation. Injected chemicals are effective indicators suggesting off pattern / zone fluid loss. The turbidity test and titration method used for polymer and surfactant detection in the field could only provide rough estimates of breakthrough times and concentrations. The polymer and surfactant breakthrough sequence seems to follow that of the tracer test. No high pH has been observed in the produced fluid to date, which suggests quite possibly an unfavorable separation of pH and surfactant fronts. The reasons include high consumption due to higher than expected clay content, and also fluid loss from the pattern.

C.3.4 Production Response

During ASP slug injection, the injection rate was maintained at 800 bpd. Later on during the polymer drive phase, as the polymer concentration was progressively decreased the injection rate was increased accordingly (shown in Figure C.6). On the producer side, as can be seen from Figure C.9, the two wells on the south side of the pilot, Martin 10A and Martin 12, were set at a maximum production rate of roughly 500bpd, whereas Martin 34 and Martin 37, situated on the north side, were set at lower rates initially but raised to higher rates later on (especially Martin 37).

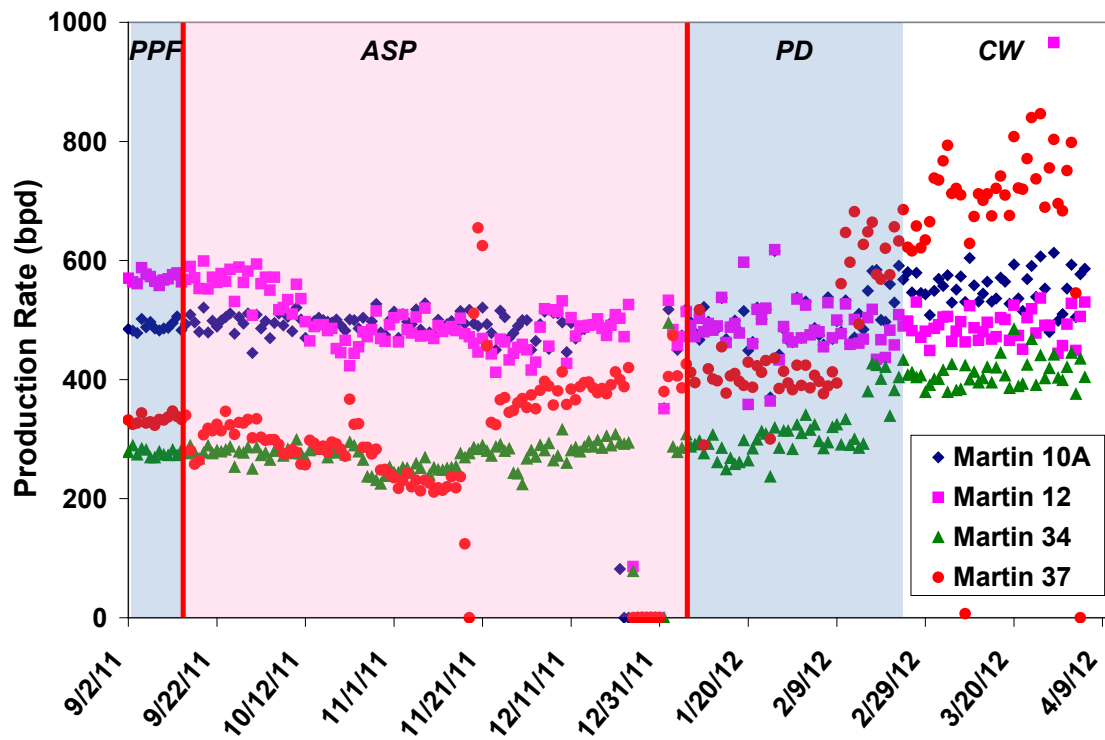


Figure C.9 Daily Production Rate of the Four Producers in the Pattern since Polymer Pre-Flush.

By pulling fluid faster on the south side of the pilot, the initial intention of such a production schedule was to counterbalance the influence of the natural water influx (SW

to NE), and to distribute injected chemicals more evenly within the pattern area. Later on, it was discovered that polymer showed up at Martin 6 well outside the pattern (consistent with tracer response). A high-perm conduit was suspected to exist between the injector and Martin 6. A decision was made at that point to bump up the production rate on the Martin 37 well (nearest to injector) and thus pull more fluid out from in-pattern producers. It was hoped this would weaken the impact of any high-perm thief zones.

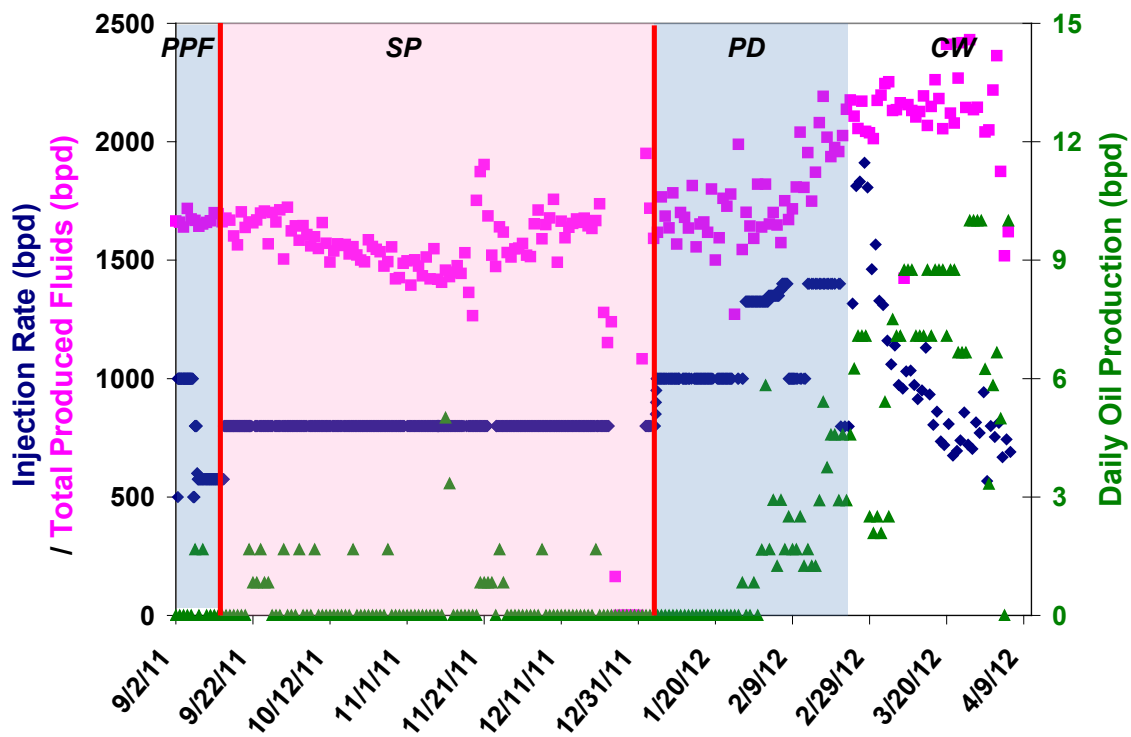


Figure C.10 Pilot Injection and Production Rates, along with Daily Oil Production.

Figure C.10 plots out the total injection and production rates from pilot wells, along with daily oil production rate from the four pilot producers combined. The total injection volume is always lower than the total fluid produced due to 1) the rate constraints put in place on the wells; and 2) the fact that an active aquifer is continuously

charging the reservoir. No appreciable oil production enhancement was observed throughout the ASP slug injection period. The daily oil rate started to pick up roughly half way through the polymer drive injection, and has continued to grow.

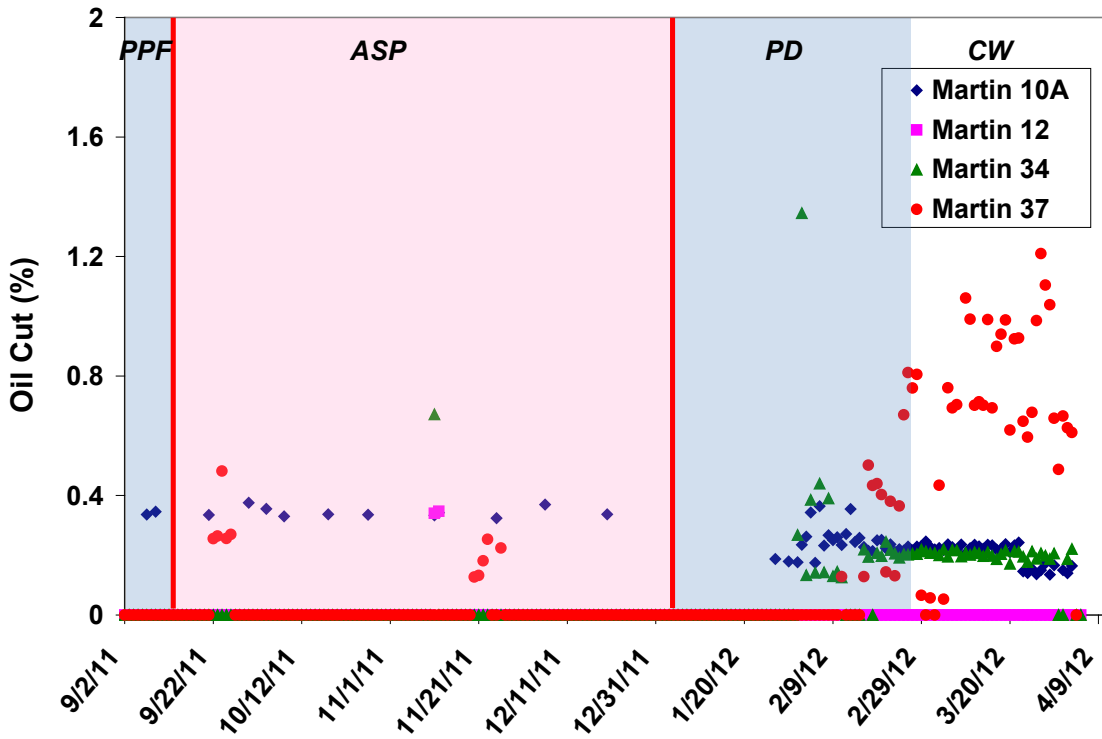


Figure C.11 Daily Oil Cut of the Four Producers in the Pattern since Polymer Pre-Flush.

Figure C.11 shows the oil cut on individual pilot producers since the start of the pre-flush. As seen, the oil cut did not show much change throughout the ASP slug injection, but started to rise about half way through the polymer drive. Martin 37 well shows the strongest response, with oil cut rising from zero to about 1.5%. This is in agreement with tracer response and the fact that M37 is the closest well to the injection. The stronger production response on M37 seems to correlate well with the higher production rate imposed on this well towards the end.

To date, the performance of the pilot has been far below expectation. Produced fluid samples were checked frequently for injected chemicals. Polymer was the first chemical to be detected. Surfactant has also been detected in the Martin 37. No alkali has been detected in the produced fluid, suggesting the possibility of high alkali consumption in the reservoir. The inability to propagate the pH and surfactant front simultaneously would result in poor oil solubilization and high interfacial tension. Insufficient alkali injection is of course only one possible reason among others that could adversely impact the pilot performance.

C.4 PILOT RISKS AND UNCERTAINTIES

There are many factors that can greatly affect the outcome of a pilot. Dean (2011) conducted a comprehensive review of the potential risks associated with chemical floods. Not all of the factors are applicable to the Brookshire pilot. The following is a list of possible problems that may affect the results from this pilot.

C.4.1 Higher Swept Pore Volume

The injected mass of surfactant and polymer injected is based on an estimated swept pore volume, so an underestimated pore volume could result in insufficient surfactant injection. Thus it would be impossible the slug to reach the producers. This typically occurs if there is a good bit of fluid flux into and out of the pilot pattern. This can also occur if injection occurs out of the target zone due to the presence of fractures or unanticipated flow behind pipe. Each of these scenarios can adversely affect the pilot performance since not enough of the injected fluids would be injected into the target zone. Based on a polymer injectivity study conducted in our group (Lee, 2012), a larger injection zone height can help match injection pressure data, which in the meantime

obviously suggests the possibility of a higher swept pore volume or injection into an undesired zone.

Poor confinement of chemicals within the pilot area also adversely affects the project performance, since effectively a lesser amount of chemicals would go into the target reservoir volume. The low overall tracer recovery, only about 24% recovered, suggests fluid loss from the pattern. The breakthrough of tracer into the Martin 6 is also an indication of preferred flow pathways that are not well understood.

C.4.2 Existence of Thief Zones / Unconstrained Fracture Growth

The existence of a high-permeability streak connecting the injector to outer wells can hurt sweep inside the pilot area and lower recovery. The inter-well tracer program results show very complicated breakthrough profiles. Earlier breakthrough on some of the out-of-pilot (and faraway) producers (for instance, Martin 6 well) seems to suggest the existence of such thief zones and more heterogeneity than was expected in the area.

The injectivity response observed in the field is extremely puzzling in the sense that it is completely unexpected and much higher than both analytical and simulation predictions. The injected fluid viscosity and the filtration ratio were constantly monitored. The viscosity remained at the target level throughout the project. Thus the high injectivity was probably not due to poor injection fluid quality (lower than expected viscosity), although other degradation processes (such as exposure to oxygen of some sulfite in fluid) could occur during polymer pumping and transport in the reservoir. An injectivity simulation study (Lee, 2012) shows that a pre-existing fracture in the injector can help explain the high injectivity. This would result in the EOR chemicals being injected out of zone, and may explain the poor oil recovery in the pilot.

C.4.3 Higher Surfactant Retention

Higher-than-expected surfactant retention will result in lower oil recovery and less favorable economics. The best way to prevent this from happening is to do realistic and accurate coreflood experiments with representative reservoir core under reservoir conditions. This unfortunately could not be accomplished for the Brookshire Dome project due to the poor quality of core plugs from the field. One way to reconcile this in the field is to inject more than sufficient surfactant mass so that even higher than expected retention will not cause severe damage. For the Brookshire project, a larger than designed pore volume (0.4 instead of 0.3PV) of surfactant slug was actually injected to accommodate the fact that the surfactant retention in the reservoir was a bit of an unknown.

An increase in alkali consumption together with surfactant adsorption may be another possible reason for the pilot performance. Common solutions include pre-flooding the reservoir to unload the clays of divalent cations, increasing the alkali concentration and / or changing to a surfactant that is more tolerant to divalent ions. Accurate mineralogy information needs to be collected. A core plug from the field was sent for XRD analysis for Brookshire project. The results however were not self-consistent, which made the clay content estimation even more difficult.

In the field, no high-pH (~ 10 to 11) fluid sample has been detected yet in any producer, whereas surfactant breakthrough was interpreted to have occurred on the adjacent Martin 37 well. The separation of pH and surfactant fronts seems to suggest higher alkali consumption in the reservoir, which delayed the pH front propagation in the reservoir. This situation was particularly undesirable since proper phase behavior, and thus oil mobilization, depends on the presence of both the alkali (in-situ soap generation)

and the synthetic surfactant. It seems as if this may be a likely reason for the poor oil recovery seen in the pilot.

C.4.4 Viscous Microemulsion Formation

In the classic Winsor (1954) microemulsion theory, the formation of Type III (or middle phase) microemulsion is of key importance for achieving ultra-low IFT. The flow behavior of microemulsion phase also has a direct impact on surfactant flood performance (Bennett, 1981; Walker, 2012; Solairaj, 2012). High microemulsion viscosity will significantly increase surfactant retention; adversely affect mobility control requirements and oil recovery results. Careful visual inspection of the middle phase is therefore a very important task during phase behavior screening. By using a branched main surfactant (Levitt *et al.*, 2006) and a hydrophilic co-solvent (Sahni *et al.*, 2010), the current surfactant formulation showed improved phase behavior and reduced microemulsion viscosity. The data in Figure C.12 show the low shear microemulsion viscosities at two C_{23} values.

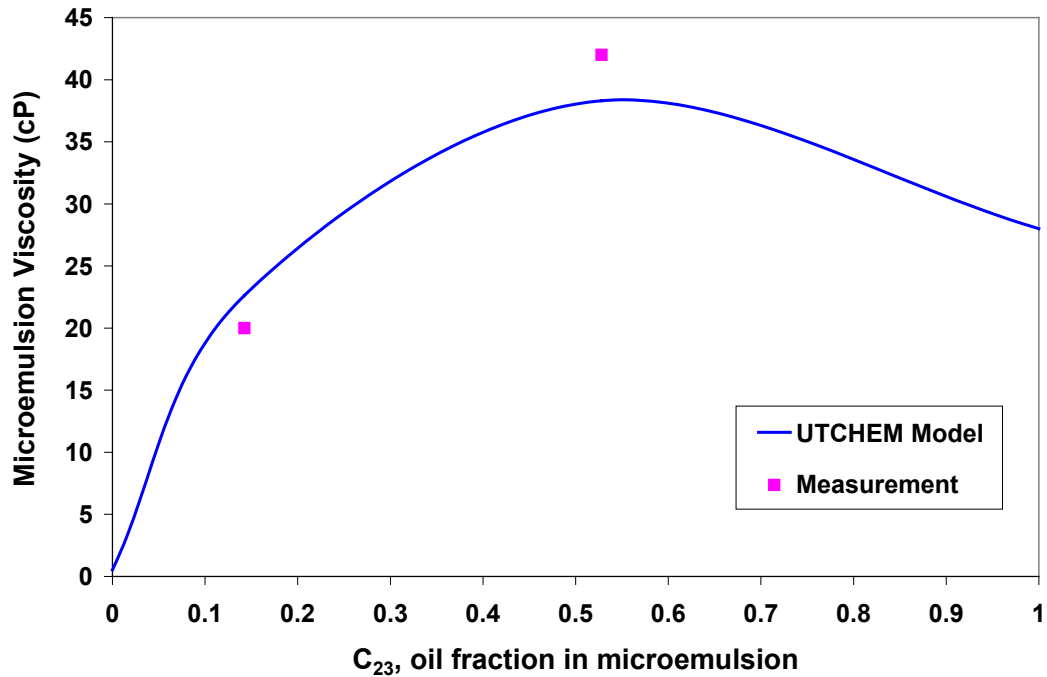


Figure C.12 Experimental and Modeled Microemulsion Viscosity at 55°C vs. C_{23} .

In UTCHEM simulation, microemulsion viscosity is modeled by a liquid phase viscosity model (UTCHEM, 2000), where the required input parameters are determined by matching laboratory measured viscosities at different compositions. The microemulsion viscosity varies between the brine (left) and oil (right) viscosity boundaries. Where C_{23} equals zero, the viscosity is the brine viscosity. When C_{23} equals one, the viscosity is the oil viscosity. At about 0.5 C_{23} , the microemulsion viscosity shows a maximum of about 43cP. As can be seen from Figure C.12, the UTCHEM model is able to predict lab measured microemulsion viscosities using solubilization parameters from phase behavior tests. There are however other complexities to this problem.

The non-Newtonian behavior of the microemulsion phase, as shown in Figure C.13, cannot be captured in the UTCHEM model. Similar behavior has been reported elsewhere (Bennett, 1981; Walker, 2012).

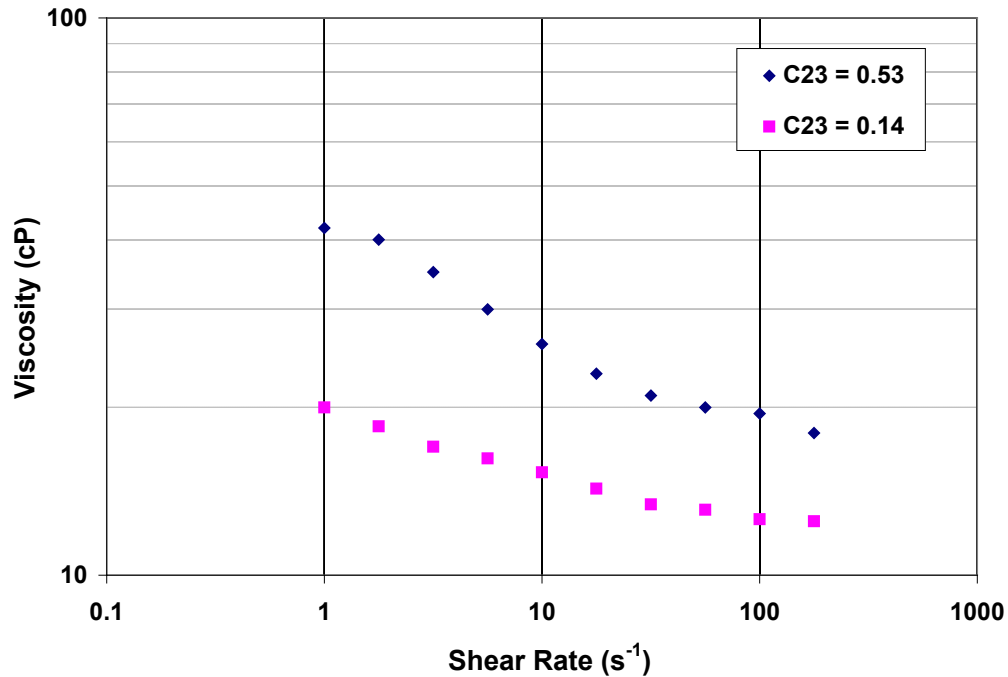


Figure C.13 Non-Newtonian Behavior of Microemulsion Viscosity at 55°C.

Considering the different mixing conditions in a phase behavior pipette and the pore space of a reservoir rock, the microemulsion viscosity in the field could be quite different from lab measurement. A more viscous microemulsion will cause a more serious problem in the field than in a 1D linear core flood. On a more “open” reservoir scale, the viscous microemulsion phase can act like a “diverting agent” to the injected fluid behind if the mobility control is not ensured. As a result, phase trapping and high surfactant retention will lead to a poor oil recovery. The fact that the injectivity remained almost constant (see Figure C.7) during slug and drive injection seems to suggest a possibility of the injected fluid trying to avoid the high viscosity microemulsion zone, since otherwise a steady drop of injectivity would be observed.

C.4.5 Low Initial Oil Saturation

The economics of any tertiary EOR process are very sensitive to the remaining oil saturation in the target zone. The waterflood residual oil saturation should ideally be determined as accurately as possible before planning the EOR pilot, using a method such as single well chemical tracer test (SWCTT). For a small scale pilot project such as the Brookshire Dome pilot it was not cost effective to conduct such a test. It is unlikely that this was the reason for the poor pilot performance. The increase in injectivity at the start of EOR chemical injection indicates that the waterflood residual oil was being displaced by the injected chemicals.

C.5 SECTION SUMMARY

An ASP flood in a mature waterflooded field was implemented in the Brookshire Dome field, Texas. Chemical injection in the field went smoothly without any injectivity issues as was originally feared. The injectivity remained remarkably stable throughout the flood even when injection rates and polymer concentration was changed. The unexpectedly high injectivity suggests the presence of fractures in the injector or unconstrained fracture growth induced by injection. This could lead to fluid loss to out-of-pattern zones, and viscosity breakdown in the wellbore. All these could severely impair the pilot performance.

The mobilization of waterflood residual oil by the surfactant slug (formation of an oil bank) was clearly indicated by the drastic increase of injectivity upon ASP slug injection. Production rates on the pilot producers were adjusted in real time based on field observation and response. Daily oil rate started to increase about half way through the polymer drive and has now reached a plateau. Production responses were observed in the Martin 34 and 37 wells, two of more close-by producers to the injector, as expected and suggested by the tracer test. Martin 37 started to show a 1 to 2% oil cut on towards the

end of the polymer flood. The oil recovery obtained was far below the expected recovery. There are many factors, risks, and uncertainties involved in the field trial that could have impacted this final performance.

Conclusions

A systematic laboratory design was carried out to optimize the chemical formulation for an ASP pilot flood. Lab-scale simulation model accurately history matched the coreflood experiment and sets up foundation for pilot-scale numerical study. Different operating strategies were investigated using a pilot-scale model, as well as the sensitivities of project economics to various design parameters. A field execution plan was proposed based on the results of the simulation study. A surface facility conceptual design was put together based on the practical needs and conditions in the field. Positive production responses have been observed from several nearby producers, and are under careful monitoring. More specifically, the technical accomplishments of this pilot project include:

- A systematic and successful laboratory design process was carried out in research lab at the University of Texas. The four-step design approach, composed of a) process and material selection; b) formulation optimization; c) coreflood validation; 4) lab-scale simulation, could be easily transferred to other EOR projects. The optimal formulation recovered over 90% residual oil from Berea coreflood. Lab-scale simulation model accurately history matched the coreflood experiment and set up foundation for pilot-scale numerical study.
- Pilot-scale simulation model was set up based on available information in hand. Different operating strategies were investigated, as well as the sensitivities of project economics to various design parameters. A field execution plan was proposed based on the results of this simulation study.
- A surface facility conceptual design was put together based on the practical needs and conditions in the field. All field preparations, on-site equipment installation,

chemical ordering and delivering were carried out in a timely and efficient manner. Flood injection was completely without any major issues. Good field management ensured a smooth operation and an effective communication with different parties involved.

- Residual oil mobilization and accumulation oil in front of surfactant slug (formation of oil bank) were clearly shown by drastic increase of injectivity upon ASP slug injection. Production rates on the pilot producers were adjusted in real time based on field observation and response. Daily oil rate started to increase about half way through the polymer drive and is still continuing to grow. Production responses were observed on Martin 34 and 37, two of more close-by producers to the injector, as expected and suggested by the tracer test. Martin 37 starts to show stronger oil production on towards the end.

There are many factors, risks, and uncertainties involved in the field trial that could impact the final performance. More thorough investigation needs to be conducted when more data and information are collected from the field. Some of key lessons learned throughout the project, among others, include:

- Good quality reservoir core is crucial to the design process, and should be collected and used whenever possible for more realistic (compared to Berea) coreflood experiment. Invaluable information could therefore be obtained. Chemical (surfactant and alkali) consumption in the reservoir can be much better estimated. And such knowledge is of key importance to the design process. Endpoint relative permeability and residual phase saturation are two other (among many) important sets of parameters can more accurately estimated using reservoir core, and they are absolutely crucial in simulation studies.

- For ASP processes that make use of alkali and naphthenic acid reaction to generate soap, the phase behavior and thus oil solubilization capacity of the chemical formulation are always greatly impacted by the amount of alkali present in the system. By itself, the synthetic surfactant can seldom render optimal phase behavior. It is therefore imperative that sufficient synthetic surfactant and alkali always coexist in the system. However, in rocks with high clay content, alkali could be consumed very quickly which leads to a separation between surfactant and pH (alkali) fronts. Then the system is no longer optimum and loses its ability to mobilize residual oil. Therefore, it is important to monitor surfactant breakthrough and pH values of effluents from coreflood and produced fluids in the field. It is necessary oftentimes to add more alkali to compensate higher than expected consumption in the reservoir.
- Mobility ratio is a key parameter to a successful APS flood design. This is especially important when considering the possibility of highly viscous and non-Newtonian microemulsion formation in the reservoir. Careful laboratory characterization of microemulsion rheology is therefore of key importance. Improved rheology model could help better understand the flow behavior of microemulsion phase in the reservoir.
- All numerical simulations are based upon assumptions. This is particularly true when building the geological model. Lack of good reservoir cores in most cases makes the situation even worse. By no means can a successfully lab-scale history match on a coreflood guarantee the quality of a field-scale run. The results need to be interpreted with extreme caution.
- The injection of chemicals marks the beginning of a flood. But oftentimes even this starting point cannot be well understood. Polymer injectivity has long been a

hot research topic, and yet most simulation models today have hard time matching the injectivity in the field. Better and probably more fundamental understanding of various injectivity related issues is most definitely needed.

Bibliography

- Bennett, K.E., Davis, H.T., Macosko, C.W., and Scriven L.E., Microemulsion Rheology: Newtonian and Non-Newtonian Regimes, Paper SPE 10061, presented at the SPE ATCE, San Antonio, Texas, 5-7 October, 1981.
- Choi, S.K., pH Sensitive Polymers for Novel Conformance Control and Polymer Flooding Applications, PhD Dissertation, The University of Texas at Austin, Austin, Texas, 2008.
- Dean, R.M., Selection and Evaluation of Surfactants for Field Pilots, MS Thesis, The University of Texas at Austin, Austin, Texas, 2011.
- Delshad, M., Pope, G., and Sepehrnoori, K., A Compositional Simulator for Modeling Surfactant Enhanced Aquifer Remediation 1. Formulation, Journal of Contaminant Hydrology, 23 (1996), 303-327.
- Flaaten, A.K., Experimental Study of Microemulsion Characterization and Optimization in Enhanced Oil Recovery: A Design Approach for Reservoirs with High Salinity and Hardness, MS Thesis, The University of Texas at Austin, Austin, Texas, 2007.
- Flatten, A.K., Nguyen, Q.P., Pope, G.A., and Zhang, J., A Systematic Laboratory Approach to Low-Cost, High-Performance Chemical Flooding, Paper SPE 113469, presented at the Symposium on Improved Oil Recovery, Tulsa, Oklahoma, 19-23 April, 2008.
- Jackson, A.J., Experimental Study of the Benefits of Sodium Carbonate on Surfactants for Enhanced Oil Recovery, MS Thesis, The University of Texas at Austin, Austin, Texas, 2006.
- Jain, A.K., Dhawan, A.K., and Misra, T.R., ASP Flood Pilot in Jhalora (K-IV) – A Case Study, Paper SPE 153667, resented at the SPE Oil and Gas India Conference and Exhibition, Mumbei, India, 28-30 March, 2012.
- Lake, L. W., Enhanced Oil Recovery, Prentice Hall (1989).
- Lee, K., Impact of Fracture Creation and Growth on Well Injectivity and Reservoir Sweep during Waterflooding and Chemical EOR Processes, PhD Dissertation, The University of Texas at Austin, Austin, Texas, 2012.
- Levitt, D.B., Experimental Evaluation of High Performance EOR Surfactants for a Dolomite Oil Reservoir, MS Thesis, The University of Texas at Austin, Austin, Texas, 2006.
- Levitt, D. B., Jackson, A. C., Heinsen, C. Britton, L. N., Malik, T., Dwarakanath, V., and Pope, G.A., Identification and Evaluation of High-Performance EOR Surfactants, SPE Reservoir Evaluation and Engineering, 12 (2009), 243-253.

- Mohammadi, H., Mechanistic Modeling, Design, and Optimization of Alkaline / Surfactant / Polymer Flooding, PhD Dissertation, The University of Texas at Austin, Austin, 2008.
- Mohnot, S.M., Bae, J.H., and Foley, W.L., A Study of Mineral/Alkali Reactions, SPE Reservoir Engineering, 2 (1987), 653-663.
- Novosad, Z., and Novosad, J., Determination of Alkalinity Losses Resulting From Hydrogen Ion Exchange in Alkaline Flooding, SPE Journal, 24 (1984), 49-52.
- Qu, Z., Zhang, Y., Zhang, X., P., and Dai, J., A Successful ASP Flooding Pilot in Gudong Oil Field, Paper SPE 39613, resented at the SPE/DOE Improved Oil Recovery Symposium, Tulsa, Oklahoma, 19-22 April, 1998.
- Sharma, A., Azizi-Yarand, A., Clayton, B., etc., The Design and Execution of an Alkaline-Surfactant-Polymer Pilot Test, Paper SPE 154318, resented at the 18th SPE Improved Oil Recovery Symposium, Tulsa, Oklahoma, 14-18 April, 2012.
- Sahni, V., Experimental Evaluation of Co-solvents in Development of High Performance Alkali/Surfactant/Polymer Formulations for Enhanced Oil Recovery, M.S. Thesis, The University of Texas at Austin, Austin, Texas, 2009.
- Sahni, V., Dean, R.M., Britton, C., Kim, D., Weerasooriya, U., and Gary, P.A., The Role of Co-Solvents and Co-Surfactants in Making Chemical Floods Robust, Paper SPE 130007, presented at the SPE Improved Recovery Symposium, Tulsa, Oklahoma, 24-28 April, 2010.
- Solairaj, S., New Method of Predicting Optimum Surfactant Structure for EOR, MS Thesis, The University of Texas at Austin, Austin, Texas, 2011.
- Solairaj, S., Britton, C., Kim, D., Weerasooriya, U., and Pope, G.A., Measurement and Analysis of Surfactant Retention, Paper SPE 154247, presented at the SPE Improved Recovery Symposium, Tulsa, Oklahoma, 14-18 April, 2012.
- Sydansk, R.D., Elevated-Temperature Caustic/Sandstone Interaction: Implications for Improving Oil Recovery, SPE Journal, 22 (1982), 453-462.
- UTCHEM-9, Volume II: Technical Documentation for UTCHEM 9.0, A Three-Dimensional Chemical Flooding Simulator, The University of Texas at Austin, Texas, 2000.
- Veedu, F.K., Scale-up Methodology for Chemical Flooding, MS Thesis, The University of Texas at Austin, Austin, Texas, 2010.
- Walker, D.L, Britton, C., Kim, D., Dufour, S. Weerasooriya, U., and Pope, G.A., The Impact of Microemulsion Viscosity on Oil Recovery, Paper SPE 154275, presented at the SPE Improved Recovery Symposium, Tulsa, Oklahoma, 14-18 April, 2012.

- Yang, H., Britton, C., Liyanage, P.J., Solairaj, S., Kim, D., Nguyen, Q., Weerasooriya, U., and Pope, G.A., Low-cost, High-performance Chemicals for Enhanced Oil Recovery, Paper SPE 129978, presented at the SPE Improved Recovery Symposium, Tulsa, Oklahoma, 24-28 April, 2010.
- Yang, H.T., Development of Improved ASP Formulation for Reactive and Non-reactive Crude Oils, MS Thesis, The University of Texas at Austin, Austin, Texas, 2010.
- Zhao, P, Jackson, A.C., Britton, C., and Pope, G.A., Development of High-Performance Surfactants for Difficult Oils, Paper SPE 113432, presented at the Symposium on Improved Oil Recovery, Tulsa, Oklahoma, 19-23 April, 2008.

List of Tables

Table A.1: Composition of Field Water Samples (from Heater Treater).	6
Table A.2: Mixing Sheet for Preparing 1L SBB (TDS = 7360.74 mg/L).	6
Table A.3: Composition of SBB (TDS = 7360.74 mg/L).....	6
Table A.4: X-Ray Diffraction Analysis of Core Sample at 2468' Depth (from CoreLab).	8
Table A.5: Summary of Group 1 (Alcohol Ether Sulfates) Surfactant Screening	14
Table A.6: Summary of Group 2 (ABS) Surfactant Screening.....	16
Table A.7: Summary of Group 3 (Surfactant Mixtures or New Molecules) Surfactant Screening.	18
Table A.8: Summary of Screening Experiments for Formulation Optimization.	22
Table A.8: Summary of Screening Experiments for Formulation Optimization (Cont.).....	23
Table A.8: Summary of Screening Experiments for Formulation Optimization (Cont.).....	24
Table A.8: Summary of Screening Experiments for Formulation Optimization (Cont.).....	25
Table A.8: Summary of Screening Experiments for Formulation Optimization (Cont.).....	26
Table A.8: Summary of Screening Experiments for Formulation Optimization (Cont.).....	27
Table A.9: Berea Core Properties for Coreflood GB-2.	39
Table A.10: Permeability and Relative Permeability Values of Berea Core GB-2.	39
Table A.11: Saturation Data for Berea Core GB-2.....	39

Table A.12: Fluid Viscosities Measured at 55°C and 10s ⁻¹ .	44
Table A.13: Alkali Surfactant Polymer Slug Data for GB-2 Coreflood.	44
Table A.14: Polymer Drive Data for GB-2 Coreflood.	45
Table B.1 Phase Behavior Parameters to Match the Experimental Data Shown in Figure B.1 and Figure B.2.	51
Table B.2 Review of Core and Fluid Properties for GB-2 Coreflood.	54
Table B.3 Summary of Simulation Inputs for GB-2 Coreflood.	56
Table B.4 Areal and Volumetric Calculations for Pilot Pattern.	60
Table B.5 5-Layer Model: Individual Layer Properties.	62
Table B.6 5-Layer Model: Reservoir Size and Dimensions.	63
Table B.7 9-Layer Model: Individual Layer Properties.	63
Table B.8 9-Layer Model: Reservoir Size and Dimensions.	63
Table B.9 5-Layer Model: S _o and Oil in Place after 5000 Days of Waterflood.	69
Table B.10 9-Layer Model: S _o and Oil in Place after 5000 Days of Waterflood.	69
Table B.11 Producer Rates for Base Case Simulation (from tracer test).	71
Table B.12 Different Strategies Investigated in this Section.	71
Table B.13 Simulation Results Summary for Different Operating Strategies.	81
Table C.1 ASP Pilot Final Injection Schedule.	98
Table C.2 Brookshire Dome Field ASP Pilot Timeline.	99

List of Figures

Figure A.1: Lateral Continuity of the Catahoula Sand within the Pattern (Injector: Martin 24; Producers: Martin 37, 34, 12 and 10A).....	4
Figure A.2: Well Locations in Brookshire Dome Field (pilot pattern in red box).	5
Figure A.3: Core Plugs from the Field (broken apart and muddy looking).	7
Figure A.4: B-3 Solubilization Plot after One Month Settling at WOR=1 (1.5wt% Alfoterra L167-7S + 0.5wt% Petrostep S-2 + 2wt% IBA).	10
Figure A.5: B-4 Solubilization Plot after 20 Days Settling at WOR = 4(1.5 wt%Alfoterra L167-7S + 0.5 wt%Petrostep S-2 + 2wt% IBA).	11
Figure A.6: B-11 Phase Behavior Pipettes after 1 Week Settling.	12
Figure A.7: B-12 Phase Behavior Pipettes after 1 Week Settling.....	13
Figure A.8: B-33 Phase Behavior Pipettes after 3 Weeks' Settling.	19
Figure A.9: B-34 Phase Behavior Pipettes after 3 Weeks' Settling.	19
Figure A.10: B-65 Phase Behavior Pipettes after 2 Weeks' Settling.	28
Figure A.11: B-65 Solubilization Plot after 33 Days Settling at WOR = 1 (0.5 wt% Petrostep S13-B + 0.2 wt% Neodol 25-12).	28
Figure A.12: B-67 Phase Behavior Pipettes after 2 Weeks' Settling.	29
Figure A.13: B-67 Solubilization Plot after 26 Days Settling at WOR = 2.33 (0.5 wt% Petrostep S13-B + 0.2 wt% Neodol 25-12).	29
Figure A.14: B-73 Phase Behavior Pipettes after 2 Weeks' Settling.	30
Figure A.15: B-73 Solubilization Plot after 20 Days Settling at WOR = 1 (0.2 wt% Petrostep S13-B + 0.2 wt% Neodol 25-12).	30
Figure A.16: B-74 Phase Behavior Pipettes after 3 Weeks' Settling.	31

Figure A.17: B-74 Solubilization Plot after 20 Days Settling at WOR = 1 (0.5 wt% Petrostep S13-C + 0.2 wt% Neodol 25-12).	31
Figure A.18: B-91 Phase Behavior Pipettes after 3 Weeks' Settling.	32
Figure A.19: B-91 Solubilization Plot after 20 Days Settling at WOR = 1 (0.3wt% Petrostep S13-C + 0.1 wt% Neodol 25-12).	32
Figure A.20: Activity Map for 0.3wt% Petrostep S13-B + 0.1 wt% Neodol 25-12.	33
Figure A.21: Activity Map for 0.3wt% Petrostep S13-C + 0.1 wt% Neodol 25-12.	33
Figure A.22: GB-2 Brine Flood Pressure ($q = 2.64\text{ml/min}$, $\mu_w = 0.54\text{cP}$).	40
Figure A.23: GB-2 Oil Flood Pressure ($q = 0.54\text{ml/min}$, $\mu_o = 28\text{cP}$).	41
Figure A.24: GB-2 Water Flood Pressure ($q = 0.054\text{ml/min}$, $\mu_w = 0.54\text{cP}$).	42
Figure A.25: Corey Model Estimation of Relative Permeability ($n = 2$).	43
Figure A.26: Polymer Viscosities for GB-2 at 55°C and 10s^{-1} .	44
Figure A.27: GB-2 ASP Pressure ($q = 0.04\text{ml/min}$).	46
Figure A.28: GB-2 Oil Recovery.	47
Figure A.29: GB-2 Effluent pH and Emulsion Cut.	47
Figure B.1: Phase Behavior Match for 50% Oil Concentration.	50
Figure B.2: Phase Behavior Match for 30% Oil Concentration.	51
Figure B.3: UTCHEM Model Fit to Lab Data: Viscosity vs. Salinity (2000ppm Floppam 3330S at 55°C).	52
Figure B.4: UTCHEM Model Fit to Lab Data: Viscosity vs. Concentration (Floppam 3330S in SBB of 0.243meq/ml at 55°C).	52
Figure B.5: UTCHEM Model Fit to Lab Data: Viscosity vs. Shear Rate (2000ppm Floppam 3330S in 100% SBB at 55°C).	53

Figure B.6: Relative Permeability Curves used in UTCHEM Coreflood Simulation.	
	55
Figure B.7: Capillary Desaturation Curve for Oil in Simulation Model.....	55
Figure B.8: Comparison of Simulated and Measured Oil Recovery and Oil Cut for GB-2 Coreflood.	57
Figure B.9: Comparison of the Effluent pH between UTCHEM and Experimental Data for GB-2 Coreflood.	58
Figure B.10: Simulated Salinity, IFT and Oil Saturation for GB-2 at 0.5 PV...58	
Figure B.11: Areal View of the Well Placement in the Simulation Model.	59
Figure B.12: Spinner Survey Results Provided by Weatherford.	62
Figure B.13: Detailed Bromide Tracer Response for All Monitoring Wells 70 Days after Injection.	65
Figure B.14: Tracer Concentration Response Simulated using UTCHEM.	67
Figure B.15: Tracer Concentration Response Simulated using UTCHEM. Note that the simulation assumes all the wells produce from day 1 while in reality the wells were drilled over a period of time.	68
Figure B.16: Areal View of Post-Waterflood Oil Saturation of Layer 1, 2, 3, and 5 for Coarser Model (5-layer).	70
Figure B.17: Cumulative Oil Recovery and Oil Production Rate for Case 1 (base case ASP injection).	72
Figure B.18: Areal View of Post Chemical Flood Oil Saturation of Layer 1, 2, 3, and 5 for Case 1 (base case ASP injection).	73
Figure B.19: Cumulative Oil Recovery and Oil Production Rate for Case 2 (2X ASP injection).	74

Figure B.20: Areal View of Post Chemical Flood Oil Saturation of Layer 1, 2, 3, and 5 for Case 2 (2X ASP injection).	75
Figure B.21: Cumulative Oil Recovery and Oil Production Rate for Case 3 (ASP bottom layer injection).	76
Figure B.22: Areal View of Post Chemical Flood Oil Saturation of Layer 1, 3, 4, and 5 for Case 3 (ASP bottom layer injection).	77
Figure B.23: Cumulative Oil Recovery and Oil Production Rate for Case 4 (Polymer Pre-flush and ASP flood).	78
Figure B.24: Areal View of Post Chemical Flood Oil Saturation of Layer 1, 2, 3, and 5 for Case 4 (Polymer Pre-flush and ASP flood).	79
Figure B.25: Cumulative Oil Recovery and Oil Production Rate for Case 5 (ASP with doubled production rates).	80
Figure B.26: Areal View of Post Chemical Flood Oil Saturation of Layer 1, 2, 3, and 5 for Case 5 (ASP with doubled production rates).	81
Figure B.27: Cum. Oil Production Comparison between 5 Cases Studied.	82
Figure B.28: Cum. Oil Production and Total Oil Rate Comparison between 5-Layer and 9-Layer Models.	84
Figure B.29: Cumulative Oil Recovery and Oil Production Rate for ASP Simulation with 2000 ppm Polymer.	85
Figure B.30: Cumulative Oil Recovery and Oil Production Rate for ASP Simulation with 3000 ppm Polymer.	86
Figure B.31: Effect of Polymer Concentration on the Recovery Results of ASP Flood.	86
Figure B.32: Chemical Mass Sensitivity Study: Base Case.	88
Figure B.33: Chemical Mass Sensitivity Study: 15% Less Chemical Mass.	88

Figure B.34:	Chemical Mass Sensitivity Study: 15% More Chemical Mass.	89
Figure B.35:	Chemical Mass Sensitivity Study: 30% Less Chemical Mass.....	89
Figure B.36:	Cum. Oil Production Comparison between the Chemical Mass Sensitivity Cases.	90
Figure B.37:	Dependence of Cum. Production on Total Injected Chemical Mass (or Swept Pore Volume).	90
Figure B.38:	pH Breakthrough Profiles on M37 and M34 with Two Different Cation Exchange Capacities.	93
Figure B.39:	pH and Surfactant Breakthrough Profiles on M34 with Two Different Cation Exchange Capacities.	94
Figure C.1	Surface Facilities Installed at Pilot Location.	101
Figure C.2	Solubilization Plot Comparison between Field QC Test (solid lines & filled symbols) and Original Lab Results (dash lines & open symbols) (0.3wt% Petrostep S13-C + 0.1 wt% Neodol 25-12).	103
Figure C.3	QC Viscosity Measurements of Different 3430S Polymer (EOR90) Batches (@ 2500 ppm & 55°C).	103
Figure C.4	Theoretical Calculation of Polymer Injectivity and Surface Pressure.	104
Figure C.5	Polymer Pre-Flush (PPF) Injection Data.	105
Figure C.6	Injection Data throughout the Entire Chemical Injection Sequence (PPF: polymer pre-flush; ASP: surfactant slug; PD: polymer drive; CW: chase water).	106
Figure C.7	Injectivity and Polymer Viscosity Profiles throughout the Chemical Injection Sequence.	107
Figure C.8	Field Injectivity Response at the Onset of ASP Slug Injection: Indication of Oil Mobilization.	108

Figure C.9	Daily Production Rate of the Four Producers in the Pattern since Polymer Pre-Flush.	110
Figure C.10	Pilot Injection and Production Rates, along with Daily Oil Production. 111	
Figure C.11	Daily Oil Cut of the Four Producers in the Pattern since Polymer Pre- Flush.....	112
Figure C.12	Experimental and Modeled Microemulsion Viscosity at 55°C vs. C ₂₃ .	117
Figure C.13	Non-Newtonian Behavior of Microemulsion Viscosity at 55°C. ...	118